UNIVERSITAT DE BARCELONA

Endothelial Mitofusin 2 deficiency improves systemic metabolic health and delays age-associated decline

Íñigo Chivite Araiz

Endothelial Mitofusin 2 deficiency improves systemic metabolic health and delays age-associated decline

Íñigo Chivite Araiz

PhD. Thesis 2020

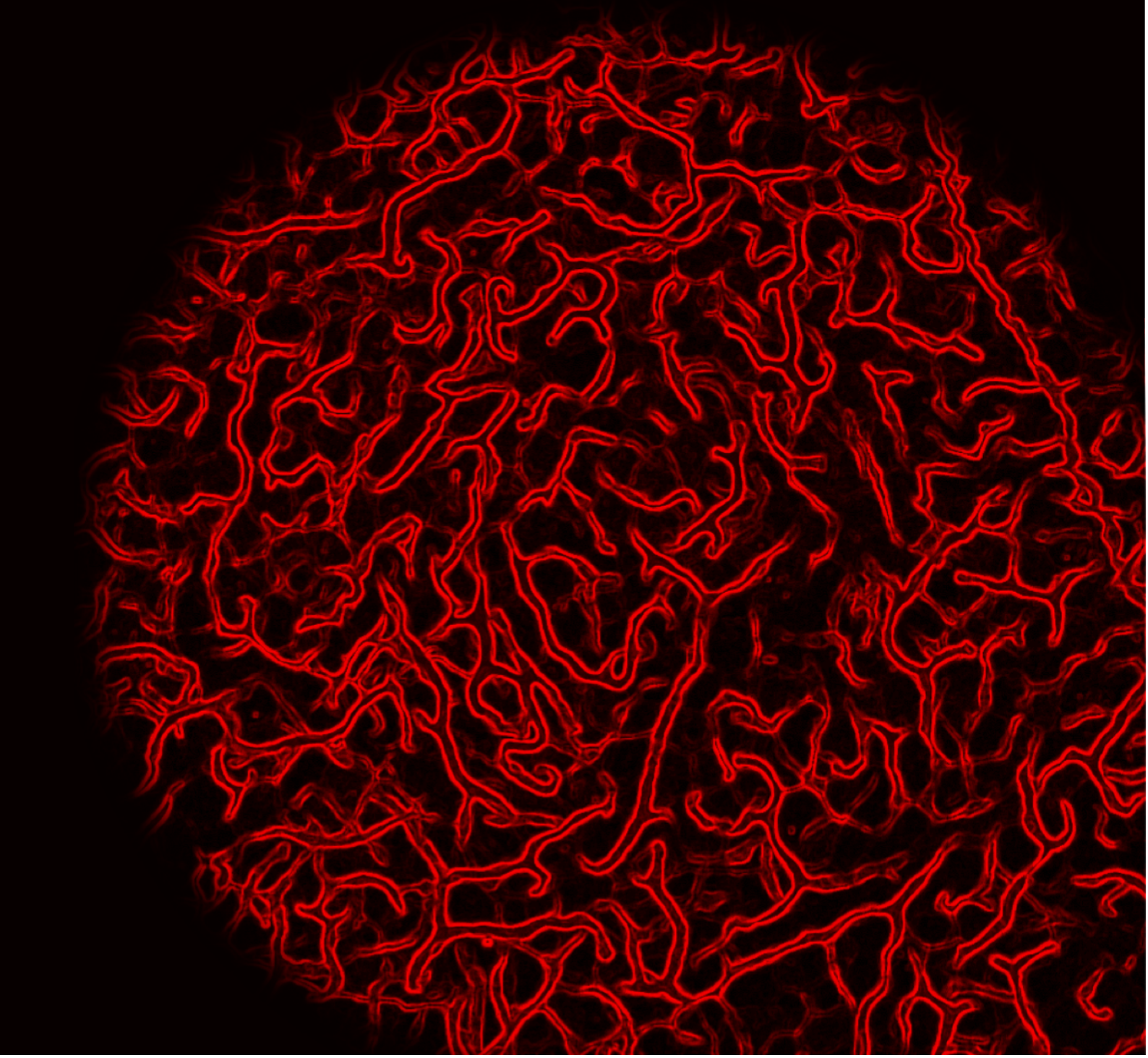

Facultat de Medicina i Ciències de la Salut

Programa de Doctorat en Biomedicina

Endothelial Mitofusin 2 deficiency improves systemic metabolic health and delays age-associated decline

Memòria presentada per
Íñigo Chivite Araiz
per optar al títol de doctor per la Universitat de Barcelona.

Aquesta tesi ha estat realitzada sota la direcció de
Marc Claret Carles i **Mariona Graupera i Garcia-Milà**
en el Laboratori de Control Neuronal del Metabolisme ubicat en l'Institut d'Investigacions Biomèdiques August Pi i Sunyer (IDIBAPS)

_____
Doctorand

Íñigo Chivite Araiz

_____	_____	_____
Director de la tesi	Co-directora de la tesi	Tutor
Marc Claret Carles	**Mariona Graupera i Garcia-Milà**	**Pablo Miguel García-Rovés González**

Barcelona, Setembre 2019

To my grandparents,
to my parents,
to my siblings,

Zion National Park (Utah, USA)

“La dificultad de la pendiente te hace olvidar que no paras de subir y progresar”

(Si tu me dices ven lo dejo todo… pero dime ven, Albert Espinosa)

ACKNOWLEDGEMENTS

AKNOWLEDGEMENTS

El trabajo que esta redactado a continuación no habría sido posible sin el apoyo y la ayuda de muchas de las personas que me han acompañado durante estos últimos años. Gracias a todos vosotros he podido completar este camino sin perder la ilusión, y experimentando un proceso de creciendo personal y profesional. Me es imposible describir lo que cada uno de vosotros me ha aportado, es por ello por lo que en las próximas líneas solo quiero dejar unas pequeñas pistas. De esta forma, al releerlas con el paso de los años, pueda desenterrar el sentimiento y recuerdo que guardo de cada uno de vosotros, y así volver a revivir estos fantásticos años.

Primeramente, agradecer a team "M&M" (Marc y Mariona), por la oportunidad, la confianza, la ayuda y la dedicación que me habéis dado. Marc, de ti me quedo con la practicidad y el pragmatismo, así como con la diplomacia que tienes la capacidad de conservar en cada momento. Mariona, de ti destaco esa inagotable fuente de energía y positivismo que tienes y contagias. Gracias a los dos.

Esta tesis es imposible entenderla sin mi paso previo por el laboratorio de las ONAs. Helena, Adri, las Anas y Erika. Si no fuera por vosotras jamás hubiera comenzado una tesis doctoral. Gracias a que me hicisteis partícipe de vuestro trabajo, de la dedicación que demostrabais, de los momentos de ilusión y desilusión, de las risas y de las lágrimas y de las conversaciones que eran terapias, aprendí lo bueno y lo no tan bueno de la investigación científica. Gracias de corazón.

A mi familia de acogida en Barcelona: Javi, Lorena, Raffa, Simone, Clara, Niels, Laura, Fotis, Elisenda, Andrea, Judit, las Anas y Erika. La ciencia nos acercó y la vida nos unió. Habría sido muy difícil sobrevivir en esta ciudad sin vosotros. Gabi, tu siempre serás mi madre en Barcelona, y Estefanía la hermana gemela que, por desgracia, nos separaron al nacer.

Un salto mortal me metió de lleno en el NeuCoMe lab, ahora sí en la tesis. Alicia y Sara gracias por enseñarme a andar por este nuevo laboratorio, abrirme puertas y guiarme. Seguís siendo mis referentes, cada una con su estilo, pero lo sois. Alicia, esos refranes, frases hechas, y ese "Que es lo que digo yo siempre…" son tu seña de identidad. Sara, siempre me quedará la duda de si fuimos novios en una vida anterior, si no, no me explico esta especie de tensión que en algún que otro día dejas aflorar y que sabemos que algún día terminará en los tribunales. Macarena, tus charlas inspiradoras y revolucionarias y esa motivación innata que tienes por la ciencia, son alucinantes. Una bocana de positivismo, pero siempre con los pies en la tierra y las ideas claras, muy claras. Roberta, la brasi-germana, la perfecta fusión de afecto y rectitud. Soy tu protegido y tu "pichu", y por eso se que me enseñas a volar para dejar que me estrelle, pero siempre, siempre estás ahí para levantarme otra vez. Arnaud, la antítesis de la seriedad y el

cachondeo en una misma persona. En cierta manera me recuerdas a mi, tu molestar sí, pero a ti, que no te toquen. Gracias por compartir tus vivencias, no lo sabes, pero las tendré muy en cuenta en mis futuras decisiones. María, tu que me tienes que sufrir de compañero de ordenador y de poyata, tienes el cielo ganado. Los caminos nos vuelven a juntar después de unos cuantos años, pero tu sonrisa y tu manera de ser, siguen generando un perfecto buen rollo de trabajo. Miriam y Elena, acabáis de llegar, pero en este corto tiempo os habéis mostrado atentas a escucharme y ayudarme. De verdad gracias a todos porque sin vuestras conversaciones, escucha, consejos, apoyo y ayuda (jamás olvidare a todos reunidos alrededor del LAS4000 revelando aquella mancha negra que me esforzaba por decir que era un WB) no me podría imaginar hoy escribiendo mi tesis.

A los compañeros del grupo RG. Ainhoa y Rebeca, gracias por darme la confianza de poder acercarme a vosotras a preguntaros cualquier cosa que necesitara con la seguridad de que me resolveríais el problema, fuera el que fuera. Hugo y Joan, gracias por las preguntas y por generar discusión en mis “Què fas?”, con una mención especial a Rosa y Ramón por su incesante curiosidad, así como por proponerme experimentos. Con ello habéis favorecido a que crezca la ilusión por mi proyecto. A Berta, y sus miradas confidentes por encima del ordenador a altas horas de la tarde. Marta F, Ana Lu, Montse y Gary, gracias simplemente por generar un buen ambiente. Gary, echaré en falta tus comentarios sinceros, alentadores y tu sonrisa, buena suerte.

A los Novials Sara, Juli, La Portu (Joana), Carlos Valeria, Franchi por aquel año de aventuras que decidimos vivir en Menorca, Italia y Munich y, cada viernes noche, en Barcelona. Sara, gracias por nuestras conversaciones a cerca de esta montaña rusa llamada “Tesis Doctoral” y nuestros viajes de reset completo, tan necesarios como el de Holanda o Islandia, has sido un gran apoyo. Juli, gracias por tus consejos y ayuda prestada siempre que te iba a buscar, y también por haber sido el motor social de la 5ª. Ahora, Guillermo, Elia, Oriol, Arturo, Dani, las nuevas generaciones de predocs, toman el relevo institucionalizando las cervezas de los viernes. Seguid así y hacedme un hueco junto Óscar y Gema, los postdocs con espíritu joven, que no fallan.

A Marce y sus consejos y ayuda desinteresada cuando la he necesitado, a Joan Marc, los Santamaría, los Ferrer, Marta Julia y la Patri simplemente por haber generado un buen ambiente de trabajo, que aunque no sabemos valorarlo en el día a día, en muy necesario. Gracias a todos de verdad.

A los amistades y conocidos del resto del IDIBAPS, ya sea por medio del CE, o la Phd Community, o las manifestaciones por los derechos de los investigadores predoctorales. Parece mentira,

pero el simple hecho de preguntar “¿Cómo va…?” y ese “¡Ánimo que ya falta menos!”, son dignos de mencionar y agradecer. Gracias Marcos, Mire, Martí y Nuria por materializar ese viaje que tanta ilusión teníamos en hacer y que me ayudó a coger aire y fuerzas para afrontar esta última etapa. Mire y Marti, por esas jornadas maratonianas de curro + preparación del viaje + los preparativos de Sant Jordi. ¡Brindemos por ello!

A esas personas que os habéis hecho querer, no solo, pero en especial por el apoyo de los últimos meses. Nuria y Laia, por esas cervezas, cafés, meriendas y visitas inesperadas cualquier excusa ha bastado para que despegase el culo de la silla y descansara la vista del ordenador. Jon, por sacarme a correr y hacer que me mueva, y siempre, siempre preocuparte por cómo estoy y preguntarme “¿Qué tal…?”, aunque sabes que te espera una chapa, un poco pesada. Gracias de corazón.

Saioa, Mónica y a ella que no os ha faltado la comprensión y las palabras de ánimo. A los biologuchos: Amaia, Sandra y David. Simplemente por formar parte de mi vida y por las aventuras que hemos vivido y nos quedan por vivir juntos. A la coadrillica: los Javis, Nacho, Noelia y Julián, que siempre se encargan de recordarme que por muy lejos que me vaya, siempre habrá un hueco para mí en Pamplona.

Pablo, no hay palabras para describirte. Simplemente no existen. Sé que quieres que la próxima vida la pasemos juntos en el infierno… pero es que, ya sólo por como eres conmigo te has ganado el cielo una y mil veces. Y eso tan solo hablando de los 6 últimos meses y no de los más de 15 años que llevamos compartidos. Has sido una pieza calve para mí durante este tiempo, mi confidente sin filtros, mi almohada y mi trampolín, aguantándome las largas horas de conversación y dándome consejos hasta cuando me admitías que “ya no sé que decir”, pero aún y todo ahí seguías. No me faltes nunca.

Y para mi familia, para quien va dedicada esta tesis. Es imposible imaginarme hoy tal y como soy sin vosotros. Quiero agradecer a los abuelos, por la apuesta decidida que tuvieron porque sus hijos cambiaran de vida y al trabajo duro de sol a sol, que lo posibilitó. Mis padres y hermanos que conjuntamente me habéis hecho fuerte ante la adversidad, me habéis enseñado a no tirar la toalla y a confiar en uno mismo, así como a relativizar, sin menospreciar. Valores, sin duda imprescindibles, y que han posibilitado el éxito de esta tesis.

Gracias a todos de corazón.

ABSTRACT

ABSTRACT

Blood vessels distribute nutrients and oxygen to every single cell in the body. Endothelial cells define the vessel wall, and thus they are ideally located to crucially modulate nutrient availability and act as metabolic gatekeepers of the organism. In recent years, mitochondrial dynamics has emerged as a bioenergetic adaptation process to cellular metabolic demands. Mitofusins are GTPase-like proteins implicated in external mitochondrial membrane fusion. Our hypothesis is that mitochondrial fusion in endothelial cells is implicated in energy balance and metabolic control.

In order to address this hypothesis, we generated mice lacking either Mitofusin 1 (Mfn1) or Mitofusin 2 (Mfn2) into adulthood by breeding a tamoxifen-inducible endothelial Cre line (*PdgfbiCreER*^{T2}) with Mfn1 or Mfn2 floxed animals (hereafter called *Mfn1*$^{\Delta EC}$ and *Mfn2*$^{\Delta EC}$ respectively). *Mfn2*$^{i\Delta EC}$ mice showed a progressive reduction (~25%) in body weight when compared to control counterparts. Intestinal nutrient absorption, food intake and locomotor activity were unaltered in knockout mice. However, enhanced energy expenditure and a shift towards lipid oxidation was observed, while the thermogenesis capacity was not different between groups. Consistent with this phenotype, *Mfn2*$^{i\Delta EC}$ mice exhibited lower fat mass and improved glucose tolerance and insulin sensitivity in the face of unaltered insulin release. Collectively, these results indicate that loss of Mfn2 in endothelial cells causes a lean phenotype as the consequence of enhanced lipid metabolism. However, endothelial *Mfn1* deletion did not alter systemic metabolism.

Upon high-fat diet administration, *Mfn2*$^{i\Delta EC}$ mice showed complete resistance to its obesogenic effects. In concordance with lower body weight due to reduced adiposity, mutant mice exhibited improved glucose homeostasis. Moreover, induction of endothelial Mfn2 ablation in established obesity reduced body weight to standard diet control levels and improved metabolic alterations. Interestingly, *Mfn1*$^{i\Delta EC}$ mice do not show any metabolic alteration when fed high-fat diet.

Aged *Mfn2*$^{i\Delta EC}$ mice preserved young-like health-span parameters. Indeed, mutant mice exhibited improved age-associated physiological parameters such as kidney function or anaemia. Diverse motor and cognitive parameters were also preserved in old *Mfn2*$^{i\Delta EC}$ mice. Collectively, our results indicate that Mfn2 in endothelial cells is implicated in systemic energy homeostasis control as well as in ageing progression in mice.

ABBREVIATIONS

ABBREVIATIONS

Abbreviation	Definition
4-OHT	4-hydroxytamoxifen
ACR	Albumin to creatinine ratio
AKT	Protein kinase - B
ANG	Angiopoietin
AR	Aspect ratio
AT/ATs	Adipose tissue / tissues
ATP	Adenosine triphosphate
AUC	Area under the curve
BBB	Blood brain barrier
BMI	Body mass index
BMR	Basal metabolic rate
BP	Blood pressure
CD31	Cluster of differentiation 31
CD36	Cluster of differentiation 36
CM	Cristae membrane
CR	Calorie restriction
Ct	Cycle threshold
DM	Diabetes mellitus
DRP1	Dynamin related protein
EB	Evans blue
EC / ECs	Endothelial cell / cells
EE	Energy expenditure
eNOS	Endothelial nitric oxide synthase
EPCs	Endothelial progenitor cells
ER	Endoplasmic reticulum
ET-1	Endothelin 1
ETC	Electron transport chain
eWAT	Epididymal white adipose tissue
FADH2	Flavin adenine dinucleotide
FAO	Fatty acid oxidation
FF	Form factor
FFA	Free fatty acids
FIS1	Mitochondrial fission 1

ABBREVIATIONS

FoxO1	Forkhead box protein O1
GLUT	Glucose transporters
GSIS	Glucose stimulated insulin secretion test
GTP	Guanosine triphosphate
GTT	Glucose tolerance tests
gWAT	Gonadal white adipose tissue
H&E	Hematoxylin and eosin
HCAs	Human coronary arterioles
HFD	High fat diet
Hif1-α	Hypoxia-induced factor 1-α
HOMA-IR	Homeostatic model assessment of insulin resistance index
HSL	Hormone sensitive lipase
Hsp90	Heat shock protein 90
HUVECs	Human umbilical endothelial cells
IB4	Isolectin GS-IB4
iBAT	Interscapular brown adipose tissue
IBM	Inner boundary membrane
Igf-1	Insulin-like growth factor-1
IL	Interleukin
IMM	Inner mitochondrial membrane
IMS	Intermembrane space
InsR	Insulin receptor
IP	Intraperitoneal
IR	Insulin resistance
IRS-1	Insulin receptor signalling-1
ITT	Insulin tolerance test
KO / KOs	Knockout / Knockouts
LA	Locomotor activity
LDL-C	Low - density lipoprotein cholesterol
MAO	Monoamine oxidases
MF	Macrophages
MFF	Mitochondrial fission factor
MFN / MFNs	Mitofusin / Mitofusins
MFN1	Mitofusin 1

MFN2	Mitofusin 2
MiD49	Mitochondrial dynamic protein of 49kda
MiD51	Mitochondrial dynamic protein of 51kda
mtDNA	Mitochondrial DNA
NADH	Nicotinamide adenine dinucleotide
NADPH	Nicotinamide adenine dinucleotide phosphate
nDNA	Nuclear DNA
NEFAs	Non-esterified fatty acids
Nf-κB	Nuclear transcription factor κ-light-chain-enhancer of activated B cells
NMRI	Nuclear magnetic resonance imaging
NO	Nitric oxide
NORT	Novel object recognition test
NOX4	Nicotinamide adenine dinucleotide phosphatase oxidase 4
OCT	Optimal cutting temperature
OF	Open field
OMM	Outer mitochondrial membrane
OPA1	Optic atrophy 1
OXPHOS	Oxidative phosphorylation
PBS	Phosphate-buffered saline
PCR	Polymerase chain reaction
PECs	Proliferative endothelial cells
PFA	Paraformaldehyde
PFKB3	Phosphofructokinase-2/fructose-2,6-bisphosphatase 3
PGC1α	Peroxisome proliferator-activated receptor γ coactivator-1-α
PINK1	Phosphatase and tensin homolog (PTEN)-induced putative kinase 1
POMC	Proopiomelanocortin
Ppar	Peroxisome proliferator-activated receptor
QECs	Quiescent endothelial cells
QMR	Quantitative magnetic resonance
qRT-PCR	Quantitative reverse transcription PCR
RIPA	Radioimmunoprecipitation assay buffer
RNS	Reactive nitrogen species
ROS	Reactive oxygen species
rpm	Rotations per minute

ABBREVIATIONS

RQ	Respiratory quotient
RT	Room temperature
SDS-PAGE	Sodium dodecyl sulfate polyacrylamide gels
STD	Standard diet
sWAT	Subcutaneous white adipose tissue
T1D	Type 1 diabetes
T2D	Type 2 diabetes
TAE	Tris-acetate EDTA
TCA	Tricarboxylic acid cycle
TG	Triglycerides
TIE2	Tyrosine-protein kinase receptor
TIM	Translocase of the inner membrane
TNF-α	Tumor necrosis factor α
TOM	Translocase of the outer membrane
UCPs	Uncoupling proteins
UPR^{mt}	Mitochondrial unfold protein response
VDAC	Voltage dependent anion channel
VEGF	Vascular endothelial growth factor
VOI	Volume of interest
vSMC	Vascular smooth muscle cells
vWAT	Visceral adipose tissue
WAT	White adipose tissue
WHO	World health organization

TABLE OF CONTENTS

CONTENTS

TABLE OF CONTENTS

TABLE OF CONTENTS

LIST OF FIGURES

LIST OF TABLES

INTRODUCTION

1. Energy balance and glucose homeostatic disorders

1.1 Obesity

Obesity is a chronic multifactorial disease in which a combination of biological, environmental and behavioural factors cause a state of positive energy balance that generates excessive fat accumulation and increased body weight to the extent that represents a risk to health (Phoebe A.Stapleton, 2008). Imbalance between calories intake and expended is the leading cause of overweight and obesity. Body mass index (BMI), defined as a person's weight in kilograms divided by the square of one's height in meters (kg/m^2), is commonly used to classify overweight ($25<BMI<30$) and obese ($BMI>30$) human adults. The modern lifestyle, promoting physical inactivity and the consumption of energy-dense food that are high in fat and carbohydrates, has caused a dramatic increase in the worldwide prevalence of obesity. In fact, according to the World Health Organization (WHO), it has been nearly tripled since 1975. Indeed, in 2016, more than 1,9 billion (39%) of adults were overweight, and 650 million (13%) were obese. More importantly, around 41 million preschool children (under the age of 5) were either overweight or obese.

It is well established that higher BMI is associated with increased risk of developing systemic disorders such as gastrointestinal-related diseases including gallstone, pancreatitis and non-alcoholic fatty liver. The endocrine and metabolic system is also affected by increasing the risk of diabetes, insulin resistance (IR), glucose intolerance and dyslipidaemia. Of crucial importance is the higher predisposition of obese patients to develop cardiovascular disorders such as thromboembolism, hypertension, coronary artery disease, chronic heart failure and cardiac asthma (Darvall et al., 2007; Reis et al., 2005). Moreover, obesity is associated with menstrual abnormality and infertility (Cohen et al., 2008; Maruthur et al., 2009; Obligado and Goldfarb, 2008), musculoskeletal disorders as osteoarthritis (Tukker et al., 2008) and gout (Tahmin Sarnali et al., 2010) as well as respiratory abnormalities such as hypoventilation syndrome (Poulain, 2006), pneumonia and pulmonary embolism (Tahmin Sarnali et al., 2010). Furthermore, obese patients are more susceptible to develop some types of cancers including colon, rectum, liver, endometrial, breast, ovarian, prostate, kidney and lymphomas (Basen-Engquist and Chang, 2011; Johnson and Lund, 2007; WHO-Obesity, 2018). Childhood obesity is associated with future risks, such as higher chances for developing obesity, premature death and disability in the adulthood (Tahmin Sarnali et al., 2010; Tan and Vidal-Puig, 2008; WHO-Obesity, 2018).

Current statistics show that around 300.000 annual deaths are attributed to obesity in the United States, (Flegal et al., 2004) and most of them are due to obesity-associated diseases such

as diabetes, hypertension, cardiovascular disease and cancer (Kopelman, 2000). According to the WHO, common obesity can be prevented by the promotion of losing weight through healthy eating and regular physical activity. Nutritional interventions such as calorie restriction diets and intermittent fasting have been lately proposed as potential actions to counteract obesity. Weight-loss surgery, such as electric stimulation system, gastric emptying systems, gastric balloon systems and bariatric surgery, is also available but restricted to patients with specific clinical features. All proposed therapies, targeting energy intake, will initially produce weight loss. However, the homeostatic defended feedback loop would resist further weight loss thus limiting the effectiveness (Spiegelman and Flier, 2001). Moreover, pharmaceuticals treatments that target intestinal fat absorption or serotonergic receptors in the brain are of limited efficacy (Bray and Tartaglia, 2000).

Taken together, research in obesity is mandatory to provide new insights into the molecular and physiological pathways that underlie this complex disease. This will allow the development of novel and truly effective therapies.

1.2 Diabetes mellitus

Diabetes mellitus (DM) is a group of metabolic diseases that are characterized by impaired insulin secretion and/or action, eventually leading to chronic hyperglycaemia. Thus, fasting blood glucose levels are used to diagnose DM (non-diabetic, less than 5,5 mmol/L; prediabetic, between 5,5 and 7,0 mmol/L; diabetic, more than 7,0 mmol/L). According to the WHO, the prevalence of DM has been quadrupled in the last 40 years, reaching 422 million people in 2014. Of note, 1,6 million deaths were attributed to diabetes in 2016 (WHO-Diabetes, 2018).

The defects in carbohydrate, lipid and protein metabolism in DM patients are due to deficient insulin secretion by the β-cells in the pancreas and/or action on target tissues (IR). This leads to a state of hyperglycaemia that in the long-term has been associated to damage, dysfunction and failure of heart, blood vessels, eyes (leading to blindness through diabetic retinopathy), kidneys and nerves (WHO-Diabetes, 2018).

According to the American Diabetes Association, DM can be classified into four different categories being type 1 and type 2 diabetes (T1D and T2D, respectively) the most common forms.

Type 1 diabetes

T1D, also known as insulin-dependent diabetes, is mainly due to an autoimmune destruction of the pancreatic β-cells through T-cell inflammatory (insulitis), and humoral (β-cells) responses

(Devendra et al., 2004). This leads to β-cell deficiency and dysfunction (Vetere et al., 2014), thus being unable to produce and secrete insulin. In fact, the presence of autoantibodies against pancreatic β-cells is a hallmark of T1D (Kharroubi and Darwish, 2015) which can be detected months or years before the onset of DM in the serum of patients (Couper and Donaghue, 2009). It only accounts for 5% to 10% of the diabetic patients (Maahs et al., 2010) that have complete dependence on exogenous insulin injections. T1D often produce symptoms such as lack of energy, excessive thirst (polydipsia), excessive excretion of urine (polyuria), involuntary urination (enuresis), constant hunger, sudden weight loss, blurred vision (International Diabetes Federation, 2017). T1D patients are also more susceptible to develop other autoimmune diseases (American Diabetes Association, 2014).

Other types of T1D (idiopathic T1D and fulminant T1D) have been described in which no antibodies against β-cells are detected in the serum of the patients (Kharroubi and Darwish, 2015).

Type 2 diabetes

T2D, formerly named non-insulin dependent diabetes, is characterized by insulin insensitivity as a result of IR and relative insulin deficiency due to partial pancreatic β-cell failure (Kahn, 1994; Robbins et al., 2010; Robertson, 1995). IR in target tissues such as liver, muscle and adipose tissues (ATs) increases the demand for insulin. The pancreatic β-cells cannot meet this demand due to their functionality defects (Halban et al., 2014). As a result of this impairment, blood glucagon levels and hepatic glucose production are increased upon fasting and not suppressed after feeding. This results in glucose homeostasis dysregulation that leads to hyperglycaemia. T2D is characterized by β-cell loss due to apoptosis (Butler et al., 2003) that is caused by multiple mechanisms collectively termed as glucotoxicity. These mechanisms include: a) enhanced generation of reactive oxygen species (ROS) as a consequence of chronically increased glucose metabolism in β-cells (Kajimoto and Kaneto, 2004), b) sustained elevation to cytotoxic levels of cellular Ca^{+2} (Donath and Halban, 2004), c) defective β-cell secretory activity including pro-Islet Amyloid Associated Peptide, which promote endoplasmic reticulum (ER) stress (Araki et al., 2003; Donath and Halban, 2004), and inflammatory Interleukin (IL)-1β (Maedler et al., 2002).

T2D compromises around 90% to 95% of DM patients, having reached 425 million in 2017. T2D symptoms are similar to the T1D, including increased thirst and urination, tiredness and slow-healing wounds apart from recurrent infections. During the first stages, T2D can be asymptomatic and its diagnosis is normally delayed for years, increasing the incidence of long-term complications.

The increased incidence of T2D has occurred in parallel with obesity as is the major cause of IR development in peripheral tissues (Reinehr, 2013; 2000). Furthermore, obesity and hyperlipidaemia can also cause β-cell apoptosis due to the abnormal accumulation of lipids in β-cells, thus impairing their functionality (Unger and Orci, 2001; Wrede et al., 2002).

Therefore, it is of paramount importance to further investigate the crosstalk among obesity, DM and IR, to better understand the mechanisms underlying these diseases. Given the direct relationship between obesity and T2D development, it is reasonable to believe that an efficient treatment for obesity will also lead to reduced T2D incidence.

2. Impaired mitochondrial function leads to metabolic disorders

2.1 Mitochondria

Definition

The mitochondrion is a cytoplasmatic organelle that is responsible for energy generation in the cell by metabolizing organic substances (carbohydrates, lipids and proteins) to produce adenosine triphosphate (ATP) via oxidative phosphorylation (OXPHOS) (Kusminski and Scherer, 2012; Osellame et al., 2012; Rogge, 2009). It is believed that mitochondria are evolutionarily derived from alphaproteobacterial that operated within cells in endosymbiosis (Wallin, 1927). Across evolution, the genes of the endosymbiont were transferred to the genome (nuclear DNA; nDNA) of the host cell. In humans, the mitochondrial DNA (mtDNA) encodes for 37 genes, including 13 key proteins of the OXPHOS system that require specific mitochondrial translation and transduction machinery. Additionally, around 1500 nDNA-encoded proteins (Pagliarini et al., 2008) are processed in the cell cytoplasm and imported to the mitochondria at the correct stoichiometry via a complex and largely enigmatic process (Ryan and Hoogenraad, 2007; Schmidt et al., 2010).

Structure

Structurally, mitochondria are double-bound-membrane organelles. Both membranes are composed of phospholipidic bilayers and proteins, that enclose the intermembrane space (IMS). The outer mitochondrial membrane (OMM) isolates the organelle from the cytoplasm, allowing the passage of metabolites through the voltage-dependent anion channel (VDAC) (Colombini et al., 1996) and the nuclear-encoded proteins through the translocase of the outer membrane (TOM) (Pfanner and Wiedemann, 2002). In addition, two regions in charge of establishing inter-organelle connections have been described: mitochondria-associated ER membrane, that

interact with ER and inter-mitochondrial junctions that interact with other mitochondria (Cogliati et al., 2016).

The IMS is the smallest sub-compartment of the mitochondria. It contains soluble proteins involved in various biological process and acts as a hub between the cytoplasm and the mitochondrial matrix (Herrmann and Riemer, 2010). Of crucial importance for the correct functionality of the mitochondria is the higher concentration of protons (H^+), lowering the pH between 0,2 to 1 units when compared with the cytoplasm or the matrix (Cortese et al., 1992; Herrmann and Riemer, 2010; Porcelli et al., 2005). The inner mitochondrial membrane (IMM) separates the matrix from the IMS and can be subdivided in the inner boundary membrane (IBM) and the cristae membrane (CM) (Figure 1).

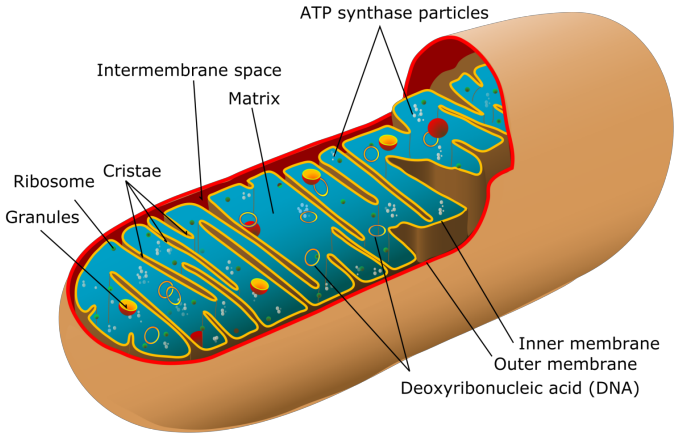

Figure 1: Schematic representation of mitochondrion structure

The IBM contains translocases (translocase of the inner membrane; TIM complexes) that import nuclear-encoded proteins to the mitochondria (Van Der Laan et al., 2016). CM are invaginations of the IMM that form bag-like structures separated from the IMS by narrow tubular junctions (Cogliati et al., 2016). Optic atrophy 1 (OPA1) and MICOS complex are the master regulators of cristae dynamics (Frezza et al., 2006; Pfanner et al., 2014).

The respiratory complexes, that constitute the electron transport chain (ETC), and the ATP synthase are embedded on the CM. This characteristic structural organization suggest that cristae are specialized compartments influencing the diffusion of key molecules, thus modulating the OXPHOS system (Cogliati et al., 2016). The matrix is the innermost compartment of the mitochondria that contains hundreds of enzymes required for substrate metabolism processes such as the fatty acid oxidation (FAO) and the Krebs cycle (also known as tricarboxylic acid cycle (TCA)) as well as the mtDNA and the necessary machinery for DNA replication.

INTRODUCTION

ATP production and ROS

The ETC complexes couple the oxidation of Nicotinamide adenine dinucleotide (NADH) or Flavin adenine dinucleotide (FADH2), that are produced during glycolysis, the TCA cycle or the β-oxidation of fatty acids. Electrons are transferred to complex I (NADH dehydrogenase) or complex II (Succinate dehydrogenase), and then translocated stepwise to coenzyme Q and consecutively to complex III (Ubiquinol-cytochrome c reductase), complex IV (Cytochrome c oxidase) that finally reduce the molecular oxygen (O_2) producing water. This transference of electrons throughout the complexes of the ETC is coupled with the transport of protons (H^+) from the matrix across the IMM into the IMS, generating an electrochemical gradient that powers the ATP synthase to finally produce ATP (Bhatti et al., 2017) (Figure 2).

The continuous electron translocation through the ETC complexes is an imperfect process in which between 0,4% to 4% of all oxygen consumed is incompletely reduced and leads to the production of ROS such as superoxide anion (O_2^-) and hydroxyl radical (OH) among others. In addition to ROS, ETC also generates reactive nitrogen species (RNS) such as nitric oxide (NO). Numerous studies show that excessive ROS and RNS production dramatically damage cellular structures. However, in recent years it has been evident that these reactive chemical species also exert crucial signalling functions, when produced in a well-regulated manner, that are fundamental for many biological processes (Di Meo et al., 2016). Indeed, they are implicated in the maintenance of homeostasis at the cellular level in healthy tissues by modulating signalling pathways acting as second messengers (Harman, 1981).

To counteract deleterious effects of oxidative damage (due to excessive production of ROS) nature has endowed the cells with adequate protective systems. First, by reducing ROS production through the dissipation of the proton gradient across de IMM via uncoupling proteins (UCPs) (Brand, 2000). This process reduces the production of ATP and generates heat as a consequence of proton leak. Second, by dampening ROS levels via antioxidants, that are defined as substances that neutralize free radicals or their actions (Ji, 1999). These are divided in enzymatic (e.g. Superoxide dismutase, Glutathione peroxidase, Catalase) and nonenzymatic (e.g. Vitamins A, C, E; carotenoids and polyphenols) antioxidative mechanisms (Dhawan, 2014). Finally, through mitophagy or apoptosis if excessive ROS levels compromise mitochondrial or cell function.

Overproduction of ROS or decreased antioxidant defences, may lead to an imbalance between pro-oxidant/antioxidant defence mechanisms thus causing oxidative stress and diverse pathologies (Dhawan, 2014). In fact, it is described that excessive generation of ROS causes

damage in the structure of the nDNA (Halliwell and Gutteridge, 2015), mitochondrial proteins, membranes and mtDNA that eventually compromise ATP generation (Dröge, 2002; Murphy, 2009) and cellular function.

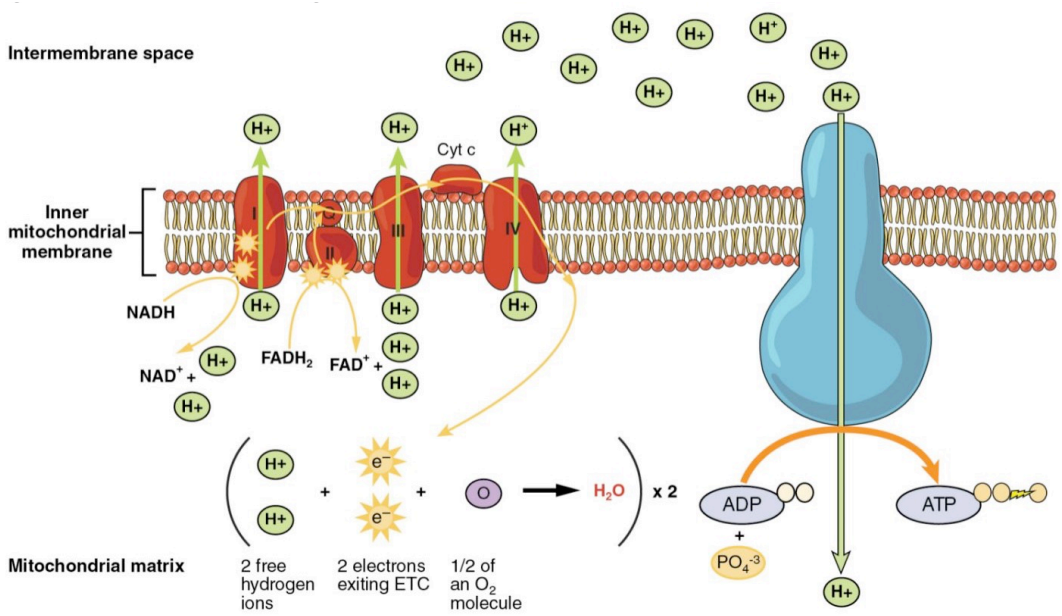

Figure 2: Schematic representation of the four complexes of the electron transport chain and the ATP synthase
As electrons flow along the ETC (red), protons (H^+) are pumped from the matrix into the intermembrane space through complexes I, III, and IV. Protons then flow back into the matrix through the ATP synthase (blue), producing ATP.

Since mitochondria is susceptible to a range of cellular and environmental stressors, that may result in mitochondrial dysfunction, specific quality control mechanisms exist to protect it against these insults. Mitochondrial quality control processes include maintenance of proteostasis via mitochondrial unfold protein response (UPR^{mt}), biogenesis, dynamics and mitophagy. For the focus of this thesis I am going to lay emphasis on mitochondrial dynamics.

2.2 Mitochondrial dynamics: a bioenergetic adaptation process

Several criteria define the dynamic nature of mitochondria. First, mitochondria are actively transported throughout the cell cytoplasm and normally positioned in high energy demanding sites. For instance, mitochondria in mammalian sperm cells are located at the proximal part of the flagellum, thus ideally located to supply ATP to the flagellar motor proteins (Fawcett, 1975; Wooley, 1970). Similarly, in muscle cells, mitochondria are situated along the myofibrils assuring a proper and uniform ATP supply to the motor proteins during muscle contraction (Ogata and Murata, 1969; Ogata and Yamasaki, 1985). In neurons, mitochondria are recruited to high energy-demand regions. Mitochondrial membrane potential studies show that mitochondria with high membrane potential migrate in the anterograde direction (from the soma to the axon

tip). On the contrary, lower membrane potential mitochondria migrate in the retrograde direction (from the axon tip to the soma) (Santel and Fuller, 2001).

Second, modifications of the internal structure of the mitochondria in response to the physiological state. Reorganization of CM shape is influenced by nutritional status, affecting the diffusion of ions, metabolites and proteins thus modulating enzymatic reactions. This reorganization is also important for cytochrome c release during apoptosis (Gilkerson et al., 2003).

Third, mitochondria also change their shape, size and number as an adaptation to the metabolic needs of the cell and in response to environmental cues (Galloway and Yoon, 2013; Westermann, 2012). Mitochondria are highly dynamic organelles that constantly undergo fusion and fission events, building large intracellular connected networks or producing small isolated fragments, respectively (Bereiter-Hahn, 1990). These constant cycles of fusion/fission allow mitochondrial content and membrane potential homogenization, thus maintaining a healthy mitochondrial population (Figure 3). Of note, mitochondrial structure and functionality are closely related to the specific cellular functions of each tissue. Therefore, mitochondrial organization and function must be considered within each cell and tissue.

Mitochondrial fission

Mitochondrial fission is driven by the constricting action of Dynamin related protein 1 (DRP1), a ubiquitous cytosolic protein with Guanosine triphosphate (GTP)ase function. It is recruited by proteins (mitochondrial fission 1 (FIS1), Mitochondrial fission factor (MFF), and mitochondrial dynamic protein of 49kDa and 51kDa (MiD49, MiD51 respectively)), that are located in the OMM fission sites. DRP1 polymerizes, generating constricting filaments around the mitochondria (Bui and Shaw, 2013) eventually splitting it into two daughter mitochondria (Figure 3).

Small fragmented mitochondria, and uncoupled respiration to ATP, is generally associated with low energetic-demanding situations such as resting cells or nutrient excess (obesity and T2D) (Collins, 2002; Liesa and Shirihai, 2013). Moreover, mitochondrial fragmentation is required for a variety of functions such as cell division, releasing of cytochrome c during apoptosis, the generation of transportable mitochondria along the cytoskeleton, and is involved in the elimination of senescent mitochondria (Detmer and Chan, 2007; Kluge, 2013; Liesa et al., 2009; Westermann, 2010). In fact, mitochondrial division frequently produce two daughter organelles with different membrane potential. Those with lower membrane potential have also reduced levels of OPA1, being less likely to re-fuse and thus, those dysfunctional mitochondrial are

removed by autophagy. This mechanism contributes to maintain a healthy mitochondrial population (Twig et al., 2008).

Mitochondrial fusion

Mitochondrial fusion is tightly regulated by a complex enzymatic machinery including Mitofusin (MFN) proteins 1 (MFN1) and 2 (MFN2) as well as OPA1, which are GTPase proteins anchored at the outer and inner membranes of the mitochondria, respectively. MFNs are homologous proteins that form homotypic (MFN1-MFN1 and MFN2-MFN2) and heterotypic (MFN1-MFN2) complexes (Chen et al., 2003a) and are in charge of merging the OMM of two adjacent mitochondria. Moreover, OPA1 controls mitochondrial IMM fusion and also cristae remodelling (Ishihara et al., 2006; Olichon et al., 2003).

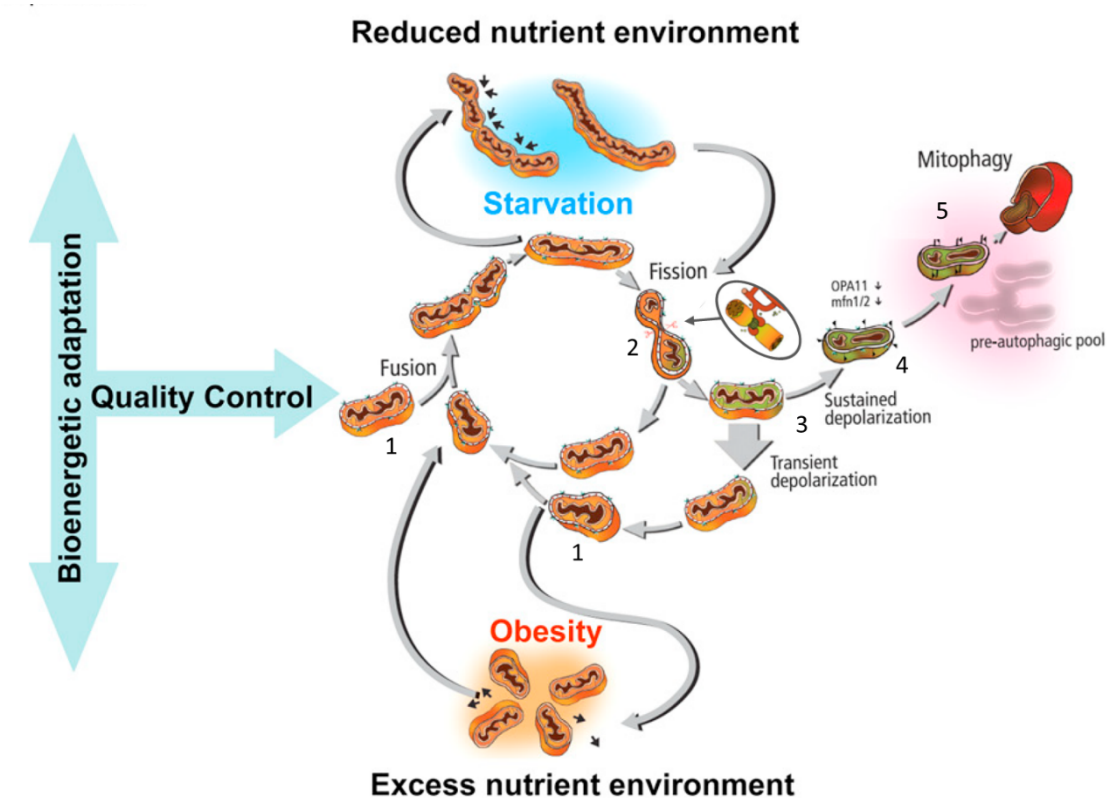

Figure 3: Mitochondrial life cycle and its adaptation to different nutritional environments
Mitochondria are highly dynamic organelles that constantly undergo fusion and fission events, building large intracellular connected networks (1) or producing small isolated fragments (2), respectively. Mitochondrial division frequently produce two daughter organelles with different membrane potential. The daughter mitochondria with higher membrane potential will return to the fusion/fission cycle (3). Those with lower membrane potential have also reduce levels of OPA1 and MFNs (4), being less likely to re-fuse and thus, those dysfunctional mitochondrial are removed by autophagy (5). In reduced nutrient environments (starvation, acute stress, and senescence) fusion is activated resulting in mitochondrial elongation (top section). In nutrient excess environments (reduced bioenergetic efficiency, increased uncoupled respiration) mitochondrial fission is activated resulting in fragmented mitochondria (bottom section). Adapted from (Liesa and Shirihai, 2013).

INTRODUCTION

Fused mitochondria are preferred when optimal mitochondrial function is needed (Westermann, 2012). It facilitates the distribution of metabolites, proteins and mtDNA while contributes to maintain electrical and biochemical connectivity (Kluge, 2013). This exchange of contents between mitochondria reduce the mitochondrial heterogeneity, allowing the IMM-ETC constituents to mix and cooperate more efficiently. Genetic material combination allows the complementation of gene products, thus preventing the accumulation of somatic mutations in the mtDNA. In this manner, mitochondrial fusion provides a pathway for defective mitochondria to regain vital components, recovering its functionality (Detmer and Chan, 2007). In general terms, interconnected mitochondrial networks are associated with high energetically-demand physiological processes, such as acute stress, starvation and G1/S phase. For this reason, metabolically active cells tend to exhibit elongated mitochondria that contribute to energy dissipation (Liesa and Shirihai, 2013; Skulachev, 2001). Conversely, mitochondrial fusion disruption results in loss of the respiratory capacity causing mitochondrial dysfunction (Chen et al., 2003a, 2005) (Figure 3).

Mitofusins

As mentioned above, Mfns are highly homologous proteins (approximately ~80% of similarity in mice (Chen et al., 2003a) and in humans (Filadi et al., 2018)). In fact, human MFN1 and MFN2 share the same relevant functional domains and both are involved in mitochondrial fusion (Zorzano et al., 2010). Mfn1 and Mfn2 proteins have GTPase activity, although Mfn2 show lower GTPase activity and reduced affinity to GTP than Mfn1 (Ishihara et al., 2004; Neuspiel et al., 2005). Despite being highly homologous it has been reported that each Mfn protein also has exclusive functions. While Mfn1 is crucial for mitochondrial interaction and fusion (Koshiba et al., 2004), Mfn2 is also present in the ER, controlling ER morphology and mitochondrial-ER interactions (de Brito and Scorrano, 2008; Ishihara et al., 2004). In fact, MFN2 is enriched at ER-mitochondrial contact regions of the OMM and has been observed an inverse correlation between MFN2 expression and mitochondrial-ER distance (de Brito and Scorrano, 2008), suggesting its importance in tethering these organelles.

Moreover, genetic deletion of *Mfn2* has been associated with ER stress (Ngoh et al., 2012; Schneeberger et al., 2013; Sebastián et al., 2012), probably as a consequence of losing mitochondrial-ER contacts (Sebastián et al., 2012). These interconnections directly affect mitochondrial lipid biosynthesis (Vance, 1990) and are crucial for the uptake of Ca^{+2} from ER (Rizzuto et al., 1998), contributing to adequate mitochondrial metabolism (Hajnóczky et al., 1995).

Importantly, it has been reported that Mfn2 also plays dynamic-independent functions (Segalés et al., 2013). In this study, muscle and liver from mice were infected with a mutant form of the human MFN2 lacking mitochondrial fusion activity. Infected mice showed enhanced mitochondrial function and stimulated glucose metabolism, without changes in mitochondrial morphology. These results suggest that Mfn2 regulates mitochondrial bioenergetics independently of mitochondrial conformation alterations (Segalés et al., 2013).

2.3 Mitochondrial dysfunction & disease: the role of mitofusins

Given the pivotal role of mitochondria in cellular bioenergetics, mitochondrial dysfunction is present in many pathophysiological processes, including metabolic disorders such as obesity and T2D (Gao et al., 2014). However, given the scope of this thesis, I will focus this section on mitochondrial dynamics and Mfns alterations.

It is well known that obesity has an impact on mitochondrial dynamics (Jheng et al., 2015; Lahera et al., 2017). For instance, reduced Mfns expression and increased expression of fission proteins was shown in the skeletal muscle of high-fat diet (HFD)-induced obese mice (Liu et al., 2014). Consistent with this, alterations in mitochondrial mass and density, accompanied by reduced *Mfn2* expression, have been reported in skeletal muscle of obese and T2D rats and patients (Bach et al., 2003; Kelley, 2002). Decreased Mfn2 expression was also observed in AT of HFD-fed mice, finding that was corroborated in AT from obese versus lean human subjects (Mancini et al., 2019).

Given these evidences, specific studies genetically manipulating Mfns have been performed. Global deletion of Mfn proteins in mice is embryonically lethal (Chen et al., 2003a), thus tissue-specific conditional strategies are required. For instance, congenital *Mfn1* and *Mfn2* deletion in mouse muscle show decreased oxygen consumption, mitochondrial dysfunction and reduced endurance exercise capacity (Bell et al., 2019; Chen et al., 2010b). However, upon ageing, only *Mfn2* deletion in muscle was sufficient to show reduced exercise performance (Sebastián et al., 2016).

Other studies show divergent phenotypes upon Mfn1 or Mfn2 ablation. For instance, *Mfn2* hepatic deletion showed increased ROS generation and glucose metabolism alterations (Sebastián et al., 2012). Conversely, Mfn1 deficient hepatocytes, displayed increased mitochondrial respiratory capacity and reduced respiratory quotient (RQ), improving glucose metabolic parameters upon HFD administration (Kulkarni et al., 2016). Another example are the studies performed in hypothalamic Proopiomelanocortin (POMC) neurons. While *Mfn2* deleted

neurons developed obesity (Schneeberger et al., 2013), Mfn1 deficient POMC neurons exhibited defective pancreatic insulin release (Ramírez et al., 2017).

Specific deletion of Mfns in AT demonstrated that *Mfn2,* but not *Mfn1,* is crucial for brown adipocyte thermogenic function, causing hypertrophy and cold intolerance. Surprisingly, upon HFD administration, Mfn2-deficient mice were protected from IR while no effect was shown upon *Mfn1* deletion (Boutant et al., 2017; Mahdaviani et al., 2017). Moreover, it has been reported reduced Mfns expression in WAT of HFD-fed mice. Consistent with this observation, mice with *Mfn2* deletion in adipocytes developed an obese phenotype characterized by increased food intake, adiposity and impaired glucose metabolism (Mancini et al., 2019).

Interestingly, most of the phenotypes observed upon *Mfn2* deletion are the consequence of increased oxidative stress and elevated ROS production, either via direct mechanisms or secondary to promotion of ER-stress (reviewed in (Zeeshan et al., 2016)).

3. The cardiovascular system and endothelial cells

The cardiovascular system is formed by the heart and interconnected closed tubular structures, known as vessels, that transport blood through a complex network composed by arteries, veins and capillaries. All vascularized tissues rely on blood vessels for the continuous nutrient and oxygen supply, waste product collection, and distribution of signalling molecules and hormones. Briefly, highly-oxygenated blood is pumped by the heart through the arteries, arterioles and capillary beds. Capillaries form extensive networks that, due to their thin walls, substances can easily pass through by diffusion, filtration or osmosis. Oxygen and nutrients move out from the bloodstream into the tissues and cells, while waste products move into the capillaries. Deoxygenated blood is returned through venules and veins to the heart. Finally, blood enters in the pulmonary circulatory system to be replenished with oxygen (Adams and Alitalo, 2007; Carmeliet, 2005).

The innermost layer of the blood vessels (tunica intima), consists of a continuous monolayer formed by tightly attached endothelial cells (ECs) that line the luminal surface of the blood vessels. During embryogenesis, vessels arise *de novo* in a process named “vasculogenesis”, in which mesoderm-derived cells (angioblasts) are appropriately differentiated into ECs and organized creating a primitive vascular plexus of capillaries (Risau and Flamme, 1995). Subsequently, ECs proliferate producing new sprouts that will progressively expand this vascular plexus forming new blood vessels from pre-existing ones in a process named “angiogenesis”. This process is mainly orchestrated by vascular endothelial growth factor (VEGF)-A, that when

secreted from non-vascularized tissues, promotes angiogenesis in ECs. Vascular expansion will generate highly branched, tree-like tubular networks that need to stabilize by forming tight EC junctions, recruiting mural cells and forming an extracellular matrix that will provide surface contact with the residing tissues. Vascular remodelling, consisting of a pruning process to eliminate redundant vessels, is mandatory to finally acquire a fully functional and optimized vasculature (Ferrara and Kerbel, 2005). Once vessels become stable and angiogenesis is not further required, VEGF-A signal decreases favouring a shift in the endothelial behaviour from active-proliferative to stable-quiescent (Potente et al., 2011). In healthy adult tissues, vessels rarely proliferate and are usually found in a quiescent state. Of note, ECs preserve a high plasticity to sense and respond to angiogenic signals (Carmeliet, 2000; Potente et al., 2011).

Vascular network structure formation and differentiation, coupled with residing tissues development, is mandatory. ECs need to reach every cell of the organism to be able to fulfil their tissue-specific tasks. Thus, ECs are not all alike. Depending on the type of vessel or organ in which they are located, ECs exhibit different molecular patterns and functional properties that cause extensive heterogeneity in the endothelium (Aird, 2007; Herron et al., 2019; Marcu et al., 2018; Nolan et al., 2013). ECs specialization arises from cell-intrinsic developmental programs as well as signalling molecules from the microenvironment (growth factors, mechanical forces, metabolic stimuli and cell-matrix and cell-cell interactions), further confirming the aforementioned exceptional ECs plasticity (extensively reviewed in (Potente and Mäkinen, 2017)). Although ECs heterogeneity is essential for their function, it hinders scientific research. There are few protein/mRNA markers that are specifically or uniformly expressed across the endothelium (Garlanda and Dejana, 1997).

One of the most relevant features of the endothelium that distinguishes it from other tissues is its ubiquitous localization. ECs are distributed throughout the organism, invading organs until achieving direct contact with almost every single cell of the organism. This distinctive feature posits them as key players in maintaining vascular and residing organs homeostasis. Moreover, the importance of ECs is highlighted not only by their large number (around one trillion/adult human), nor by their ubiquitous distribution, but also by the immense exchange surface with the plasma (4,000-7,000 m^2/adult human) (Bianconi et al., 2013; Jaffe, 1987). This extensive contact area facilitates a precise sensing of the environmental cues that thanks to the impressive plasticity of the endothelium allow accurate responses. For instance, during AT expansion ECs shift from quiescent to a proliferative state, thus conquering non-vascularized areas. Hence, ECs are at the crux of nutrient supply and demand to the extent of being considered as the metabolic gatekeepers of the organism (Graupera and Claret, 2018).

4. Metabolic disorders and vascular dysfunction

Many studies have reported that metabolic disorders, such as obesity and T2D, are accompanied by EC dysfunction and decreased vascular density (Phoebe A.Stapleton, 2008; Steinberg et al., 1996). Excessive fat accumulation is a hallmark of obesity that causes AT expandability, either by hypertrophy (increased adipocyte volume) or hyperplasia (increased adipocyte number). This process requires coordinated vascular angiogenesis to guarantee sustained AT growth.

Importantly, pathological increase in adiposity also implies the development of hypoxia, secretion of proinflammatory cytokines, certain adipokines and free fatty acids (FFA) by adipocytes. The continued release of these factors generates a low-grade inflammation status, causing oxidative stress and compromising vascular function (Galili et al., 2007; Knudson et al., 2005; Vigili de Kreutzenberg et al., 2000; Virdis et al., 2011) (Figure 4).

4.1 Hypoxia and inflammation

Studies in genetic and diet-induced obese rodents show that impaired white adipose tissue (WAT) expansion-associated angiogenesis leads to a reduction in O_2 supply, consequently inducing hypoxic genes such as hypoxia-induced factor 1- alpha (Hif1-α) (Rausch et al., 2008; Yin et al., 2009). This, rather than stimulating angiogenesis, actually accelerates AT fibrosis (Halberg et al., 2009). Independently or hypoxia-related, the inflammatory machinery of adipocytes in response to stress is activated. It has been reported that AT expansion in humans and animal models is associated with enhanced expression of inflammatory cytokines such as IL-1, IL-6 and tumour necrosis factor-alpha (TNF-α), mainly inducing pro-inflammatory M1-macrophages infiltration (Guzik et al., 2017; Weisberg et al., 2003). Not only the infiltration but also the localization of the macrophages is important. More than 90% of the macrophages infiltrated in AT in obese mice and humans are localized surrounding death adipocytes creating “crown-like structures” (Cinti et al., 2005).

4.2 Oxidative stress

In addition to inflammation, oxidative stress has emerged as a mediator of obesity-induced endothelial dysfunction (Huang et al., 2015). Inflamed AT is characterized by excessive ROS production, and it is intimately related with increased levels of oxidative stress markers in plasma of both obese mice and humans (Furukawa et al., 2004; Salgado-Somoza et al., 2010).

Obesity compromised NO production in ECs and blunted NO signalling cascade in the nearby smooth muscle cells (vSMC). Given that NO is a key promoter of vessel dilatation (Palmer et al.,

1987; Zembowicz et al., 1991), obesity promote vessel constriction (Hirase and Node, 2012; Mombouli and Vanhoutte, 1999). Besides, elevated circulating plasma levels of endothelin 1 (ET-1), a vasoconstrictor and proatherogenic endothelial factor, has been found in obese patients (Ferri et al., 2009). The resulting ET-1/NO imbalance leads to pathological vessel constriction (Virdis et al., 2015). Of note, vasodilation is known to be induced to counterbalance the aforementioned hypoxic effect upon AT expansion (Prieto et al., 2010). Hence, blocking vessel dilation in the context of obesity further contributes to endothelial dysfunction.

Oxidative stress also reduces the amount of bioavailable NO, as it rapidly reacts with superoxide anion to form peroxynitrite anion ($ONOO^-$) (Moncada and Higgs, 2006). $ONOO^-$ is a potent oxidative and toxic radical that damages DNA, proteins and lipids, produces endothelial nitric oxide synthase (eNOS) uncoupling, apoptosis, tissue injuring as well as inflammation (Touyz and Briones, 2011; Wolin, 2000). As an example, it has been reported that arterial walls from obese animals are enriched in nitrotyrosine (an $ONOO^-$ marker) (Bourgoin et al., 2008; Galili et al., 2007; Marchesi et al., 2009; Sánchez et al., 2012). Importantly, some studies show that NO reduction itself blocks the endothelial protective mechanisms of this molecule against ROS-related damage in arteries of genetic and diet-induced obese mice. (Agouni et al., 2009; Erdei et al., 2006; Erdos et al., 2004; Erdös et al., 2006; Frisbee and Stepp, 2001; Galili et al., 2007; Ketonen et al., 2010a, 2010b; Kobayasi et al., 2010; Lobato et al., 2011; Marchesi et al., 2009).

ROS production also induces nicotinamide adenine dinucleotide phosphate (NADPH) oxidase activity, further augmenting oxidative stress and impairing NO production (Kähler et al., 2001). Besides, it regulates the expression of proinflammatory cytokines contributing to inflammation (Cardillo et al., 1997; Kobayasi et al., 2010; Pierce et al., 2009) and, in combination with xanthine oxidase-derived ROS, leads to eNOS uncoupling (Landmesser et al., 2003; Zou et al., 2002b, 2002a). Of note, the augmented expression of NADPH oxidase and decreased expression of antioxidative defences has been connected with the dysregulation of adipokine production (Furukawa et al., 2004).

4.3 Adipokines

Adipokines are bioactive products secreted by AT that regulate several physiological functions such as energy balance, insulin sensitization, appetite, inflammatory response, and vascular homeostasis (Eckel et al., 2005; Kim et al., 2016). Relevant vascular dysfunction-related adipokines are here briefly described.

INTRODUCTION

Adiponectin

Unlike most adipokines, adiponectin is decreased with obesity progression and is restored upon body weight reduction (Darvall et al., 2007). It has also been associated with health beneficial effects in peripheral tissues upon ectopic lipid accumulation in muscle, by promoting FAO and glucose uptake (Fruebis et al., 2001; Yamauchi et al., 2001), and in the liver, inhibiting gluconeogenesis and lipogenesis, thus preventing hyperglycaemia and steatosis (Berg et al., 2001; Xu et al., 2003).

Interestingly, it has been reported that adiponectin has cardioprotective effects, via the stimulation of NO production by eNOS phosphorylation (Chen et al., 2003b; Cheng et al., 2007) and inhibition of FFAs-induced accumulation of ROS (Motoshima et al., 2004). Recent studies report that increased plasma levels of adiponectin are related to decreased oxidative stress markers and diminished activation of nuclear transcription factor κ-light-chain-enhancer of activated B cells (NF-kB) signalling in animals (Ouchi et al., 2000). Other studies in humans and animal models show that adiponectin promotes migration of endothelial progenitor cells (EPCs) towards the damaged areas thus promoting their recovery (Fadini et al., 2007; Shibata et al., 2008). Genetic loss of adiponectin in mice induces a state of endothelial dysfunction prompting leukocyte-endothelium interactions, causing generalized vascular inflammation accompanied by reduced NO bioavailability. *In vitro* studies also show that stimulated-endothelial ROS production is suppressed by recombinant glomerular adiponectin in a dose-dependent manner by inhibiting NADPH oxidases (Motoshima et al., 2004; Ouedraogo et al., 2007).

Leptin

Leptin secretion and levels in plasma are positively correlated with fat mass (Rönnemaa et al., 1997). Leptin mainly acts on hypothalamic neurons to modulate appetite (Hussain and Khan, 2017) but leptin-resistance, in which high leptin levels are found in plasma (hyperleptinemia), or congenitally leptin deficiency is associated with obesity in humans and rodents (Chen et al., 2006; Galili et al., 2007; Park et al., 2012). *In vitro*, acute exposure to leptin stimulates NO production through protein kinase-B (AKT)-dependent eNOS activation (Blanquicett et al., 2007; Procopio et al., 2009). Conversely, hyperleptinemia reduces L-arginine (NO precursor) and induces superoxide and peroxynitrite, producing eNOS uncoupling and compromising endothelial function (Korda et al., 2008).

Resistin

Resistin levels are increased in obesity (Kusminski et al., 2005). It is reported that resistin contributes to endothelial dysfunction by promoting the expression of proinflammatory

molecules such as TNF-α and IL-6 through Nf-kB and by inducing ET-1 release (Ouchi et al., 2011; Singer and Granger, 2007). Resistin directly inactivates eNOS through ROS overproduction and by augmenting oxidative stress by enhancing NADPH oxidase activity (Chemaly et al., 2011; Chen et al., 2010a). In conclusion, resistin also favours the aforementioned mechanisms of inflammation and oxidative stress causing endothelial dysfunction.

4.4 Lipotoxicity

Uncontrolled AT expansion in the context of obesity causes an excess in circulating lipids (hyperlipidaemia), which is a leading cause of endothelial dysfunction. Continuous exposure to high levels of circulating triglycerides (TG), FFA or low-density lipoprotein cholesterol (LDL-C) are detrimental for the vasculature and metabolic tissues functionality. This is known as lipotoxicity that is defined as the pathological changes resulting from sustained elevated lipids in the circulation or tissues (DeFronzo, 2010; Duncan, 2008; van de Weijer et al., 2011).

EC dysfunction caused by lipotoxicity is mediated through diverse mechanisms, including the aforementioned inflammation and oxidative stress. ECs from diet induced-obese animals are constantly exposed to high lipid concentrations, and it has been demonstrated that this inhibits the insulin-mediated tyrosine phosphorylation of the insulin receptor signalling-1 (IRS-1) and eNOS activation in ECs (Kim et al., 2005, 2007; Potenza et al., 2009).

4.5 Hyperglycaemia and insulin resistance

IR in vascular ECs has been intimately related to the development of metabolic disorders, such as obesity and T2D, as well as hypertension, coronary artery disease and atherosclerosis (Kim et al., 2006; Muniyappa and Sowers, 2013). In this sense, it has been demonstrated in animal models (Erdei et al., 2006; Galili et al., 2007; Naderali et al., 2001) and in clinical studies (Brook et al., 2001; Perticone et al., 2001) that obesity can be the direct cause of systemic endothelial dysfunction, through the generation of vascular IR, before being detected in muscle, liver or AT. This observation suggests that ECs are more susceptible to nutrient overload (Karpoff et al., 2009; Kim et al., 2008; Lind et al., 2011; Meyer et al., 2006) and could be explained by the differential expression of glucose transporters (GLUT) among tissues.

In normoglycemic conditions, insulin signalling regulates glucose homeostasis by promoting glucose uptake in target tissues (muscle, liver and AT) via GLUT4 translocation to the cell membrane, further activating downstream glucose metabolic pathways. However, ECs express high levels of the insulin-independent GLUT1. This transporter is not downregulated upon

hyperglycaemia, resulting in excessive glucose concentrations in the cytoplasm of ECs. This observation explains why ECs are so vulnerable to hyperglycaemia (Eelen et al., 2018). Higher glucose concentrations in ECs generates ROS, eventually causing oxidative damage and vascular dysfunction observed upon diabetic disorders.

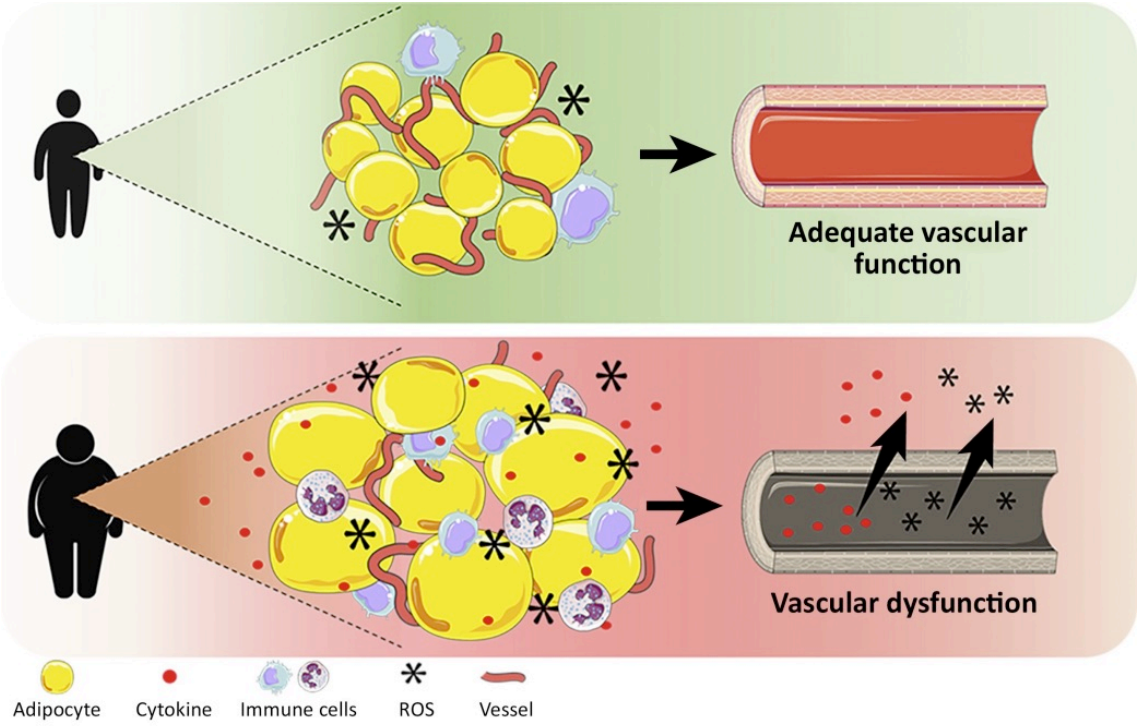

Figure 4: Obesity and metabolic disorders cause vascular dysfunction
WAT expansion is coordinated with angiogenesis. Under normal calorie intake, WAT exhibit adequate angiogenesis and inflammatory homeostasis (upper panel). However, under excess caloric intake, WAT expansion is associated with insufficient angiogenesis resulting in local hypoxia and secretion of proinflammatory cytokines, certain adipokines and FFA by adipocytes. The sustained release of these factors will generate a low-grade inflammation status, that will induce oxidative stress thus compromising vascular function (lower panel). Adapted from (Graupera and Claret, 2018).

CONCLUDING REMARKS

As shown in this section, there is controversy in defining the primary cause of vascular dysfunction under metabolic disorders situations. The current view suggests that a combination of factors as hypoxia, inflammation and lipotoxicity, creates an intricate and interrelated cocktail. This pathological microenvironment will eventually produce oxidative stress in ECs, compromising its functionality. As explained before, mitochondria are a susceptible target for oxidative stress-associated damage. Thereby, endothelial mitochondria are at the crux of oxidative stress-associated vascular dysfunction.

5. Endothelial mitochondria: at the core of vascular dysfunction

This section is focused on the particularities of the endothelial mitochondria, enlightening its contribution to the maintenance of physiological homeostasis of the organism. Given that metabolic disorders are characterized by both mitochondrial and vascular dysfunction we wonder if endothelial mitochondria could play a role in metabolic disorders-associated vasculopathies.

5.1 Endothelial mitochondria

Mitochondria are mainly recognized for their bioenergetic role, but they also integrate and participate in a variety of additional cellular processes. Interestingly, ECs rely upon anaerobic glycolysis and therefore the ATP produced by OXPHOS is considered trivial (Dagher et al., 2001; Quintero et al., 2006). It is believed that endothelial mitochondria, rather than being a cellular energy source, is a signalling platform (Darley-Usmar, 2004) allowing endothelial mitochondria to act as sensors, integrators and modulators of ECs responses to the environmental cues. In this section I describe the particular function of mitochondria in ECs.

Mitochondrial content in ECs is lower than in other cell types with higher energy requirements that rely on OXPHOS for ATP production. In rats, mitochondria occupy 2-6% of the cytoplasm volume of ECs, while in highly active tissues (such as cardiac myocytes) it increases up to 32% (Barth et al., 1992; Oldendorf et al., 1977). Variations in mitochondrial content is observed among different populations of ECs, depending on the residing organs. As an example, the highly active ECs that form the blood-brain barrier (BBB) exhibit a mitochondrial content up to 8% - 11% (Oldendorf et al., 1977). As previously mentioned, in healthy adults, most ECs remain quiescent (Eelen et al., 2018). However, under several conditions such as nutrient or oxygen deprivation, tissue damage or pathological situations such as cancer, ECs can rapidly shift to a proliferative state creating new sprouts through angiogenesis. This process is intimately associated with ECs metabolism since the endothelium must readapt their metabolism to satisfy the bioenergetics and biomass requirements of the active cells in a particular environment (De Bock et al., 2013; Potente and Carmeliet, 2017)

INTRODUCTION

Metabolic pathways

Several authors have defined ECs as “glucose addicted” (De Bock et al., 2013; Draoui et al., 2017; Polet and Feron, 2013), and this definition can be certainly used in proliferative ECs (PECs). When angiogenesis is required, proangiogenic-mediated signals, such as VEGF, upregulate glycolysis in ECs (Figure 5). This favours glucose uptake and stimulates the activity of key glycolytic enzymes, such as phosphofructokinase-2/fructose-2,6-bisphosphatase 3 (PFKB3), that is considered the main driver of glycolysis during vessel sprouting (De Bock et al., 2013). Several reasons explain why ECs rely more on anaerobic glycolysis than in glucose oxidation, despite OXPHOS yields of ATP is much higher (36 mol ATP/glucose molecule) than glycolysis (2 mol ATP/glucose molecule) (Zheng, 2012). First, non-oxygen-related energy production facilitates ECs to proliferate into hypoxic environments. Moreover, anaerobic glycolysis produces ATP in a shorter period and is restricted to the actin fibres that form lamellipodia and filopodia in ECs. As reported, glycolytic enzymes are localized in these regions during vascular sprouting (De Bock et al., 2013). Reduced OXPHOS implies less ROS production and O_2 consumption, maximizing its diffusion to the residing tissues. Finally, glycolysis provides essential glycolytic metabolites for the production of other macromolecules such as nucleotides, which are required for EC division and migration (De Bock et al., 2013; Vandekeere et al., 2015). Unlike other cell types, such as erythrocytes or

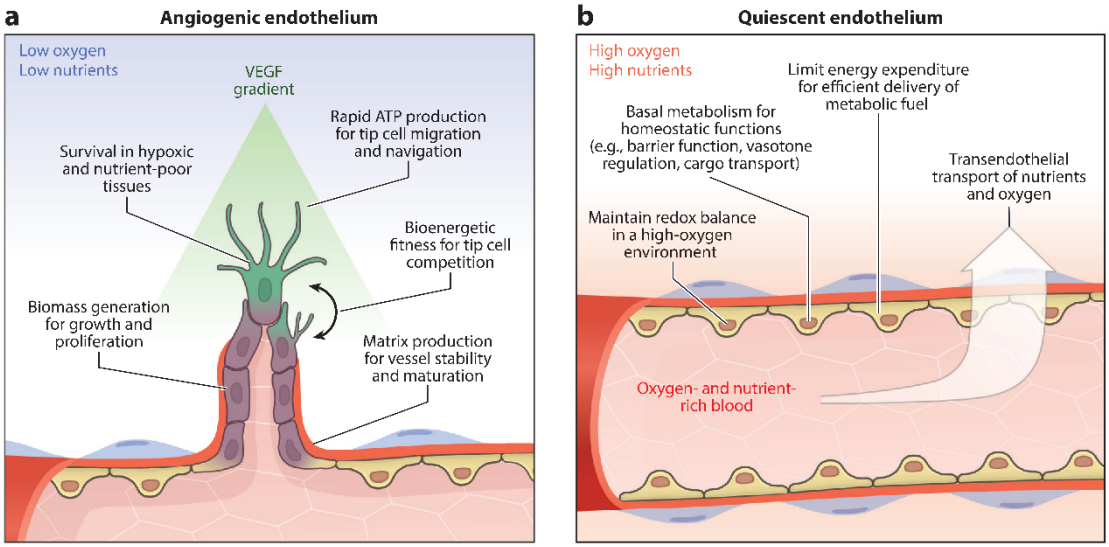

Figure 5: Metabolic requirements of proliferating and quiescent vasculature

a) Avascular tissues generate a VEGF gradient (light green) that activates the endothelium. ECs change their conformation, acquiring an invasive and motile behaviour by creating long actin-rich filopodia in a polarized manner. These are highly energy demanding processes. Furthermore, ECs need to produce biomass for the new sprout elongation, expansion and matrix production. b) Quiescent ECs rest in well-perfused vessels and facilitates the passage of O_2 and nutrients for the aerobic metabolism of the residing tissues. The basal metabolic activity of the quiescent endothelium must be controlled to prevent excessive nutrient and O_2 consumption that would make the delivery process less efficient. The high O_2 levels in the bloodstream also force ECs to maintain redox balance. Adapted from (Potente and Carmeliet, 2017).

embryonic stem cells that also rely on glycolysis for energy source (Kondoh et al., 2007), ECs conserve functional mitochondria (Blouin et al., 1977).

In contrast, ECs that are in a quiescent state (QECs) exhibit a completely different metabolic signature. In fact, a recent study found that FAO was the only significantly upregulated (3- to 4-fold) metabolic pathway in QECs when compared to PECs. Conversely, glycolysis, serine biosynthesis, TCA cycle, OXPHOS and nucleotide and fatty acid synthesis were downregulated (Kalucka et al., 2018). NADPH regeneration, necessary for redox homeostasis, has been suggested to be the primary purpose of upregulated FAO in QECs. The expression of many enzymes involved in vasculoprotection against oxidative stress are also upregulated in QECs (eNOS, prostaglandin g/h synthase PTGS1 and glutaredoxin) (Egan and FitzGerald, 2006; Heiss et al., 2015). Interestingly, several of these enzymes require NADPH as a cofactor (Davidge, 2001; Ulrich et al., 2013). Hence, QECs reprogram their metabolism, increasing FAO, to implement a vasculoprotective machinery that relies on NADPH production (Kalucka et al., 2018) (Figure 5).

Mitochondrial-mediated endothelial responses to environmental cues

a) Oxygen

Oxygen diffuses through ECs to reach perivascular tissues. ECs consume relatively low oxygen (around 15% of the EC ATP is produced via OXPHOS (De Bock et al., 2013)), thus transferring the major part of the oxygen to the residing organs (Helmlinger et al., 2000). However, under exceptional stress conditions, such as glucose deprivation or oxidative stress, EC mitochondria are able to increase respiration significantly (Mertens et al., 1990). Of note, apart from participating in oxygen diffusion, ECs have been proposed to act as an “oxygen sink” thus preventing excessive oxygen concentrations in perivascular tissues resulting in oxidative stress (Golub et al., 2011). Under hypoxic situations in which O_2 is not available, VEGF is secreted by avascularised tissues. This signalling induces mitochondrial biogenesis via AKT, resulting in increased vascular branching (Wright et al., 2008).

b) Nutrients

Dietary nutrients also affect EC function through mitochondrial mechanisms. For instance, *in vitro* ECs exposed for 24h to high glucose concentrations increase the expression of mitochondrial fission proteins. Mitochondrial dynamics alterations increase ROS production, further impairing the activation of eNOS (De Nigris et al., 2015; Shenouda et al., 2011). Moreover, sustained high glucose concentrations cause EC dysfunction through induction of mitochondrial fission as shown in venous ECs from diabetic patients (Shenouda et al., 2011). This

leads to increased ROS production, decreased mitochondrial biogenesis via downregulation of peroxisome proliferator-activated receptor γ coactivator-1-α (PGC1α) and ultimately apoptosis (Pangare and Makino, 2012; Triggle et al., 2012). Under these conditions, CM structure is altered by metalloproteinase 9 activation, resulting in altered membrane potential (Mishiro et al., 2014).

Lipids also influence the endothelium functionality. It has been reported that angiogenesis induced by VEGF is altered by cholesterol efflux from ECs, through promoting oxidative stress and mitochondrial biogenesis indirectly (Fang et al., 2013; Wright et al., 2008). Moreover, high concentrations of FFA increase ROS and proinflammatory cytokines with a negative impact on vascular function (Sawada et al., 2014; Yokoyama et al., 2014).

The effects of amino acids are less studied, but evidence show that they also affect EC function. For instance, glutamine is reported to alter EC proliferation and branching, although the underlying mechanisms remain unknown (Lohmann et al., 1999; Unterluggauer et al., 2008). Another amino acid that has been reported to modify EC function is L-arginine, that is the endothelium-NO precursor. Short-term administration of L-arginine shows that this amino acid is converted into citrulline, thus producing NO and favouring vasculoprotective effects. However, chronic long-term supplementation of arginine can be harmful to ECs (Wilson et al., 2007), by producing high levels of NO and resulting in desensitization (Abou-Mohamed et al., 2000; Bult et al., 1995; De Meyer et al., 1997; Stayner et al., 1992).

c) Hemodynamics

Vascular ECs are continuously exposed to blood hemodynamic forces named shear stress. This is a key factor that influence EC function, affecting oxidative stress and being a critical step for atherosclerosis development (Chatzizisis et al., 2007; Hsieh et al., 2014). Shear stress can increase intracellular calcium in ECs (Worthen and Nollert, 2000), that in turn enhance TCA cycle activity and ETC electron flow, resulting in increased ROS formation (Traaseth et al., 2004). Moreover, mitochondrial membrane potential is preserved upon laminar shear stress (constant flow velocity) but hyperpolarized upon pulsatile shear stress (unidirectional, but with magnitude oscillations in the flow) leading to increased ROS. In both situations, ROS can be neutralized through the inherent antioxidative defences of ECs (Scheitlin et al., 2014). Moreover, oscillatory fluid (bidirectional flow with a variation in magnitude) increases NADPH oxidase expression, enhancing superoxide production and leading to oxidative stress (Sorescu et al., 2004). This upregulates pro-atherogenic and suppresses atherogenic protective genes (Scheitlin et al., 2014).

d) ROS: one signal for all, all for one

As previously mentioned, ROS has two faces. On the one hand, controlled physiological levels of ROS are beneficial as it is a fundamental signalling molecule. On the other hand, when levels of ROS exceed the physiological threshold, oxidative stress impair ECs function. In this section, I review the specific ROS sources in ECs.

Complex I and III of the OXPHOS system are the principal producers of ROS. However, the amount of endothelial ROS *in vivo* remains uncertain (Murphy, 2009). Another ROS source is the nicotinamide adenine dinucleotide phosphatase oxidase 4 (NOX4), that is highly expressed in ECs (Chen et al., 2012). Increased NOX4 activity in ECs has been linked to increased cholesterol levels (LDL particularly) and enhanced ROS production thus leading to cell senescence (Li et al., 2016). ROS-derived NOX4 has been reported to influence endothelial relaxation, thus affecting blood pressure (Santillo et al., 2015). Besides, several reports show the implication of NOX4-mediated ROS production and signalling in cell migration and angiogenesis, hypoxia adaptive responses, oxidative stress (Amanso and Griendling, 2012) and stroke (Kleikers et al., 2014).

The growth factor adaptor protein p66Shc is another ROS source that functions in mitochondrial signalling. It generates oxygen peroxide through the oxidation of cytochrome c. High glucose or apoptotic signals have been shown to promote the translocation of p66Shc to the IMS where generates hydrogen peroxide-mediated signals (Andreyev et al., 2015; Camici et al., 2007; Giorgio et al., 2005; Paneni and Cosentino, 2012; Paneni et al., 2012; Trinei et al., 2009). Based on these observations, p66Shc seems to connect the environmental sensing and ROS-derived signals into the mitochondria.

Another ROS contributor are the monoamine oxidases (MAO), a family of enzymes localized in the OM of the mitochondria. ROS production through MAO is associated with the catabolism of catecholamines. Although MAO is expressed in ECs, its role remains poorly understood (Méresse et al., 1989). Nevertheless, MAO-derived ROS has been associated with dysfunctional EC-related situations such as cardiac remodelling and heart failure in mice (Kaludercic et al., 2010).

There also exist a process called ROS-induced ROS release, in which non-mitochondrial ROS can influence mitochondrial ROS generation (Zorov et al., 2014). This situation occurs through ROS-mediated opening of the ATP sensitive-potassium channel (mitoK_{ATP}), located in the IM. This leads to mitochondrial membrane depolarization, that is a mechanism described to protect ECs from excessive NO production (Daiber, 2010; Doughan et al., 2008). Nevertheless, it has been proposed that this mechanism is also used to amplify ROS levels, thus contributing to EC dysfunction (Zorov et al., 2014).

CONCLUDING REMARKS

All the reported ROS sources in ECs rely on mitochondrial performance. As previously described, elevated ROS production that cannot be neutralized by the inherent ROS-scavenger mechanisms produce oxidative stress leading to mitochondrial dysfunction. In this regard, mechanisms such as mitochondrial dynamics are on the crux for maintaining a healthy mitochondrial population.

Mitochondrial biogenesis, mitophagy and dynamics

Mitochondrial distribution, biogenesis and dynamics, has also been predicted to determine mitochondrial signalling in the endothelium (Park et al., 2011). ECs from rat lungs show perinuclear clustering of mitochondria, with ROS release into the nucleus, that regulate hypoxic-sensitive gene expression (Al-Mehdi et al., 2012). Moreover, in isolated human coronary arterioles (HCAs), mitochondria have been reported to be anchored to the cytoskeleton. This distribution facilitates shear stress-induced mitochondrial ROS production and subsequent dilation of (HCAs) (Liu et al., 2008).

Mitochondrial content depends on the balance between mitochondrial biogenesis and mitophagy. It is known that, similar to other tissues, PGC1α regulates mitochondrial biogenesis (Nisoli et al., 2003) and the expression of mitochondrial antioxidant enzymes (mnSOD, Catalase, Thioredoxin2), thus protecting against oxidative stress by generating new mitochondria and augmenting ROS defences (Afolayan et al., 2016; Valle et al., 2005). PGC1α seems to be also induced in PECs, since it regulates genes implicated in lipid and glucose metabolism (Leone and Kelly, 2011; Patten and Arany, 2012), it induces VEGF release (Widlansky and Gutterman, 2011) and decreases apoptosis (Li et al., 2015). Moreover, diverse models of vascular damage suggest that PGC1α exerts a protective effect against vascular dysfunction (Craige et al., 2016). Although PGC1α in ECs seems to protect ECs from oxidative stress and dysfunction, there are other studies suggesting the opposite. For instance, PGC1α is increased in ECs from diabetic rodents and humans, and specific PGC1α overexpression in ECs mimic multiple diabetic phenotypes and contributes to diverse aspects of vascular dysfunction in diabetes (Sawada et al., 2014). Collectively, these results suggest that the role of PGC1α in EC strongly depends on the context.

In a similar manner, mitophagy in ECs does not differ from other tissues, being PTEN-induced putative kinase 1 (PINK1) and Parkin the major regulators. This process allow ECs to purge defective mitochondria avoiding dysfunctional signalling and preventing apoptosis (Green et al., 2014). Mitophagy deregulation in ECs results in the accumulation of damaged mitochondria that leads to increased ROS production, inflammation and cell death. This situation has been reported in neurodegenerative disorders (Youle and Narendra, 2011), cardiovascular disease

(Craige et al., 2016) and EC dysfunction during ageing (Mai et al., 2010). Genetic knock-down of endothelial PINK1 and Parkin leads to mitophagy deregulation and subsequent mitochondrial damage and ROS accumulation, resulting in apoptosis (Wu et al., 2015). This observation suggest that the PINK-Parkin tandem may act as ECs protectors from metabolic stress derived from oxidative stress (Kluge, 2013; Wu et al., 2015).

Mitochondrial dynamics is also critical for EC function. Although little is known about mitochondrial dynamics specifically in ECs, *in vitro* studies have demonstrated that Mfns are important for endothelial functions associated with angiogenesis. Indeed, knock-down of either *Mfn1* or *Mfn2* in human umbilical endothelial cells (HUVECs) results in disrupted mitochondrial networks and reduced mitochondrial membrane potential, decreasing VEGF-mediated migration and differentiation. Interestingly, only *Mfn2* deletion resulted in decreased generation of ROS and ETC components as well as increased VEGF-stimulated Akt/eNOS signalling pathway (Lugus et al., 2011). These results indicate divergent roles for Mfn proteins in ECs. Moreover, as previously mentioned, high glucose concentration favours mitochondrial fragmentation, increases ROS production and blunts eNOS activation thereby decreasing NO bioavailability in EC *in vitro*. In this context, blocking mitochondrial fragmentation via genetic deletion of fission proteins in ECs restores eNOS activity and NO bioavailability upon high glucose concentrations (Shenouda et al., 2011).

CONCLUDING REMARKS

Mitochondria in ECs are core organelles implicated in sensing, integrating and transducing signals from the environment as well as generating a biological response in accordance. ROS has emerged as a key transducer of those signals. However, excessive ROS production in ECs mitochondria generates a toxic environment that produces oxidative stress and damages mitochondria, thus impairing EC function. These situations of excessive ROS in ECs may be the consequence of metabolic disorders-related situations, such as AT expansion and hyperglycaemia. Interestingly, *in vitro* manipulation of mitochondrial dynamics proteins results in decreased ROS production and increased eNOS activity (Lugus et al., 2011; Shenouda et al., 2011). Nevertheless, a further understanding of the mechanisms underlying EC mitochondrial dysfunction is necessary to design new therapeutic strategies to hinder the progression of metabolic disorders.

6. Endothelial cells as systemic metabolism modulators

Metabolic disorders such as obesity and T2D, are accompanied by ECs dysfunction and impaired angiogenesis (Phoebe A.Stapleton, 2008). Although these vasculopathies are currently

considered as a secondary effect of metabolic diseases, recent studies suggest that ECs could also play a primary role as systemic metabolism regulators. In this next section, I will summarize the studies in which specific manipulations of EC, have been shown to modulate systemic energy imbalance and glucose metabolic disorders.

6.1 Endothelial interference with systemic metabolism

Recent studies targeting a range of proteins in ECs have revealed novel molecular players in vascular biology implicated in, not only in the onset or the progression of metabolic diseases, but also in their protection. To date, diverse transcription factors (P53, Pgc1α, Pparγ, FoxO1, and NF-κB), proangiogenic signals (Vegf/Vegfr2; Ang2/Tie2, Dll4/Notch1), insulin cascade elements (Irs-2; insulin receptor, InsR) and fatty acid transporters (Notch1, Vegf-B/Nrp1, and Cd36), have been identified as critical modulators of the EC function and metabolism (Hagberg et al., 2010; Hasegawa et al., 2012; Hashimoto et al., 2015; Jabs et al., 2018; Konishi et al., 2017; Kubota et al., 2011; Robciuc et al., 2016; Sawada et al., 2014; Seki et al., 2018; Vicent et al., 2003; Yokoyama et al., 2014). The fact that these factors are also altered in obese and diabetic mice further supports its importance (Figure 6).

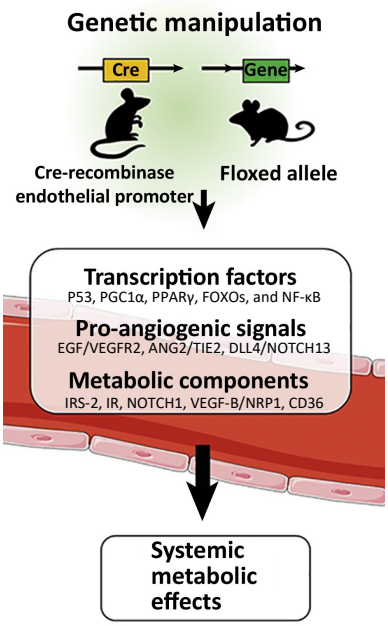

Figure 6: ECs influence systemic metabolism
Studies have shown that EC-specific deletion of certain transcription factors, pro-angiogenic signals and metabolic determinants cause systemic metabolic effects. Adapted from (Graupera and Claret, 2018).

6.2 How endothelial cells modulate systemic metabolism?

Although the mechanisms by which ECs contribute to systemic metabolism regulation are currently poorly understood, the studies previously mentioned propose diverse mechanistic insights. Based on the ECs effects, these mechanisms can be grouped in the following categories.

Modulation of NO and ROS signalling

As mentioned above, oxidative stress and NO are key elements for maintaining EC functionality. In this sense, HFD-induced obesity in mice have revealed changes in P53, Pgc1α or Irs2 expression in ECs from muscle, that have been linked to impaired NO and ROS signalling (Kubota et al., 2011; Sawada et al., 2014; Yokoyama et al., 2014). Consistent with this observation, EC-specific ablation of P53 or Pgc1α promotes NO signalling thus improving systemic metabolism (Sawada et al., 2014; Yokoyama et al., 2014). Moreover, studies targeting insulin signalling in ECs have shown that insulin itself activates NO production via Pi3k/Akt/eNOS pathway. In this sense, specific EC depletion of Irs2 or InsR causes glucose metabolism impairment (Hashimoto et al., 2015; Konishi et al., 2017; Kubota et al., 2011).

Adipose tissue vascularization

The concept that adequate AT vascularization is mandatory for healthy AT expansion (Rupnick et al., 2002) suggests that angiogenesis modulation can be a putative mechanism for treating obesity. Although this concept is controversial, it has been reported that direct inhibition of angiogenesis in AT promotes unhealthy expansion, causing inflammation and fibrosis, culminating in the progression of IR. Conversely, increased angiogenesis results in healthy AT expansion (An et al., 2017; Sung et al., 2013).

As shown in HFD-fed mice, blocking new blood vessel formation by ablating Vegf in adipocytes causes hypoxia, inflammation and apoptosis thereby causing metabolic defects (Sung et al., 2013). This observation provides proof of concept for pro-angiogenic therapies against obesity. In this line, angiogenesis induction by promoting Vegf-b/Vegfr1 signalling increases capillary density and tissue perfusion thus reducing body weight and ameliorating the metabolic complications observed in obese mice (Robciuc et al., 2016; Seki et al., 2018). Other studies have shown that angiopoietin (Ang)2 overexpression in AT promotes vascularization and systemic metabolic improvements upon HFD administration in mice (An et al., 2017). Moreover, forkhead box protein O1 (*FoxO1*) specific endothelial deletion has reveal similar results (Rudnicki et al., 2018).

Endothelial uptake of circulating lipids

Another mechanism that could allocate ECs as putative systemic metabolic modulators, is the FA transport through the endothelium. Several studies have target lipid transporters in ECs. Deletion of cluster of differentiation 36 (*Cd36*), peroxisome proliferator-activated receptor (*Ppar)-γ*) or Notch1 signalling inhibition in ECs reduces FA uptake in skeletal muscle, BAT and liver, preventing ectopic fat accumulation (Jabs et al., 2018; Kanda et al., 2009; Son et al., 2018). Similarly, blocking Vegf-b signalling in ECs diminishes the expression of FA transporters in severe obese and T2D mice, thus reducing fat deposition in muscle and pancreatic islets. In this sense, preventing lipotoxicity was shown to preserve pancreatic architecture and β-cell function, improving glucose metabolism in diabetes and obese *db/db* mice (Hagberg et al., 2010).

CONCLUDING REMARKS

The actual paradigm stating that EC dysfunction is a secondary effect of obesity and other metabolic disorders should be revised, as recent data indicates that ECs may be primary modulators of systemic energy balance and metabolism.

HYPOTHESIS & AIMS

HYPOTHESIS & AIMS

Systemic energy homeostasis is a fundamental biological process to sustain life. The vascular endothelium is strategically located, being able to adjust environmental fluctuations with physiological requirements of the underlying tissue. Mitochondria have been suggested to act as sensors, integrators and modulators of ECs responses to the constantly-changing nutritional cues. **We hypothesize that mitochondrial function and dynamics in ECs is implicated in the systemic regulation of energy balance and metabolism.**

To address this hypothesis, the following specific aims were settled up:

1. Phenotypical characterization of mice with specific deletion of mitochondrial fusion proteins (Mfn1 or Mfn2) in vascular ECs.

2. Uncover the molecular mechanisms underlying the phenotypes of mice lacking Mitofusin proteins in vascular ECs.

3. Assess the response of mice lacking endothelial Mfn1 or Mfn2 to obesogenic diets and ageing.

METHODS

1. Mice and breeding conditions

All animal work was performed in compliance with the guidelines and legislation of the Catalan Department of Agriculture, Livestock, Fisheries and Food, with procedures approved by the Animal Ethics/Research Committee of the University of Barcelona.

Breeders were kept in pathogen-free facility while after weaning sex- and age-matched mice cohorts subjected for experiments were housed in a non-pathogen free area. All of them maintained in a 12h light/dark cycle in a temperature- and humidity-controlled environment with free access to water and standard chow diet (STD) of 2,9Kcal/g (Protein 20% Kcal, fat: 13% Kcal and carbohydrates: 67% Kcal; Harlan Research Laboratories) or high fat diet (HFD) of 4,73Kcal/g (Protein 20% Kcal, fat: 45% Kcal and carbohydrates: 35% Kcal; D12451, Research Diets) for the indicated time in each experiment. When stated mice were fasted for 6h or overnight (16h).

To investigate the role of Mfn1 and Mfn2 in ECs, we have generated *Pdgfb-iCre-ER^{T2}-Mfn1$^{flox/flox}$* and *Pdgfb-iCre-ER^{T2}-Mfn2$^{flox/flox}$* by crossing *Mfn1$^{flox/flox}$* and *Mfn2$^{flox/flox}$* mice (Chen et al., 2007) with tamoxifen-inducible *Pdgfb-iCre-ER^{T2}* transgenic mice (Claxton et al., 2008). The *Cre* recombinase protein is fused to the mutant form of the human estrogen receptor (*ER^{T2}*), which is not sensitive to estrogen but is responsive to its artificial ligand, 4-Hydroxytamoxifen (4-OHT). In the absence of 4-OHT, the *CreER^{T2}* protein is kept in the cytoplasm through its sequestration by the heat shock protein 90 (Hsp90). Once present, 4-OHT allows the translocations of *CreER^{T2}* to the nucleus to mediate loxP-specific recombination events. To facilitate the nomenclature of the different mouse models used throughout the study, mouse lines will be referred as: 1) *Pdgfb-iCre-ER^{T2}-Mfn1$^{flox/flox}$* (referred as "*Mfn1$^{i\Delta EC}$*"); 2) *Pdgfb-iCre-ER^{T2}-Mfn2$^{flox/flox}$* (referred as "*Mfn2$^{i\Delta EC}$*"); 3) *Mfn1$^{flox/flox}$* (referred as "control"); and 4) *Mfn2$^{flox/flox}$* (referred as "control").

To induce *Cre* activity and generate conditional knockouts (KO) of *Mfn1* and *Mfn2* in ECs, 8-week-old control and *Mfn1$^{i\Delta EC}$*, or *Mfn2$^{i\Delta EC}$* mice received intraperitoneal (IP) injections of tamoxifen ((Sigma, T5648) 0,33mg/g body weight) during five consecutive days. After that mice were left at least for one week to recover from the IP injections (Figure 7). After tamoxifen is

Figure 7: In-vivo experimental design
Mfn1 or *Mfn2* gene was induced in 8-week-old mice by tamoxifen administration. Mice were left at least for one week to recover from the IP injections before subjected for experiments.

administered, it is oxidized in the liver by cytochrome P450 isoenzymes to 4-OHT among other metabolites, inducing *CreER^{T2}* activity (Crewe et al., 2002).

2. Mice genotyping and recombination event

For mice genotyping tail biopsies were collected before weaning. Moreover, to assess *Mfn1 or Mfn2* recombination event in the vasculature, several tissues from mice were collected two weeks after tamoxifen administration. Tissues were lysed with 600µl of 50mM NaOH (Sigma). Samples were boiled at 100ºC for 15', vortexed to facilitate the tissue digestion and cooled down. Then, 200µl of 1M Tris HCl pH7,5 (PanReac) was added to each sample. Samples were vortexed, spun down and kept at 4ºC until processed for DNA amplification. For bone, pituitary and hypothalamus samples (DNA extraction kit; gDNA Mini Tissue Kit CS11204 or gDNA Micro Tissue Kit CS11203 from Invitrogen) was used to isolated and purified DNA.

2.1 Polymerase chain reaction

Polymerase chain reactions (PCR) were performed preparing the following mix: 1µl of DNA sample, 10µl of EconoTaqMIX (Promega), 2µl of 5µM primer pool (forward + reverse) and ddH_2O water up to 20µl. Primers sequence, amplification programs and PCR products from the different PCRs performed in this project are summarized in Table 1.

PCR system 9700 (Applied biosystems) was used to perform PCRs. PCR products and a DNA ladder were then load on a 3% agarose (Sigma) gel diluted in Tris-Acetate-EDTA (TAE) buffer 1X (from a TAE 50X stock: 242g Tris base (Sigma), 57,1ml acetic acid glacial (Panreac) and 100ml EDTA 0,5M pH8 (Gibco, #15575) in ddH_2O) with Midori green dye (Nippon Genetics) (10µl/100ml agarose solution). Gel was run enough time to achieve adequate separation of the PCR product bands.

PCR	Primers sequence (5'-3')	Amplification program	PCR bands
Pdgfb Cre	FW: CCAGCCGCCGTCGCAACT RV: GCCGCCGGGATCACTCTCG FW IL-2 internal control: CTAGGCCACAGAATTGAAAGATCT RV IL-2 internal control: GTAGGTGGAAATTCTAGCATCATCC	1) Denaturation: 94ºC/4' 2) 35 cycles Denaturation: 94ºC/30" Annealing: 57,5ºC/45" Elongation: 72ºC/1' 3) Cooling: 4ºC/hold	Cre band: 500bp Internal control: 350bp
Mfn1	FW: TTGGTAATCTTTAGCGGTGCTC RV: AGCAGTTGGTTGTGTGACCA	1) Denaturation: 94ºC/30" 2) 35 cycles	WT band: 350bp

		Denaturation: 94°C/30"	Unexcised
		Annealing: 58°C/1'	conditional:
		Elongation: 72°C/1'	450bp
		3) Elongation: 72°C/1'	
		4) Cooling: 4°C/hold	
Mfn1	FW: TTGGTAATCTTTAGCGGTGCTC	1) Denaturation: 94°C/5'	Excised
deletion	RV: TTAAAGACACGGCTAATGGCAG	2) 35 cycles	band: 325bp
		Denaturation: 94°C/30"	WT band:
		Annealing: 58°C/1'	691bp
		Elongation: 72°C/1'	Unexcised
		3) Elongation: 72°C/1'	conditional:
		4) Cooling: 4°C/hold	793bp
Mfn2	FW: GAAGTAGGCAGTCTCCATCG	1) Denaturation: 94°C/5'	WT band:
	RV: AACATCGCTCAGCCTGAACC	2) 35 cycles	145bp
		Denaturation: 94°C/30"	Unexcised
		Annealing: 60°C/1'	conditional:
		Elongation: 72°C/1'	180bp
		3) Elongation: 72°C/1'	
		4) Cooling: 4°C/hold	
Mfn2	FW: GAAGTAGGCAGTCTCCATCG	1) Denaturation: 94°C/5'	Excised
deletion	RV: CCAAGAAGAGCATGTGTGC	2) 35 cycles	band: 240bp
		Denaturation: 94°C/30"	WT band:
		Annealing: 60°C/1'	710bp
		Elongation: 72°C/1'	Unexcised
		3) Elongation: 72°C/1'	conditional:
		4) Cooling: 4°C/hold	810bp

Table 1: PCR conditions, primer sequences and amplified DNA bands

3. Physiological parameters

3.1 Body weight

Mice were weekly weighted in a scale from weaning. During body weight assessment any other physiological test was performed, and mice manipulation was avoided in order not to affect the mice body weight profile.

3.2 Body composition

Quantitative magnetic resonance

Body composition in anaesthetized live mice was measured to asses absolute amount of body fat and lean tissue via quantitative magnetic resonance (QMR) instrument, EchoMRI, (Echo Medical Systems). This technique was performed for the in direct calorimetry studies in

collaboration with Ruben Nogueiras' group at the Department of Physiology (CIMUS, University of Santiago).

Nuclear magnetic resonance imaging

Body composition in anaesthetized live mice was measured to assess the differential distribution of fat among the animal models used in this study. Nuclear magnetic resonance imaging (NMRI) studies were conducted on a 7.0 T BioSpec 70/30 horizontal animal scanner (Bruker BioSpin, Ettlingen, Germany). Images were acquired by an axial Turbo RARE (Rapid Acquisition with Relaxation Enhancement) sequence without suppressing the fat signal. AT compartments were segmented semi-automatically using the image analysis software ITK-SNAP, version 3.4.0 (Yushkevich et al., 2006).

Foreground seeds are placed manually in the AT depots. An algorithm determines the boundary between the total AT and other tissues based on voxel intensity threshold. Segmentations were performed in a three-plane view and were automatically reviewed until the segmentation was satisfactory. Form the total AT volume, visceral depot was manually segmented since is well defined inside parietal peritoneum. Subcutaneous white AT (sWAT) volume was then calculated as the difference between the total and the total and the visceral white AT (vWAT).

3.3 Blood pressure and heart rate determination

Tail-cuff blood pressure (BP) and heart rate were measured for five (two for acclimation and three for measurements) consecutive days in mice cohorts of around 20- or 70-week-old mice using a computerized tail-cuff system (BP-2000 Blood Pressure Analysis System - Bioseb).

3.4 Blood collection and measurements

Plasma samples

Blood was collected via tail vein or trunk bleeds using EDTA-coated Microvettes (Starstedt) from fed or fasted animals at 10am. Microvettes were kept on ice and then centrifugated (3600 rotations per minute (rpm) for 20' at 4°C) and plasmatic supernatant was collected. Plasma was stored at -20°C.

a) Insulin plasma

Insulin plasma was measured according to the manufacturer's instructions using commercially available ELISA Kits (#90080) from Crystal Chem.

b) Free fatty acid

To assess FFA release upon fasting, plasma samples were collected before (fed state 6pm) and after fasting the animals overnight (fast state 10am). Plasma non-esterified fatty acids (NEFAs) were measured following the recommended protocol form the manufacturer (NEFA-HR (2), Fujifilm-WAKO).

Blood samples

Blood was collected via trunk in EDTAK2 coated tubes (BD Microtainer K2E Tubes, 365975). Then blood samples were kept at 4ºC for a maximum of 24h before performing a total blood hemogram analysis of the samples. Blood glucose was measured using a glucometer (Arkray) via tail tip cut.

3.5 Urine collection and measurements

Urine samples were collected at 9am over three consecutive days. Mice were gently hold allowing to urine freely on a clear plastic wrap. Then later urine was collected and kept at 4ºC for a maximum of one week.

Urine glucose was measured with a glucometer (Arkay). For renal damage analysis urine content of albumin and creatinine were measured using commercially available ELISA Kits (Crystal Chem; #80630 and #80350, respectively).

3.6 Faeces collection and measurements

Faeces were collected daily from the mice cage for four consecutive days and kept at -20ºC. Later samples were heated at 60ºC for desiccation of the sample. For that sample weight was monitored every 2h till a stable weight was achieved. For TG measurements see section 9.1.

Nitrogen content

Nitrogen content in faeces was determined by the Kjeldahl method. This technique was performed in collaboration with Xabier Remesar's group at the Department of Nitrogen-Obesity (University of Barcelona). Briefly, 1g of samples were digested in 15ml of concentrated sulfuric acid (H_2SO_4) with 7g of copper (II) sulphate ($CuSO_4$). The mixture was boiled at 400ºC and then were cooled down by adding water. Then the pH of the mixture was increased by using sodium hydroxide (45% NaOH solution). This transforms the ammonium (NH_4^+) ions (which are dissolved in the liquid) to ammonia (NH_3), which is a gas. Then ammonia is distilled into boric acid (H_3BO_3) and borate anions formed are titrated with standardized hydrochloric acid (HCl), which is

calculated the content of nitrogen representing the amount of crude protein in the sample. Most proteins contain 16% of nitrogen, thus the conversion factor is 6,25.

Gross energy

Energy content in faeces was measured using a calorimetric bomb in the Animal Nutrition Laboratory SERIDA (Villaviciosa, Spain).

3.7 Neuro-state tests

Experiments in aged mice required a previous clinical and neurological evaluation to guarantee a healthy status of the mice for performing the behavioural tests. A summary of different tests performed, and its evaluation criteria are shown in Table 2.

Test	Description	Range	System evaluated
Outreach response	Holding the animal by the tail and move it towards a plane surface.	When are the paws extended? 0 = the paws are not extended. 1 = after the contact with the surface. 2 = before the contact with the whiskers. 3 = after the contact with the whiskers. 4 = when the movement starts.	Visual/ vestibular
Visual capacity	Bring a pencil closer to the mice when holding the animal by the tail and move it towards a plane surface.	When are the paws extended? 0 = the paws are not extended. 1 = after the contact with the pencil. 2 = before the contact with the whiskers.	Visual
Twisting	Hold the mice by the tail.	0 = no twisting 1 = twisting	Vestibular
Stand up reflex	Throw the mice making a loop.	0 = land on their paws. 1 = land sidewise and turn. 2 = land on its back and turn. 3 = land on its back and is not able to turn	Vestibular
Negative geotaxis	The mouse is left in an angled grill facing the lower part.	0 = turn and go up in the grill. 1 = turn and stays in the same position. 2 = moves without turning. 3 = does not move for 30”. 4 = falls.	Vestibular/ strength

Corneal reflex	Bring a swag closer to the animal eye.	0 = no reaction. 1 = one blink. 2 = multiple blinks.	Corneal reflex
Outer ear withdrawal reflex		0 = no reaction. 1 = a tiny retraction of the outer ear. 2 = multiple retraction of the outer ear.	Touch
Flight response	Touch the back of the mice with a finger.	0 = no reaction. 1 = escape after strong touch. 2 = escape after a soft touch. 3 = escape when the hand is getting closer.	Touch/reflex
Paw withdrawal reflex	Pressing the back-paw joint with forceps.	0 = no reaction. 1 = soft retraction. 2 = moderate retraction. 3 = quick retraction. 4 = quick and repeated retraction.	Nociception
Piloerection		0 = absence. 1 = presence.	Anxiety/ excitation
Tail elevation	Tail elevation degree	0 = flaccid. 1 = horizontal. 2 = elevated.	Anxiety/ excitation

Table 2: Test performed to assess the neurological state of the animals

3.8 Physical activity

Open field

Unidentified mice were placed individually in the centre of a novel open space; an opaque plexiglass box (35x35x35cm) in a room illuminated at ≈30lux. Exploratory activity was recorded by a camera for 15', subsequently mice were identified and returned to their home cage (Figure 8). After each trial, the arena was cleaned with a disinfectant and left for 2' to eliminate aversive odours. Videos were automatically analysed by a video tracking software (Smart v3.0; Panlab). Open field (OF) test was performed in mice cohorts of around 20 or 70 weeks of age.

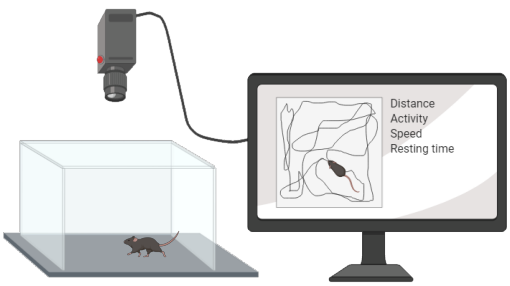

Figure 8: Schematic representation of the open field test

Rotarod

Motor coordination and balance were evaluated on an accelerating rotarod apparatus. Mice were placed on a motorized rod (30mm diameter) (Figure 9). The rotation speed gradually increased from 5 to 40 rpm over the course of 300". The time latency was recorded when the mice were unable to keep in the rod and fell. Two tests were performed daily for five consecutive days. Five tries were given to each mouse to improve its previous results, if not the highest latency was recorded. Last day tests recordings were considered for the result.

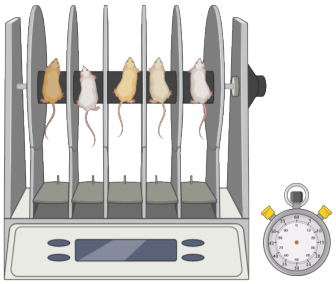

Figure 9: Representative image of mice performing the accelerating rotarod

Balance beam

Mice were placed on a wooden squared prism of 1m long, 15mm of flat surface resting 50cm from the bench. The beam was placed creating a bridge between two flat open spaces. The test consisted of two sessions separated by 4h. Animals were allowed to run for 2' along the beam that was divided into 14 segments of 5cm each (Figure 10). The latency to run 30 frames was recorded as a result.

Figure 10: Schematic representation of the balance beam test

3.9 Cognition

Novel object recognition test (NORT) was performed in the same arena used for the OF. Two days before performing the test, animals were exposed to the arena (10' session/day) to acclimatize with the environment. This session is referred as "familiarization". For the first object session, referred as "exploration", two identical items were placed in different locations within the arena. Mice were placed in the centre of the arena and were left free to explore the objects for 10'. The session was recorded and the time of exploration of each item was manually

recorded. A minimum of 10" of active exploration of the objects was required to keep on with the experiment.

Two hours later, the second object session, referred as "recognition", was performed. It took place in the same environment as the familiarization and exploration session. This time one of the previously exposed and a novel, that the animal was never been exposed to, were placed in the arena. Positioning of the objects within the arenas was consistent across trials. (Figure 11). The animal was left to freely explore both objects for 10'. This task takes advantage of the natural curiosity of mice to explore novel objects rather than familiar objects (Ennaceur and Meliani, 1992). Mice that fully encoded memory for the exposed objects, should remember the previously exposed object and spent more time exploring the novel object during the recognition session. Rodents with impaired memory will do not have the ability to recognize the previously exposed object, thus exploring equally both objects. The recognition session was filmed and the time of exploration of each item was manually recorded and used to calculate the discrimination index:

$$Discrimination\ index = \frac{time\ exploring\ novel\ object - time\ exploring\ familiar\ object}{total\ time\ exploring\ both\ objects}$$

Discrimination index values equals to 0, indicates equal exploration on both objects, equals to 1 preference for the novel, and equals to -1 preference for the familiar.

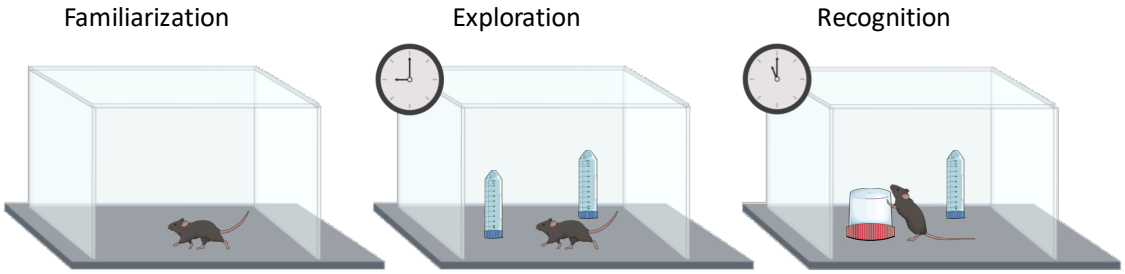

Figure 11: Schematic representation of the NORT

3.10 Neuromuscular function

Mice were left in a grill facing down 25cm from the bench. The mice have to make an effort against the gravity forces and their body weight (Figure 12). The latency to fall is recorded and data were corrected by body weight.

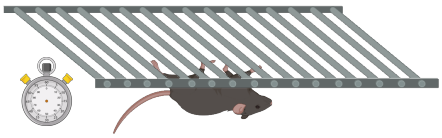

Figure 12: Schematic representation of the strength test performed

3.11 Skeletal analysis

Femur samples from around 20- and 70-week-old mice were dissected and cleaned of soft tissue. High-resolution images from the femur were acquired using a microtomographic imaging system (Skyscan 1076; SkyScan). Samples were scanned in air at 50kV and 200µA with an exposure time of 800ms, using a 1-mm aluminium filter and an isotropic voxel size of 9µm. Two-dimensional images were obtained every 0,6º for 180º rotation. Two-dimensional captions were subsequently reconstructed in order to obtain 3D images using *NRecon* reconstruction software and analysed with *CT-Analyser* (SkyScan).

For trabecular measurements, manual volume of interest (VOI) was employed, starting at 100 slices from the distal growth plate of the femur and extending to the diaphysis for 150 slices. Thus, VOI was manually drawn every 25 stacks. Cortical measurements were performed by delineating the femur medial cortex for 100 slices around the femoral midshaft. A Gaussian noise filter was applied for the reconstruction and a global binary threshold was manually established at 15 for trabecular analysis and 100 for cortical analysis.

In order to determine the bone mineral density of the samples, we scanned two different phantoms fitting with the size of the mice femurs (2-mm diameter approximately). Once two-dimensional images were obtained under the same settings as samples, the reconstruction was achieved with the same software conditions as for trabecular measurements. The phantoms used are made of hydroxyapatite and they have a known density of 0,75g/cm^3 and 0,25g/cm^3. This allowed us to compare our samples with known densities achieving a real bone mineral density value for our samples.

These studies were conducted in the laboratory of Francesc Ventura at the Department of Physiological Science at the University of Barcelona.

3.12 Lifespan

Mice were housed in the animal house facilities in *ad libitum* chow diet and water conditions. In order to minimize the disturbance of the animal, monthly body weight was monitored. From 50 weeks of age onwards, mice were checked regularly to report development of any possible age-associated pathology and to guaranteed healthy life conditions of the mice. Date of death were recorded, and post-mortem necropsy was performed to the mice to identify the cause of death.

4. Feeding, metabolic and energy expenditure assessments

4.1 Daily food intake

Mice were individually housed and acclimatized for 1 week prior to study. Food intake was measured for 5 consecutive days at different ages (specified in each experiment). A known amount of food was given to each mouse the first day and food was reweighted daily. Food consumed by the animal was calculated by difference.

4.2 Glucose tolerant test

To evaluate glucose homeostasis, glucose tolerant test (GTT) was performed in sex- and age-matched mice cohorts. Briefly, an adequate bolus of glucose was injected in mice and by assessing blood glucose clearance, differences in glucose uptake by peripheral tissues were evaluated. Glucose uptake by peripheral tissues depends on the quantity of insulin present in the blood and on the sensitivity to insulin by peripheral tissues.

Body weight of overnight fasted animals were recorded to calculate a suitable dose of glucose for each mouse. Initial glucose was measured with a glucometer (Arkay) from tail vein blood. Afterwards, mice were IP injected with a 2g/kg dose of D-glucose (Fresenius Kabi). Blood glucose levels were measured at 15, 30, 60 and 120 minutes after glucose injection via tail tip cut.

4.3 Insulin tolerance test

To evaluate IR, insulin tolerance test (ITT) was performed in sex- and age-matched cohorts of mice. Similar to GTT, in ITT blood glucose is monitored after an adequate insulin bolus was administered via IP injection. The degree of blood glucose clearance is indicative of the sensitivity to insulin by the peripheral tissues. Differences in body weight and composition compromise insulin sensitivity, for that insulin dose was optimized for each mice model and treatment.

Body weight from 5-6h food-deprived mice was recorded to calculate a suitable dose of insulin (Lilly) for each mouse. Initial glucose was measured with a glucometer (Arkay) from tail vein blood. Afterwards, insulin (0,2 to 0,4UI/Kg; specified in each experiment) was IP injected. Blood glucose levels were measured at 15, 30, 60 and 120 minutes after glucose injection via tail tip cut.

4.4 Glucose-stimulated insulin secretion

To evaluated insulin release by the pancreas, a glucose-stimulated insulin secretion test (GSIS) was performed in sex- and age-matched mice cohorts. In order to force the pancreas to release insulin stored and produce the novo insulin, a dose of 3g/kg of glucose was administered via IP to overnight fasted mice. Glucose was measured with a glucometer (Arkay) and blood samples were collected in EDTA-coated Microvettes (Starstedt) to measure plasma insulin content, from the tail vein. Those measures were performed in the basal state and 2 (stored insulin release), 5 and 20 (*de novo* insulin release) minutes after glucose injection.

4.5 Homeostatic model assessment of insulin resistance index

Overnight fasting blood samples were obtained for serum insulin determinations and plasma glucose was measured using the glucometer in order to calculate the homeostatic model assessment of IR index (HOMA-IR) using the following formula:

HOMA IR = [Fasting insulin (mg/dL) x Fasting glucose (mU/L)] / 405 (Yokoyama et al., 2003)

4.6 Indirect calorimetry

Indirect calorimetry studies were performed using a TSE LAbMaster Metabolic cage system (TSE Systems), in collaboration with Ruben Nogueiras' group at the Department of Physiology (CIMUS, University of Santiago). Individually housed mice were acclimatized for 24h into the test chambers and monitored for 48 additional hours. The system determines the volumes of O_2 consumed and the CO_2 produced. This data was used for the calculation of the RQ and to indirectly determine energy expenditure (EE). In the abbreviated Weir equation kcal per day are calculated as follows: [3.94(VO2) + 1.11 (VCO2)]1.44 (Weir, 1949). Food intake and locomotor activity (LA) (measured by beam breaks) were measured in parallel.

RQ is calculated as the ratio between CO_2 volume eliminated and O_2 volume consumed, obtained by indirect calorimetry studies. This value typically ranges between 0,7, indicating that fat is being metabolized and 1,0 for carbohydrates utilization.

4.7 Thermal imaging

Skin temperature surrounding the interscapular brown adipose tissue (iBAT) area was measured using a high-resolution infrared camera (FLIR systems). Four pictures were taken from each mouse and the average temperature was calculated.

5. Immunofluorescence

5.1 Frozen tissue

Freshly isolated tissue (liver and muscle) was snap-frozen, embedded in optimal cutting temperature (OCT) compound and stored at -80°C. Immunofluorescence was performed on 5µm sections that were cut at the cryostat and placed on Poly-L-Lysine treated microscope slide. First, samples were washed 3 times in phosphate-buffered saline (PBS) for 10'. To avoid unspecific signal, samples were incubated with blocking solution (PBS 5% donkey serum) for 1h at RT. After that primary antibody, cluster of differentiation 31 (CD31) (ab28364) was added 1:50 in blocking solution and samples were kept overnight at 4°C in a humid chamber. The next day samples were washed 3 times in PBS for 10' and incubated with secondary antibody conjugated with Alexa dye 549 (A21207, Invitrogen) 1:1000 in blocking solution, for 1h, at room temperature (RT) in a dark humid chamber. Then samples were washed 3 times in PBS for 10’ and mounted with mounting media (S3023, DAKO). Images were taken in a fluorescent microscope Olymous Bx-41-TR using a 40X objective. CD31 immunostaining was used to determine vessel density using Image J.

5.2 Whole mount adipose tissue

Fresh isolated ATs were fixed overnight at 4ºC in 4% paraformaldehyde (PFA). Then tissues were washed with gently rocking 3 times for 10’ and stored at 4ºC in PBS with 0,005% NaAz. Immunofluorescence was performed on small ATs pieces that were incubated in blocking solution (PBS 5% donkey serum) for 2h at RT. Primary antibody TOM20 (Santa Cruz, sc-11415) was incubated overnight at RT with 300rpm shaking. The following day samples were washed over day in permeabilization solution (PBS 0,3% Triton 100X). Secondary antibody conjugated with Alexa dye 488 1:250 and isolectin GS-IB4-568 (IB4) (Molecular probes I21412) 1:300 in permeabilization solution was incubated overnight at 4ºC 300rpm shaking. Next day samples were washed with permeabilization solution, gently rocking 3 times for 10’ and stored at 4ºC in PBS with 0,005% NaAz covered from light.

For IB4 quantification, confocal images were taken using a 20X objective. All images in maximal z-stack projections, were processed and analysed using Image J. Vessel density was calculated by measuring IB4 positive area within affixed square template (200µm^2). For TOM20 analysis, confocal images were taken using a 63X zoomX4. All images were processed with Image J and quantified using a specific macro generated for this quantification.

6. Vessel permeability assay

Vessel permeability was assessed in 13-week-old mice cohorts. Briefly, mice were anaesthetized with isoflurane and injected with 200µl of 0,5% evans blue (EB) solution in PBS via tail vein. After that mice were placed back into their cage for 30'. After that, tissues were weighted and incubated in 500µl formamide for 24h at 55°C. then, samples were centrifuged and absorbance at 612nm was measure. Extravasated EB tissue content (mg) was calculated and normalized per mg of tissue (Radu and Chernoff, 2013).

7. Gene expression analysis

7.1 RNA extraction and quantification

To analyse gene expression frozen tissues were pulverized under liquid nitrogen and 50mg portions were transferred to RNAse free tubes. For RNA extraction TRIzol reagent (Invitrogen) protocol was used. Briefly, samples were homogenized in 1ml TRIzol reagent using a high-speed tissue homogenizer (Ika Ultra Turrax T8.10). ATs samples were centrifuged for 15' at 12000g at 4°C, then clear supernatant was placed in a new tube (this additional centrifugation was only performed in ATs samples to remove excessive fat). Next, 200µl chloroform/ml TRIzol reagent was added and samples were shaken vigorously for 30". After 3' of incubation at RT, samples were centrifuged as before. Then the upper-aqueous phase was transferred to a new tube and 500µl chloroform/ml TRIzol reagent of 2-propanol (Sigma) was added. Subsequently, samples were left at -20°C and centrifuged for 10' at 12000g at 4°C. Then 1 volume of 70% EtOH was added and samples were vortexed followed by a 10' centrifugation at 12000g at 4°C. Then RNA pellets were left to dry for 5-10' by air-drying and were resuspended in a suitable amount of RNAse free water. Finally, RNA samples were left for 10' at 55°C to facilitate dissolution and were subjected for quantification in the Nanodrop (Thermo Scientific).

7.2 cDNA synthesis

cDNA was synthetized from 1µg of RNA using the High Capacity cDNA Reverse Transcription Kit (Applied Biosystems) following the recommended protocol form the manufacturer. Briefly, 10µl of the reaction mix (Table 3) was added to 10µl of diluted RNA sample in RNAse free water. Tubes were placed in a thermal cycler, and retrostrasncription was archived following the program: 10' at 25°C, 2h at 37°C, 5' at 85°C, hold at 4°C.

Reagents	Volume for 20 µl reaction
10x RT buffer	2 µl
25x dNTPs mix	0,8 µl
10x Random primers	2 µl
RNAse inhibitor	1 µl
RT enzyme	1 µl
Nuclease free water	3,2 µl
Total volume	10 µl

Table 3: RT reaction mix

7.3 Quantitative reverse transcription PCR

Quantitative reverse transcription PCR (qRT-PCR) was performed using Premix Ex Taq™ (Takara) and run in an ABI Prism 7900HT sequence detection system. For the reactions, 5µl of cDNA samples (diluted in 1/10 in nuclease-free water) were mixed 5µl of the Taqman Gene Expression assay FAM/TAMRA primers (Applied Biosystems) (diluted 1/11 in Universal PCR Mastermix with ROX dye (Takara)). The archived following the program: 10' at 25°C, 2h at 37°C, 5' at 85°C, hold at 4°C. qRT-PCR program includes Segment 1: 1 cycle of 30" at 95°C and Segment 2: 40 cycles of 5" at 95°C and 1' at 65°C. Results were expressed in cycle threshold (Ct) values.

Name	Reference	Company
β-actin	Mm00607939_s1	Applied Biosystems
Cdh5	Mm00486938_m1	Applied Biosystems
Cidea	Mm00432554_m1	Applied Biosystems
Dio2	Mm00515664_m1	Applied Biosystems
Elovl3	Mm00468164_m1	Applied Biosystems
Hprt	Mm00446968_m1	Applied Biosystems
Kdr	Mm00440099_m1	Applied Biosystems
Mfn1	Mm00612599_m1	Applied Biosystems
Mfn2	Mm00500120_m1	Applied Biosystems
Opa1	Mm00453879_m1	Applied Biosystems
PGC1α	Mm01208835_m1	Applied Biosystems
Prdm16	Mm00712556_m1	Applied Biosystems
Tbp	Mm00446971_m1	Applied Biosystems
Tmem26	Mm01173641_m1	Applied Biosystems
Tnfrsf9/Cd137	Mm00441899_m1	Applied Biosystems
Ucp1	Mm00494069_m1	Applied Biosystems

Table 4: Probes used for gene expression analysis

Samples were always run and referred to the housekeeping Ct values and to a standard curve performed with a pool of the cDNA samples of the experiment (1/10 dilution, 6 points). For internal controls Hypoxanthine ribosyl transferase (*Hprt*), actin (*β-act*) and TATA-box protein (*Tbp*) were used. Probes used for gene expression analysis are shown in Table 4.

8. Protein analysis

8.1 Protein extraction and quantification

To analyse gene expression frozen tissues were pulverized under liquid nitrogen and 50mg portions were transferred to centrifuge tubes. For protein extraction samples were homogenized in 400-500µl of lysis buffer (Radioimmunoprecipitation assay buffer (RIPA buffer (Sigma)) with 1X protease (Sigma) and 1X phosphatase inhibitors (PhosphoSTOP; Roche) using a high-speed tissue homogenizer (Ika Ultra Turrax T8.10). Tissue lysates were kept on ice for 15' and then centrifuged at 12000g for 15' at 4ºC. Supernatants were collected and subjected for quantification using the BCA protein assay kit (Pierce), following the instructions of the manufacturer. WATs were diluted 1:5, while the rest of tissues 1:10 in lysis buffer. Then protein samples were diluted in sample buffer 4X (For a final volume of 50ml: 200mM Tris 1M pH6,8 (12,5ml), 8% SDS (4g), (0,02%) bromophenol-blue (10mg), 40% Glycerol (20ml), 20% β-mercaptoethanol (6ml), ddH_2O up to 50ml, adjust pH=6,8) in a proportion 3volumes of protein: 1volume of sample buffer. Samples were heated for 5' at 95ºC, spun down and stored at -20ºC.

8.2 Electrophoresis and immunoblotting

Protein samples were resolved on commercial 4-12% sodium dodecyl sulphate polyacrylamide gels (SDS-PAGE) (Biorad) and separated by molecular weight using electrophoresis. Samples were run for 2h at 150V in 1X running buffer (XT MES, Biorad) and then transferred onto polyvinylidene difluoride (PVDF) membranes (Biorad). Protein transference was performed at 4ºC for 2h at 400mA in 1X transfer buffer (25mM Tris, 192mM glycine and 20% methanol). Then nonspecific protein binding sites were blocked in 5% bovine serum albumin (BSA) in containing in 1X TBS (For 500mL of TBS 10x: 6g Tris, 43,85 g NaCl, pH7,5) containing 0,01% Tween (referred as TBS-T) for 1h at RT. Next membranes were incubated with primary antibodies (Table 5) (prepared in solution: 5% BSA, 0,05% NaAz in TBS-T) overnight at 4ºC, except actin and tubulin that were incubated for 1h at RT. Then membranes were washed 3 times for 10' each in TBS-T incubated for 1h at RT with the appropriate horseradish peroxidase-conjugated secondary antibody (Table 5). Subsequently, membranes were washed 3 times for 10' each in TBS-T and

developed by using SuperSignal™ West Femto Maximum Sensitivity substrate (Thermo Scientific). Chemiluminescence was detected by ImageQuant LAS4000. Band quantification intensities by densitometry was carried out using ImageJ software. Band intensity of the target proteins were normalized by the intensity of loading controls.

Antibody	MW (kDa)	Host	Dilution	Company	Catalogue
UCP 1	32	Rabbit	1:1000	Abcam	ab10983
β-actin	42	Rabbit	1:1000	Sigma	A-2066
Total HSL	81,83	Rabbit	1:1000	Cell Signaling	4107
HSL-p660	81,83	Rabbit	1:1000	Cell Signaling	4126
HSL-p563	81,83	Rabbit	1:1000	Cell Signaling	4139
Tubulin	50	Mouse	1:1000	Sigma	T-6064
Anti-Rabbit HRP	-	Donkey	1:5000	GE Healthcare UK Limited	NA934
Anti-Mouse HRP	-	Sheep	1:5000	GE Healthcare UK Limited	NA931

Table 5: Primary and secondary antibodies used for immunoblotting

9. Biochemical measurements

9.1 Liver and faeces triglycerides

Frozen liver and faeces samples were pulverized under liquid nitrogen, and 100mg portions were digested in 3M KOH (65% ethanol) during 1h at 70ºC followed by overnight incubation at RT. Once all TG were extracted, samples were diluted to a final concentration of 100mg tissue in 500µL Tris–HCl 50mM and measured according to TG-LQ Kit's instructions (Spinreact).

9.2 Nitric Oxide and Hydrogen Peroxide measurements

NO and Hydrogen Peroxide ex-vivo amperometric measurements were performed in the laboratory of Claude Knauf at the Digestive Health Research Institute (Toulouse, France). Briefly, after dissection, tissues were washed in Krebs-Ringer bicarbonate/glucose buffer (pH 7,4) in an atmosphere of 95% O_2–5% CO_2 and then immersed in tubes containing the same medium. Spontaneous NO or H_2O_2 release was measured at 37ºC for 10' by using either a NO-specific (ISO-NOPF, World Precision Instruments) or an H_2O_2-specific (ISO-HPO, World Precision Instruments) amperometric probe implanted. The concentration of NO or H_2O_2 gas in solution was measured in real-time (TBR1025, World Precision Instruments). DataTrax2 software (World Precision Instruments) performed data acquisition. Data are expressed as delta variation of NO or H_2O_2 release from basal (Laurens et al., 2019).

RESULTS CHAPTER I:

Endothelial Mfn1 function assessment

1. *Mfn1*$^{i\Delta EC}$ mouse model validation

1.1 *Mfn1* gene recombination

Two weeks after tamoxifen injection, *Mfn1* recombination event was assessed by PCR. Specific primers were designed in order to amplify the DNA region of interest. As a result, an excision band of 325bp was amplified when proper gene recombination was achieved (Figure 13). *Mfn1* recombination was observed in all tissues tested, except in retina and pituitary. The unexcised band of 793bp was amplified and used as a reaction control of the PCR.

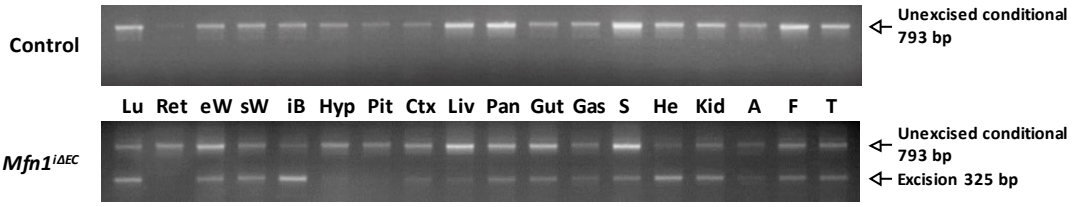

Figure 13: *Mfn1* is recombined in ECs after tamoxifen administration
Assessment of *Mfn1* recombination event by conventional PCR in the indicated tissues (Lu: Lung; Ret: Retina; eW: epididymal fat; sW: posterior subcutaneous fat; iB: interscapular brown adipose tissue; Hyp: Hypothalamus; Pit: Pituitary; Ctx: Cortex; Liv: Liver; Pan: Pancreas; Gut; Gas: Gastrocnemius; S: Spleen; He: Heart; Kid: Kidney; A: Aorta; F: Femur; T: Tail). All studies were conducted in samples from control and *Mfn1*$^{i\Delta EC}$ mice between 10-13 weeks of age.

1.2 *Mfn1*$^{i\Delta EC}$ mice do not show vascular network alterations

To assess the impact of endothelial *Mfn1* deletion in adult mice on the vascular network, we assessed the expression of vascular markers *Kdr* (Vascular endothelial growth receptor 2) and *Cdh5* (Vascular endothelial cadherin) in key metabolic tissues such as liver, muscle, epididymal WAT (eWAT), sWAT and iBAT (Figure 14 a and b). No differences were found in the expression

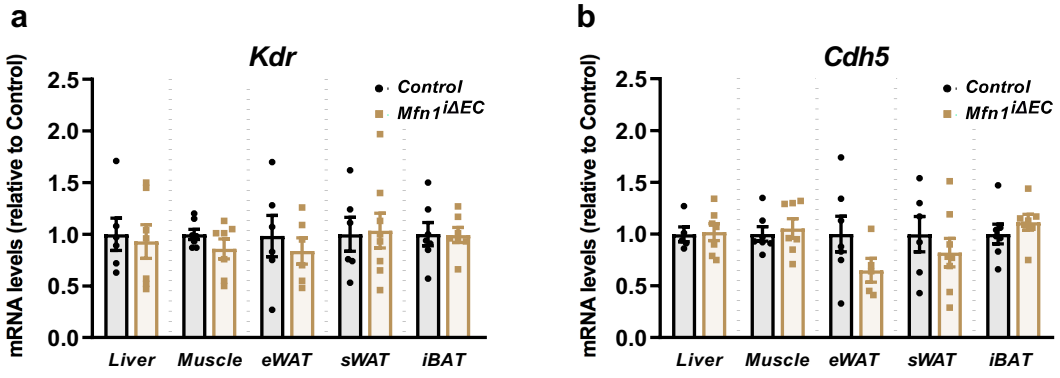

Figure 14: Equivalent ECs marker expression in control and mutant mice
a) *Kdr and* b) *Cdh5* (vascular markers) mRNA expression was assessed by qPCR in liver, muscle, eWAT, sWAT and iBAT (n=6-8/genotype). *β-actin* was used as housekeeping gene. All studies were conducted in samples from control and *Mfn1*$^{i\Delta EC}$ mice at 35 weeks of age. Statistical analysis was performed by unpaired Student's t-test. Data are expressed as mean ± SEM.

of these vascular markers in none of the analysed tissues. These results suggest that endothelial *Mfn1* deletion does not cause any significant alteration affecting the ECs population.

2. Phenotypical characterization of *Mfn1*$^{i\Delta EC}$ mice

2.1 *Mfn1*$^{i\Delta EC}$ mice do not exhibit systemic metabolism alterations under standard diet conditions

Daily tamoxifen injections were performed at 8 weeks of age, for five consecutive days, to both control and *Mfn1*$^{i\Delta EC}$ mice. Subsequently, body weight was weekly monitored. Body weight curves of both groups were overlapping (Figure 15 a). To assess if Mfn1 in ECs was modulating systemic glucose metabolism, GTT and ITT were performed. 16-week-old mutant mice showed unaltered insulin sensitivity (Figure 15 b) and no differences in glucose tolerance (Figure 15 c) when compared to their control counterparts. These results indicate that endothelial Mfn1 loss does not alter systemic metabolism of mice under STD conditions.

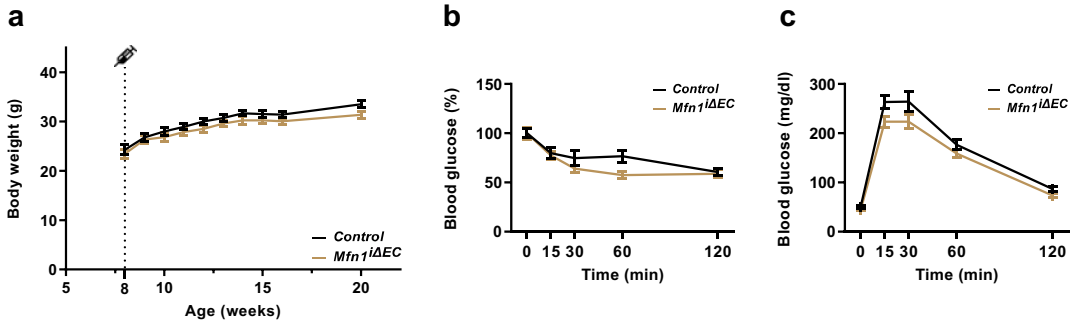

Figure 15: Endothelial Mfn1 ablation does not modify body weight or systemic glucose homeostasis
a) Body weight profile on STD (n=13-15/genotype). b) ITT (0,2UI/Kg) (n=9-11/genotype). c) GTT (n=10-16/genotype). All studies were conducted in control and *Mfn1*$^{i\Delta EC}$ mice at 16 weeks of age. Statistical analysis was performed by two-way ANOVA test. Data are expressed as mean ± SEM.

2.2 Diet-induced obesity in *Mfn1*$^{i\Delta EC}$ mice does not modify systemic glucose metabolism

Given that no changes in systemic metabolism were observed upon *Mfn1* deletion in ECs when fed with a STD, we wondered if endothelial Mfn1 loss could play a role in the development of obesity. To this end, we administered a fat-rich diet (HFD; 45% Kcal derived from lipids) starting at 11 weeks of age for 24 consecutive weeks. As expected, HFD feeding caused overweight in both control and *Mfn1*$^{i\Delta EC}$ groups but to a similar extent (Figure 16 a). Glucose homeostasis was assessed by ITT and GTT after HFD administration. No significant differences in insulin sensitivity

or glucose tolerance was observed in *Mfn1*$^{i\Delta EC}$ mice when compared to their control counterparts (Figure 16 b and c).

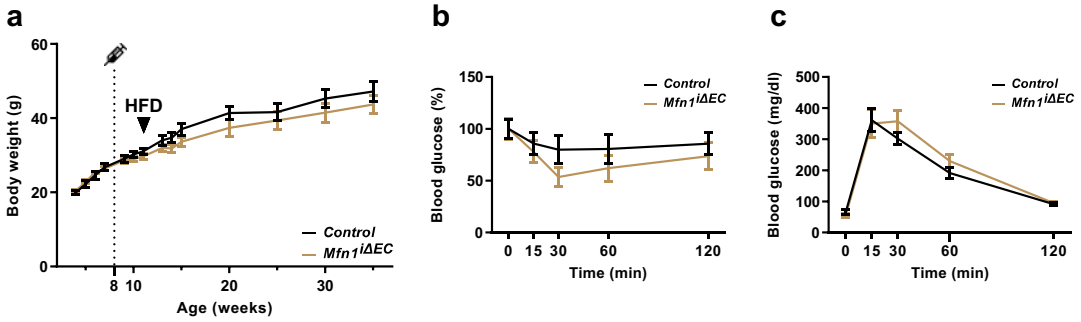

Figure 16: Unaltered body weight and glucose metabolism in *Mfn1*$^{i\Delta EC}$ mice upon HFD administration
a) Body weight profile on HFD (n=6-8/genotype). b) ITT (0,4UI/Kg) (n=6-7/genotype). c) GTT (n=6-7/genotype). All studies were conducted in control and *Mfn1*$^{i\Delta EC}$ mice at 35 weeks of age. Statistical analysis was performed by two-way ANOVA test. Data are expressed as mean ± SEM.

Given that no systemic metabolic alterations were observed upon *Mfn1* deletion in ECs, we next decided to evaluate if endothelial Mfn2 is implicated the systemic regulation of energy balance and metabolism.

RESULTS CHAPTER II:

Decoding the function of Mfn2 in ECs

1. *Mfn2*$^{i\Delta EC}$ mouse model validation

1.1 *Mfn2* gene recombination and deletion

Two weeks after tamoxifen injection, *Mfn2* recombination event was assessed by PCR. Specific primers were designed in order to amplify the DNA region of interest. As a result, an excision band of 240bp was amplified when proper gene recombination was achieved (Figure 17 a). An internal control (*IL-2* gene) was amplified as a reaction control of the PCR. *Mfn2* recombination was observed in all tissues tested, except in retina and pituitary. To further verify that *Mfn2* was deleted in vessels *in vivo*, total lung qPCR analysis from 16-week-old mice was performed. Of note, ECs make up around 20% of the total adult mouse lung cells (Singer et al., 2016). We observed a decrease in *Mfn2* mRNA, but not in other mitochondrial fusion proteins such as *Opa1* or *Mfn1* (Figure 17 b).

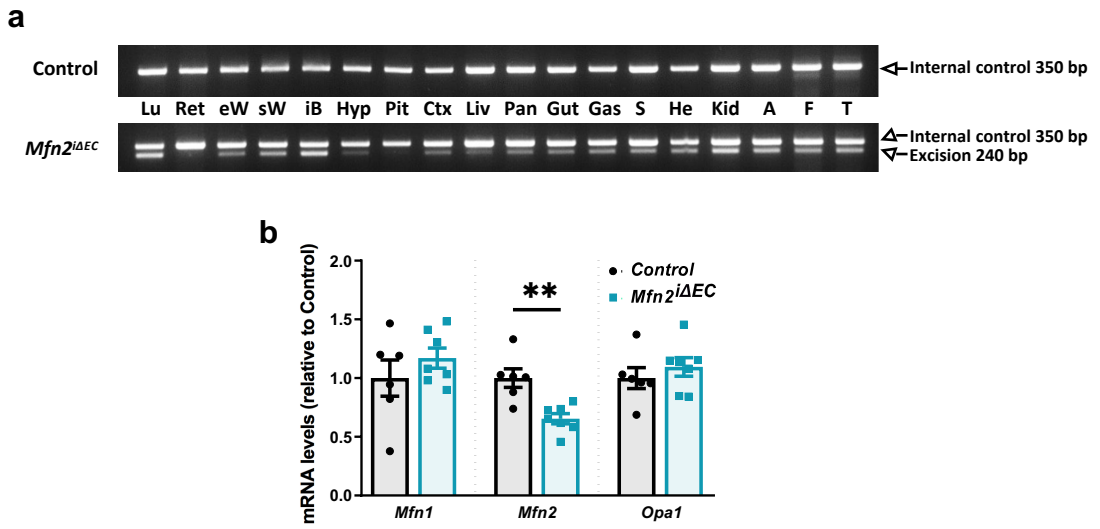

Figure 17: *Mfn2* gene is recombined in ECs after tamoxifen administration
a) Assessment of *Mfn2* deletion event by conventional PCR in the indicated tissues (Lu: Lung; Ret: Retina; eW: epididymal fat; sW: posterior subcutaneous fat; iB: interscapular brown adipose tissue; Hyp: Hypothalamus; Pit: Pituitary; Ctx: Cortex; Liv: Liver; Pan: Pancreas; Gut; Gas: Gastrocnemius; S: Spleen; He: Heart; Kid: Kidney; A: Aorta; F: Femur; T: Tail). b) Expression analysis of mitochondrial fusion genes in the lung (n=6-7/genotype). *ß-actin* was used to adjust for total RNA content. All studies were conducted in samples from control and *Mfn2*$^{i\Delta EC}$ mice between 10-16 weeks of age. Statistical analysis was performed by unpaired Student's t-test. Data are expressed as mean ± SEM. **P<0.01.

1.2 No histopathological alterations upon Mfn2 loss in ECs

Abnormal blood vessel structure and function compromise health. Given the ubiquitous nature of ECs, we analysed whether endothelial *Mfn2* deletion secondarily affected residing organs. A complete histopathological analysis was performed by the Veterinarian Faculty of the

Autonomous University of Barcelona. Mice were sacrificed at 16 weeks of age and tissues were subjected to Haematoxylin and Eosin (H&E) staining. Microscopically observation of the samples revealed no relevant anatomicopathological alterations in terms of vessel and organ structure (Table 6).

Organ	Control #1	Control #2	*Mfn2*$^{i\Delta EC}$ #1	*Mfn2*$^{i\Delta EC}$ #2	*Mfn2*$^{i\Delta EC}$ #3
Stomach	√	√	√	√	√
Duodenum	√	√	√	√	√
Jejunum	√	√	√	√	√
Ilion	√	√	√	√	√
Colon	√	√	√	√	√
Pancreas	√	√	√	√	√
Liver	*	√	√	√	√
Gallbladder	√	√	√	√	√
Kidney	√	√	√	√	√
Adrenal gland	√	√	√	√	√
Spleen	√	√	√	√	√
Mesenteric lymphatic node	√	√	√	√	√
Peyer's patches	√	√	√	√	√
Lumbar lymphatic node	√	√	√	√	√
Thymus	√	√	√	√	√
Mandibular lymphatic node	√	√	√	√	√
Salivary glands	√	√	√	√	√
Lungs	√	√	√	√	√
Trachea	√	√	√	ND	√
Thyroid	ND	√	√	√	√
Oesophagus	√	√	√	√	√
Cava vein / Aorta	√	ND	ND	ND	√
Heart / Mediastinum	√	√	√	ND	√
Breastbone / Bone narrow	√	√	√	√	√
Soleus muscle	√	√	√	√	√
Skin	√	√	√	√	√
Testicle	√	√	√	√	√
Encephalon	√	√	√	√	√
White adipose tissue	√	√	√	√	√
Brown adipose tissue	√	√	√	**	√

Table 6: No histopathological alterations upon Mfn2 loss in ECs

Evaluation of the specified tissues of control and *Mfn2*$^{i\Delta EC}$ mice at 16 weeks of age (n=2-3/genotype). (√) No pathological evidences. (*) Two small inflammatory clusters (<100µm) in the parenchyma, without pathological relevance. (**) Few microgranulomas without pathological relevance. ND: not determined (technical problems, little sample).

1.3 *Mfn2*$^{i\Delta EC}$ mice do not show alterations in the vascular network

To evaluate the impact of endothelial *Mfn2* deletion in adult mice on the vascular network, the expression of vascular markers (*Kdr* and *Cdh5)* was assessed in key metabolic tissues such as liver, muscle, eWAT, sWAT and iBAT. No differences were found in these vascular markers in none of the tissues analysed (Figure 18 a and b). Besides, CD31 immunofluorescence staining was performed in liver and muscle. For whole mount immunofluorescence performed in the different adipose depots, IB4 a membrane marker of endothelial vasculature was used. Analysis of CD31 or IB4 showed no differences in the vascular positive area of *Mfn2*$^{i\Delta EC}$ compared to

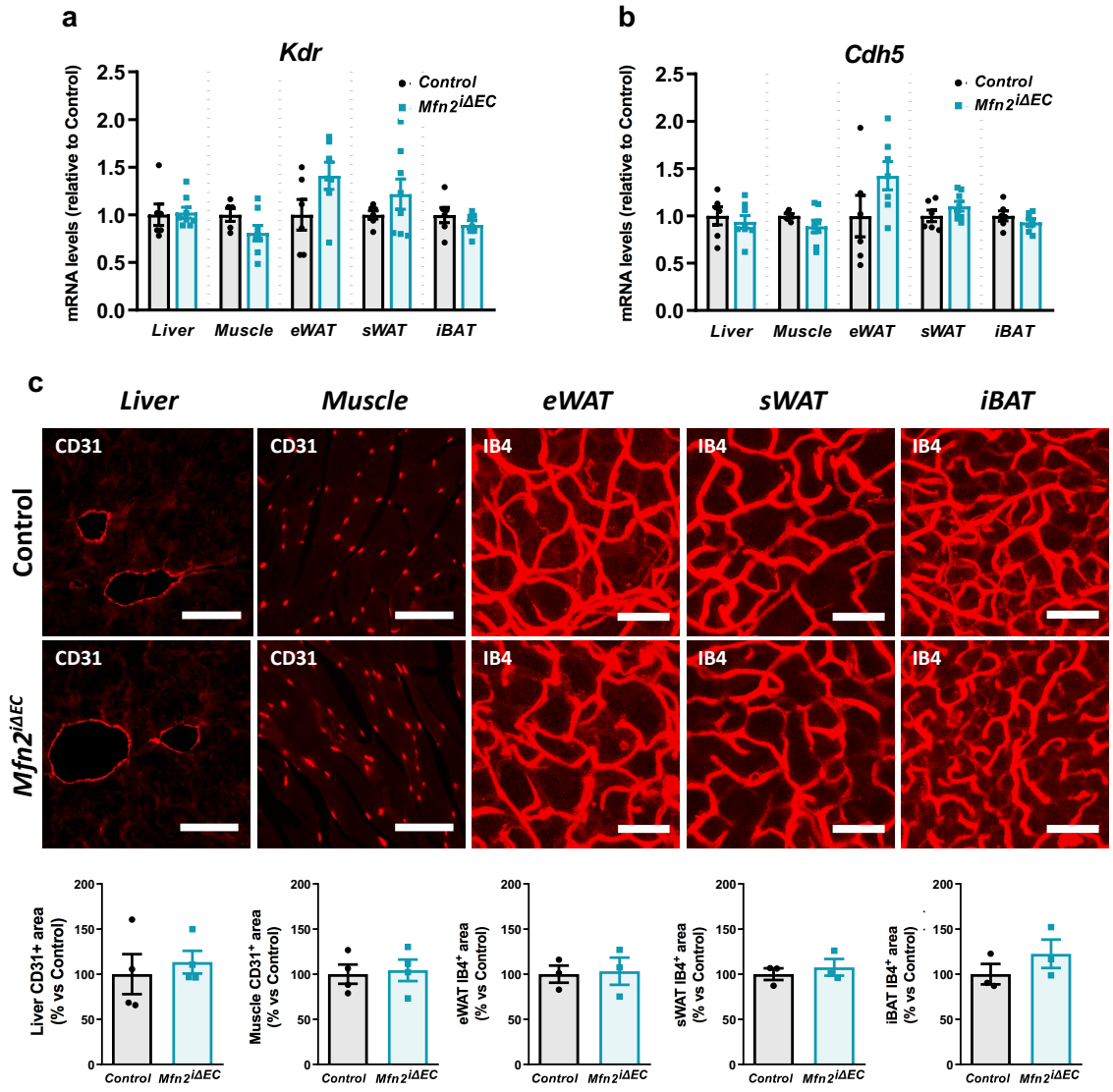

Figure 18: Equivalent vascular area and ECs marker expression in control and mutant mice
a) *Kdr and* b) *Cdh5* (vascular markers) mRNA expression was assessed by qPCR in liver, muscle, eWAT, sWAT and iBAT (n=5-8/genotype). *ϐ-actin* was used as housekeeping gene. c) Representative images of IB4 or CD31 immunofluorescence and its quantification in the specified tissues (n=3-4/genotype). Scale bar 50µm. All studies were conducted in samples from control and *Mfn2*$^{i\Delta EC}$ mice between 16-20 weeks of age. Statistical analysis was performed by unpaired Student's t-test. Data are expressed as mean ± SEM.

control mice in all of the analysed tissues (Figure 18 c). Collectively, these results indicate that endothelial *Mfn2* deletion does not alter vascular density.

1.4 Blood vessels are functional in *Mfn2*$^{i\Delta EC}$ mice

The wall of the blood vessels is lined up by tightly attached ECs forming a selective barrier that regulate the transport of substances into and out of the bloodstream. Next, we assessed if *Mfn2* deletion in ECs was affecting the function of this monolayer by measuring BP and vessel permeability. Tail BP was measured in 10-week-old mice. No differences were observed neither in diastolic/systolic pressure nor in heart rate between control and *Mfn2*$^{i\Delta EC}$ mice (Figure 19 a and b).

Besides, the fluorescent dye EB was injected in 13-week-old mice. Given that EB has a high affinity for serum albumin, this technique has been widely used to assess vessel permeability (Radu and Chernoff, 2013). No differences were observed in EB content extracted from several tissues of *Mfn2*$^{i\Delta EC}$ mice when compared to their control counterparts (Figure 19 c). Importantly, given that equivalent vascular area was measured in control and *Mfn2*$^{i\Delta EC}$ mice the results obtained reflect the leakage of EB into the residing organs.

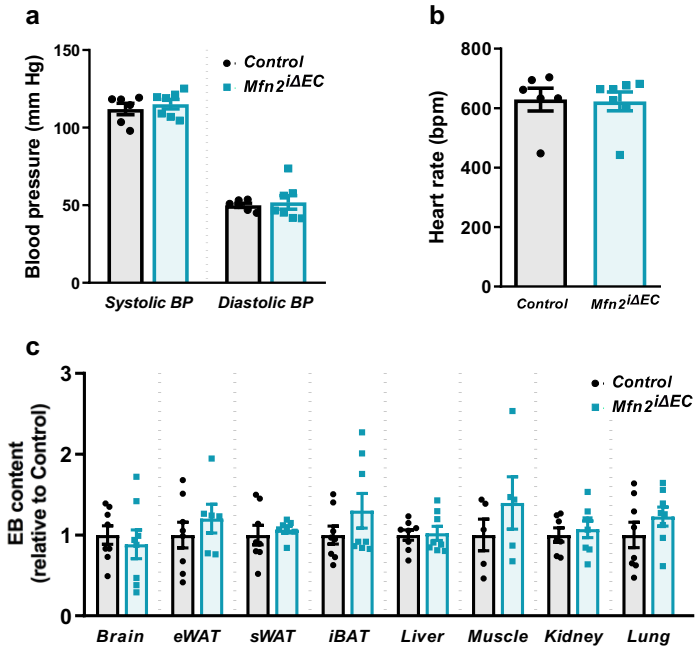

Figure 19: Mfn2 loss in ECs does not alter vascular function and permeability
a) Systolic and diastolic BP (n=6-7/genotype). b) Heart rate (n=6-7/genotype). c) EB content on the specified tissues (n=5-8/genotype). Relative EB content normalized to control. All studies were conducted in control and *Mfn2*$^{i\Delta EC}$ mice between 10-13 weeks of age. Statistical analysis was performed by unpaired Student's t-test. Data are expressed as mean ± SEM.

2. Metabolic phenotypical characterization of *Mfn2*$^{i\Delta EC}$ mice

2.1 *Mfn2*$^{i\Delta EC}$ mice show body weight reduction

Body weight from control and *Mfn2*$^{i\Delta EC}$ mice littermates was weekly monitored since weaning onwards. Tamoxifen injections were performed at 8 weeks of age, for five consecutive days, when body weights were equivalent between experimental groups. However, three weeks after tamoxifen-induced recombination (around 11 weeks of age) *Mfn2*$^{i\Delta EC}$ mice exhibited a progressive reduction of body weight reaching ~20% loss at 30 weeks of age (Figure 20).

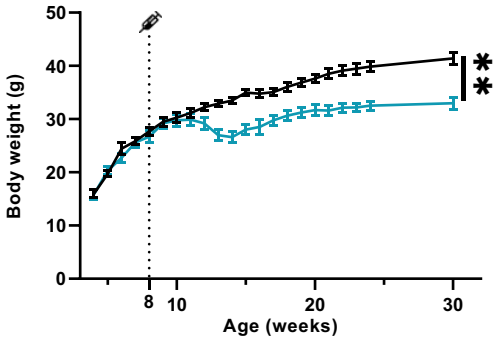

Figure 20: *Mfn2* ablation in ECs resulted in reduced body weight.
Body weight profile of control and *Mfn2*$^{i\Delta EC}$ mice fed with STD (n=7-8/genotype). Statistical analysis was performed by two-way ANOVA test. Data are expressed as mean ± SEM. **P<0.01.

Body composition analysis showed an equivalent percentage of lean mass (Figure 21 a) but a significant reduction in total fat mass (Figure 21 b). To further assess the fat mass loss, representative AT depots were collected and weighted. Consistently, posterior sWAT and eWAT showed a significant reduction. No changes were observed in iBAT mass (Figure 21 c). Together, these results indicate that body weight loss in *Mfn2*$^{i\Delta EC}$ mice is the consequence of reduced adiposity.

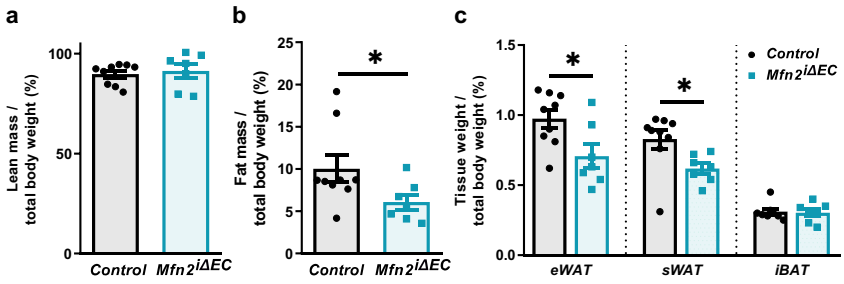

Figure 21: Reduced adiposity in *Mfn2*$^{i\Delta EC}$ mice
a) Total lean mass. b) Total fat mass. c) Discrete AT depots weight corrected by body weight. All studies were conducted in control and *Mfn2*$^{i\Delta EC}$ mice between 13-15 weeks of age (n=7-9/genotype). Statistical analysis was performed by unpaired Student's t-test. Data are expressed as mean ± SEM. *P<0.05.

2.2 Improved glucose metabolism as a consequence of body weight reduction

Glucose tolerance and insulin sensitivity were assessed in body weight-matched mice at 10 weeks of age. No differences were observed in either of the tests (Figure 22 a and b). However, at 16 weeks of age, when body weight differences were apparent, *Mfn2*$^{i\Delta EC}$ mice showed increased insulin sensitivity and improved glucose tolerance (Figure 22 c and d). GSIS test was equivalent in control and mutant mice, indicating unaltered insulin release in response to glucose (Figure 22 e). These results suggest that the improvements shown in glucose homeostasis are the consequence of reduced adiposity.

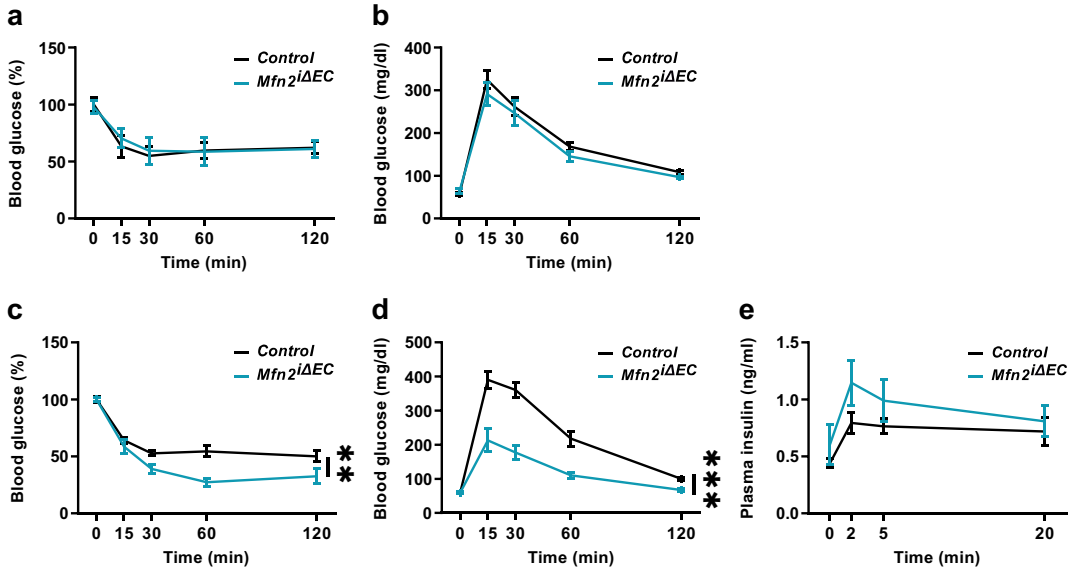

Figure 22: Glucose homeostasis in vivo in control and *Mfn2*$^{i\Delta EC}$ littermates
a) ITT (0,2UI/Kg) and b) GTT performed in body weight-matched mice at 10 weeks of age. c) ITT (0,2UI/Kg), d) GTT and e) GSIS test performed in significantly different body weight mice at 16 weeks of age (n=5-9/genotype). Statistical analysis was performed by two-way ANOVA test. Data are expressed as mean ± SEM. **P<0.01; ***P<0.001.

2.3 *Mfn2*$^{i\Delta EC}$ female mice show reduced body weight

Next, we wondered whether this lean phenotype also occurs in females. Body weight from control and *Mfn2*$^{i\Delta EC}$ female mice littermates were weekly monitored since weaning onwards. Tamoxifen injections were performed at 8 weeks of age, as described previously. A significant reduction in body weight was observed in the *Mfn2*$^{i\Delta EC}$ group, four weeks after tamoxifen administration (Figure 23 a). Afterwards, *Mfn2*$^{i\Delta EC}$ female mice were able to maintain a lighter body weight during the time recorded. Consistently, decreased adiposity was observed in the

Mfn2$^{i\Delta EC}$ group (Figure 23 b). Given the similarity between male and female phenotypes, we undertook subsequent studies only in male mice.

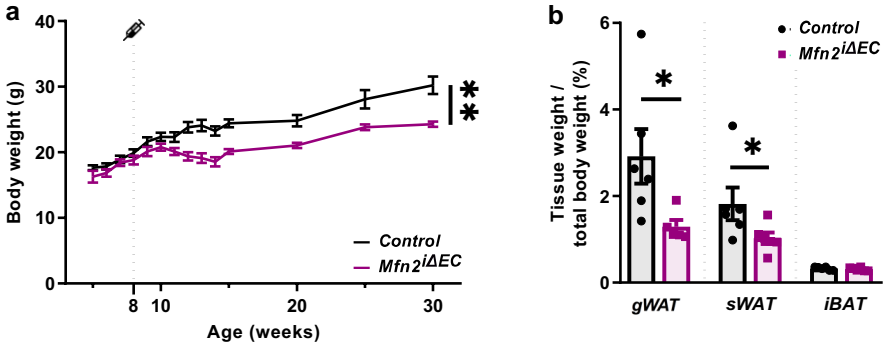

Figure 23: *Mfn2*$^{i\Delta EC}$ female mice show reduced body weight and adiposity
a) Body weight profile (n=6-7/genotype). b) Discrete AT depots (gonadal WAT; gWAT) weight corrected by body weight in control and *Mfn2*$^{i\Delta EC}$ female mice at 75 weeks of age (n=5-6/genotype). Statistical analysis was performed by two-way ANOVA test (a) and unpaired Student's t-test (b). Data are expressed as mean ± SEM. *P<0.05; **P<0.01.

2.4 *Mfn2*$^{i\Delta EC}$ mice do not show altered food intake patterns or gut malabsorption

Given the obvious reduction of body weight in mutant mice, we next assessed if food intake patterns or nutrient absorption by the gut were altered. Food intake during body weight loss

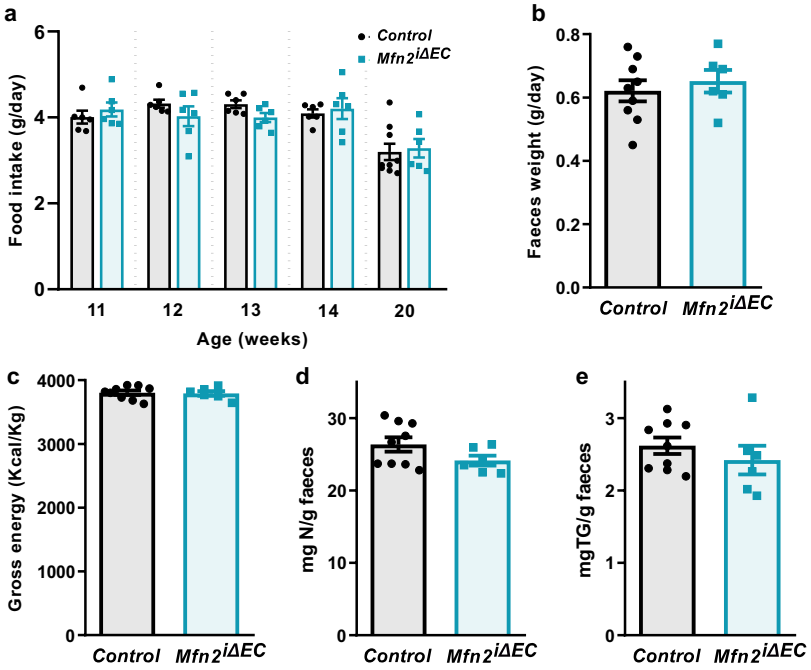

Figure 24: Food intake and nutrient absorption analysis in control and *Mfn2*$^{i\Delta EC}$ mice
a) Food intake per mouse during the body weight reduction phase (11 to 14 weeks of age) and at 20 weeks of age from control and *Mfn2*$^{i\Delta EC}$ mice (n=6-9/genotype). b) Faeces weight c) total gross energy, d) nitrogen and e) TG content per mouse, measured in faeces from control and *Mfn2*$^{i\Delta EC}$ mice (n=6-9/genotype) collected over four consecutive days at 20 weeks of age. Statistical analysis was performed by unpaired Student's t-test. Data are expressed as mean ± SEM.

(11-14 weeks of age) and stabilization (20 weeks of age), revealed no differences between groups (Figure 24 a). Besides, no differences were observed in faeces weight, faeces residual caloric content (measured by bomb calorimetry) and faeces nitrogen/triglyceride content between control and *Mfn2*$^{i\Delta EC}$ littermates at 20 weeks of age (Figure 24 b-e). These results indicate that reduced body weight is not the consequence of diminished food intake or inadequate nutrient absorption by the intestine in *Mfn2*$^{i\Delta EC}$ mice.

2.5 Increased energy expenditure causes body weight reduction in *Mfn2*$^{i\Delta EC}$ mice

To further investigate why *Mfn2*$^{i\Delta EC}$ mice are leaner, we subjected them to calorimetry chambers. Indirect calorimetry studies showed enhanced EE in mutant mice during the light phase (Figure 25 a). EE is the sum of three components: basal metabolic rate (BMR), thermogenesis and physical activity (Speakman, 2013). To exclude components from this equation, LA (Figure 25 b) was simultaneously recorded. No changes were observed in this parameter.

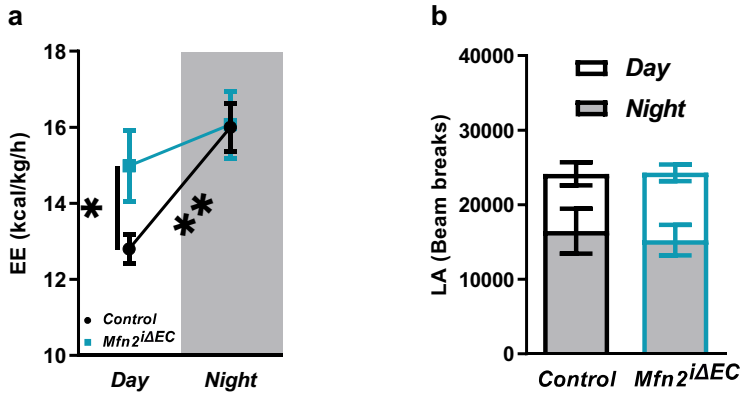

Figure 25: *Mfn2*$^{i\Delta EC}$ mice show increased EE in the absence of changes in locomotor activity
a) EE corrected by lean mass. b) Locomotor activity (LA) measured by beam breaks. All studies were conducted in control and *Mfn2*$^{i\Delta EC}$ mice at 13 weeks of age (n=7-9/genotype). Statistical analysis was performed by one-way ANOVA test; corrected by two-stage step-up method of Benjamini, Krieger and Yekutieli. Data are expressed as mean ± SEM. *P<0.05; **P<0.01.

We next assessed the thermogenic capacity of control and *Mfn2*$^{i\Delta EC}$ mice. First, we indirectly measured potential thermogenesis changes by the analysis of expression of several well-known markers of thermogenesis in iBAT including UCP1 protein levels. No significant changes were observed in the expression of these thermogenic markers (Figure 26 a and b). To measure thermogenesis in a more direct manner, we used infrared thermography. This strategy revealed no differences in iBAT temperature between control and *Mfn2*$^{i\Delta EC}$ mice (Figure 26 c). Given that

browning of WAT may contribute to whole-body EE, we next evaluated the expression of thermogenic genes and markers of brown adipocyte precursors in sWAT. No differences in the expression of these molecular markers were observed (Figure 26 d and e). Collectively, these data indicate that Mfn2 depletion does neither result in enhanced BAT activity nor WAT browning suggesting an augmented BMR in *Mfn2*$^{i\Delta EC}$ mice as the likely cause of increased EE.

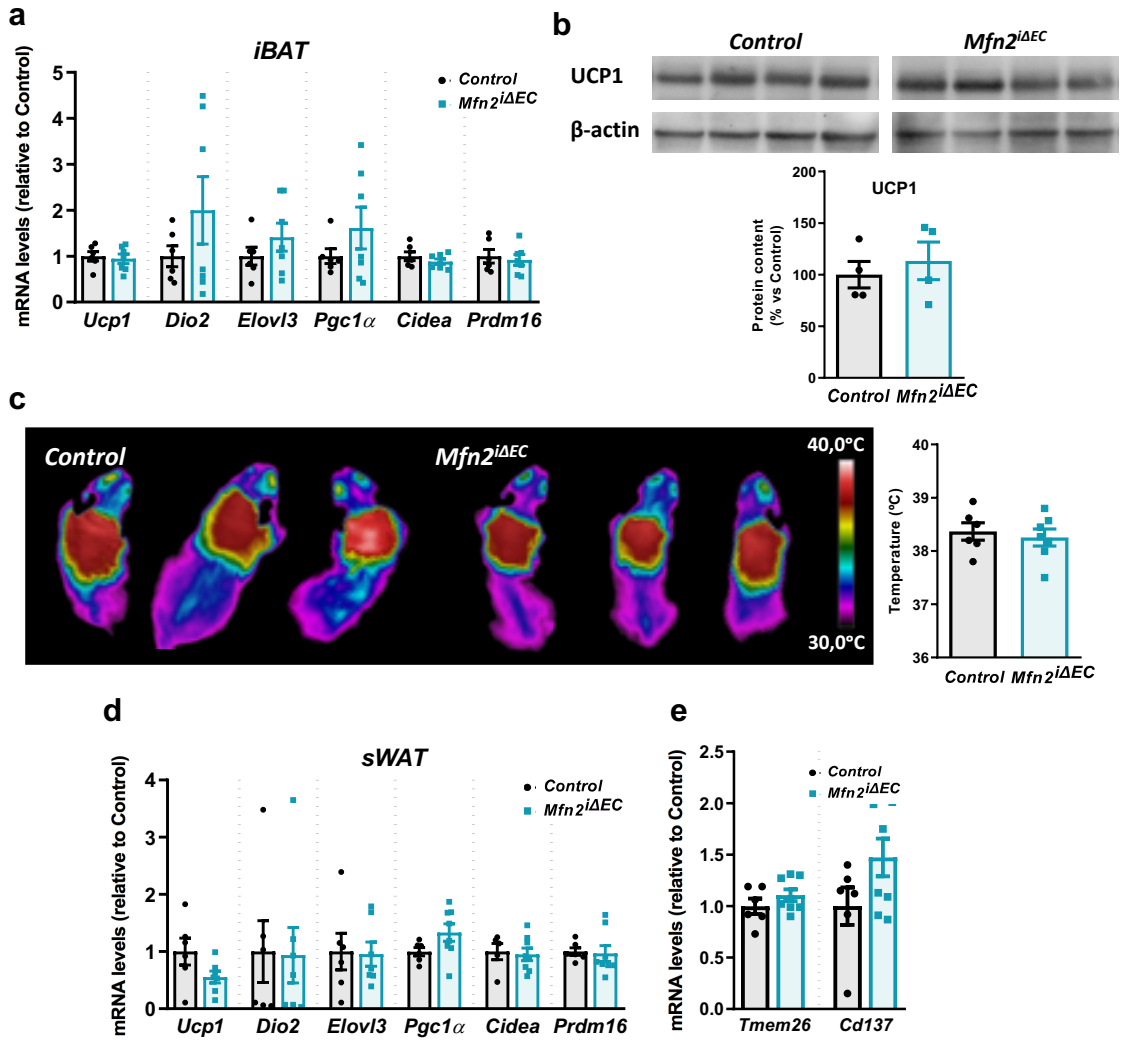

Figure 26: *Mfn2*$^{i\Delta EC}$ mice do not exhibit enhanced thermogenesis

a) Gene expression of the thermogenic markers assessed by qPCR in iBAT (n=6-7/genotype). *Tbp* was used to adjust for total RNA content. mRNA levels were normalized to control. b) Immunoblot analysis and quantification of Ucp1 expression in iBAT (n=4/genotype). β-Actin was used to adjust for total protein content. Protein content is expressed relative to controls. c) Representative thermic images of the interscapular area and quantification (n=6-7/genotype). d) Thermogenic and e) beige adipocyte marker expression analysis in sWAT (n=6-7/genotype). *Tbp* was used to adjust for total RNA content. mRNA levels were normalized to controls. All studies were conducted in control and *Mfn2*$^{i\Delta EC}$ mice at 15 weeks of age. Statistical analysis was performed by unpaired Student's t-test. Data are expressed as mean ± SEM.

2.6 *Mfn2*$^{i\Delta EC}$ mice show increased lipolytic capacity

Next, we wondered if reduced adiposity in *Mfn2*$^{i\Delta EC}$ mice could be explained, at least in part, by uneven metabolic substrate utilization by tissues. RQ showed a normal fluctuation between the light and dark phase in control mice, characterized by predominant lipid oxidation during the resting (light) phase and increased carbohydrate utilization in the active (dark) phase. Notably, this switch is significantly attenuated in the *Mfn2*$^{i\Delta EC}$ group, displaying a tendency to preferentially oxidise lipids during both phases. Quantitative analysis of the RQ values showed a significant decrease in the mutant group during the dark phase (Figure 27). This suggests a sustained lipid oxidation rate in of *Mfn2*$^{i\Delta EC}$ mice when compared to control counterparts.

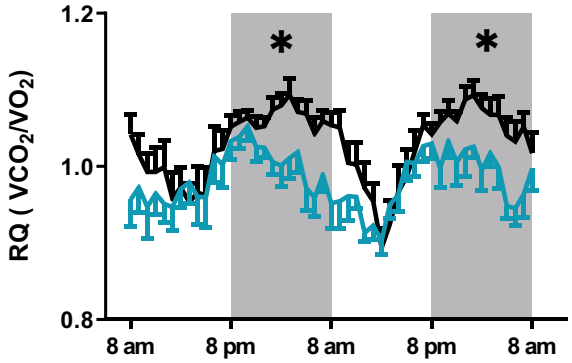

Figure 27: *Mfn2*$^{i\Delta EC}$ mice show enhanced lipid oxidation
RQ measured in control and *Mfn2*$^{i\Delta EC}$ mice at 15 weeks of age (n=7-9/genotype). Statistical analysis was performed by one-way ANOVA test; corrected by two-stage step-up method of Benjamini, Krieger and Yekutieli. Data are expressed as mean ± SEM. *P<0.05.

To further investigate the increased lipolytic capacity of *Mfn2*$^{i\Delta EC}$ mice, we initially collected adipose depots and plasma from 15-week-old animals under *ad libitum* fed or overnight-16h fasting conditions. As expected, a significant decrease in adiposity was observed upon fasting in the control group. Reduced adiposity levels in *Mfn2*$^{i\Delta EC}$ group were not further modified upon fasting (Figure 28 a). Interestingly, fasting-induced lipolysis was exacerbated in the *Mfn2*$^{i\Delta EC}$ group as reflected by increased plasma FFA levels (Figure 28 b).

Hormone-sensitive lipase (HSL) is a key enzyme of the lipolytic pathway. HSL activation is mainly driven by phosphorylation at Ser660 and Ser563. To molecularly verify whether lipolysis was perturbed in our model, whole eWAT depots from both groups under *ad libitum* and overnight fasting conditions were subjected to immunoblotting. Increased protein levels of the active HSL forms were observed after fasting in a similar magnitude in each group (Figure 28 c and d). However, HSL was aberrantly activated in *Mfn2*$^{i\Delta EC}$ mice during fed conditions when compared

to the control group (Figure 28 c and e). These results suggest that despite the fasting-induced lipolysis molecular response is occurring in both groups to a similar extent, *ad libitum* fed *Mfn2*$^{i\Delta EC}$ mice show a sustained activation of the lipolytic pathway likely leading to decreased adiposity and resulting in body weight reduction.

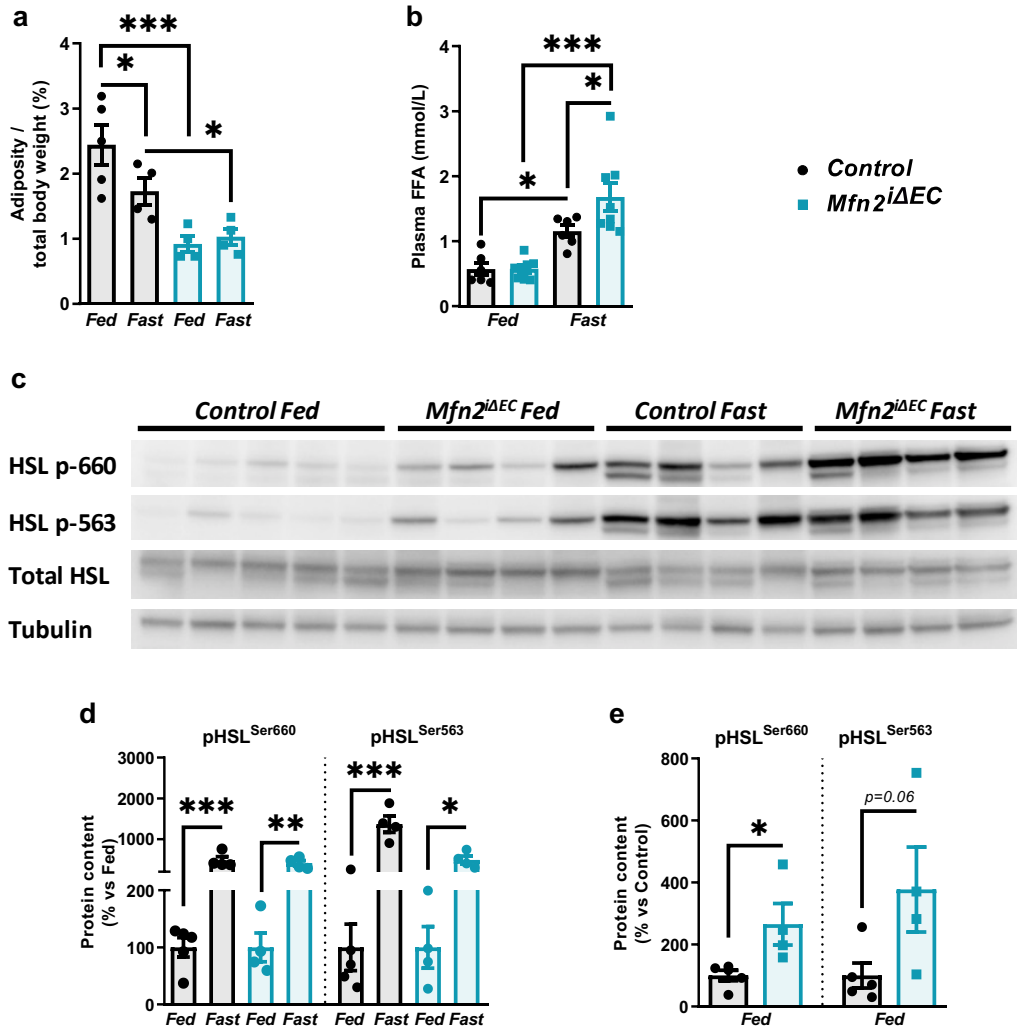

Figure 28: *Mfn2*$^{i\Delta EC}$ mice show increased lipolysis in fed conditions

a) Adiposity calculated by the combined sum of sWAT and eWAT depots weight normalized by body weight (n=4-5/genotype/nutritional status). b) Plasma FFA levels (n=6-8/genotype/nutritional status). c) Immunoblot analysis of eWAT using the indicated antibodies. d-e) Densitometric quantification of HSL phosphorylation levels at Ser660 and Ser563 (n=4-5/genotype/nutritional status). All studies were conducted in control and *Mfn2*$^{i\Delta EC}$ mice at 15 weeks of age under *ad libitum* (fed group) or upon overnight fasting (fast group). Statistical analysis was performed by one-way ANOVA test; corrected by two-stage step-up method of Benjamini, Krieger and Yekutieli (a, b and d) and by unpaired Student's t-test (e). Data are expressed as mean ± SEM. *P<0.05; **P<0.01; ***P<0.001.

2.7 Mfn2 loss in ECs results in less and enlarged mitochondria

To further uncover the molecular mechanisms underlying the metabolic phenotype upon *Mfn2* deletion in ECs, we next assessed mitochondria structural parameters. We specifically focused

on WAT as reduced adiposity is a consistent attribute of our mouse model. To this aim, a double immunofluorescence for IB4 (vascular maker) and Tom20 (mitochondrial marker) was performed in whole-mount sWAT (Figure 29 a). Quantification of confocal microscopy images, revealed decreased number of mitochondria in mutant mice (Figure 29 b) although the total area covered by mitochondria in vessels was equivalent (Figure 29 c). Consistently, mitochondria perimeter (Figure 29 d) and area (Figure 29 e) was increased in the vasculature of *Mfn2*$^{i\Delta EC}$ mice. No differences in aspect ratio (AR) (Figure 29 f) or form factor (FF) were observed (Figure 29 g). These results suggest a differential mitochondrial conformation in ECs upon *Mfn2* deletion.

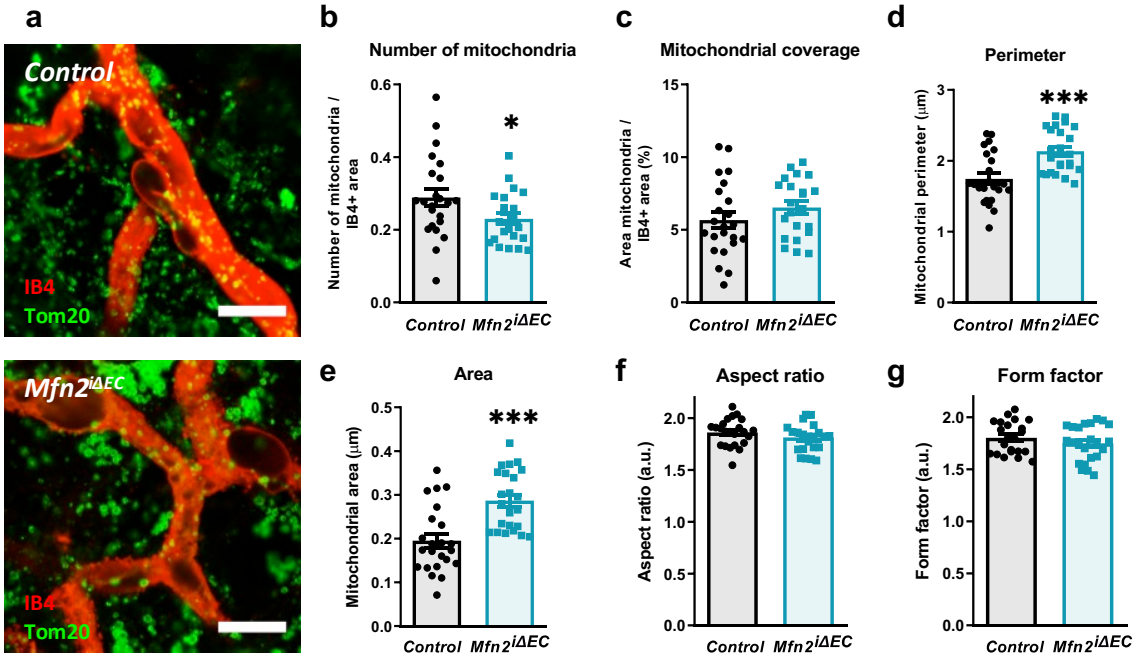

Figure 29: Reduced density and enlarged mitochondria in ECs of sWAT from mutant mice
a) Representative confocal microscopy images of double IB4 and Tom20 immunofluorescence in sWAT. b) Number of mitochondria normalized by the IB4 positive area. c) IB4 positive area covered by mitochondria. d) Perimeter and e) area of each mitochondrion. f) AR. g) FF. All studies were conducted in control and *Mfn2*$^{i\Delta EC}$ mice at 20 weeks of age upon overnight fasting (n=1405-1789 mitochondria in 6274-6590 µm^2 IB4 area/3 mice/genotype). Scale bar 50µm. Statistical analysis was performed by unpaired Student's t-test. Data are expressed as mean ± SEM. *P<0.05; ***P<0.001.

2.8 Endothelial *Mfn2* deletion increases NO and reduce ROS levels in white adipose tissue

Genetic deletion of *Mfn2* is associated with excessive ROS production and oxidative stress (Jiang et al., 2018; Schneeberger et al., 2013; Sebastián et al., 2012). Therefore, we conducted amperometric measures of ROS and NO production in *ex vivo* tissues from control and *Mfn2*$^{i\Delta EC}$ mice. We found a significant decrease in hydroxide peroxide (H_2O_2) levels in key metabolic

tissues such as the hypothalamus (Hyp), liver, eWAT, and iBAT (Figure 30 a-d). Notably, we also observed a significant increase in NO levels but exclusively in sWAT (Figure 30 e).

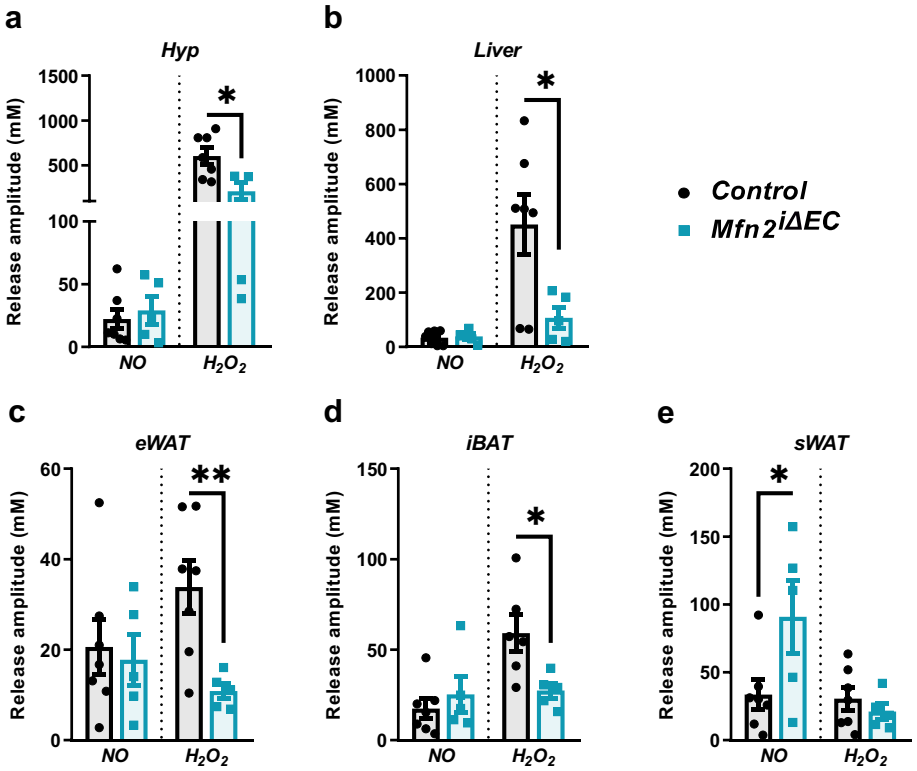

Figure 30: H_2O_2 and NO release in tissues from *Mfn2*$^{i\Delta EC}$ mice
Nitric oxide (NO) and hydroxide peroxide (H_2O_2) release in a) hypothalamus (Hyp), b) liver, c) eWAT, d) iBAT and e) sWAT *ex vivo* explants. All studies were conducted in control and *Mfn2*$^{i\Delta EC}$ mice at 13 weeks of age (n=4-7/genotype). Statistical analysis was performed by unpaired Student's t-test. Data are expressed as mean ± SEM. *P<0.05; **P<0.01.

3. *Mfn2*$^{i\Delta EC}$ mice are resistant to obesogenic diets

Mfn2$^{i\Delta EC}$ mice showed reduced adiposity that was accompanied by body weight decrease and improved glucose homeostasis. This phenotype could represent an advantage in the context of metabolically-related pathologies, such as obesity and T2D. In order to mimic these pathological conditions, we assessed the impact of HFD exposure on *Mfn2*$^{i\Delta EC}$ mice using two independent but complementary approaches. First, we evaluated the potential beneficial effects of endothelial *Mfn2* deletion upon the development of obesity (preventive study). To this aim, *Mfn2* deletion was induced before HFD exposure. In a second approach, we wanted to assess the impact of endothelial *Mfn2* deletion in counterbalancing established obesity (curative study). In this case, tamoxifen-mediated *Mfn2* deletion in ECs was induced in obese animals.

3.1 Mice lacking Mfn2 in ECs are resistant to diet-induced obesity

Mice were maintained under STD conditions since weaning. At 8 weeks of age, *Mfn2* deletion was induced by tamoxifen injection using our regular protocol. Two weeks after the last tamoxifen injection, mice were switch to HFD for 19 consecutive weeks. At 25 weeks of age, glucose metabolism was assessed, and tissues were collected at the end of the experiment (Figure 31). Parallel cohorts of control and mutant mice on STD and HFD were monitored.

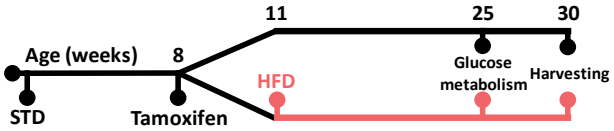

Figure 31: Experimental design for the preventive strategy
Mfn2 deletion was induced at 8 weeks of age. Three weeks later mice were exposed to 45% fat enriched diet for 19 weeks. Glucose metabolism was assessed five weeks before the end of the experiment.

Body weight gain upon HFD administration was highly effective in the control group. Indeed, around 20% difference in body weight increase was recorded between HFD and STD control groups. Remarkably, *Mfn2*$^{i\Delta EC}$ mice fed with either STD or HFD exhibited the same absolute body weight values, indicating complete resistance of *Mfn2*$^{i\Delta EC}$ mice to develop diet-induced obesity (Figure 32 a and b). These results demonstrate that endothelial deletion of *Mfn2* protects against obesity in a preventive manner.

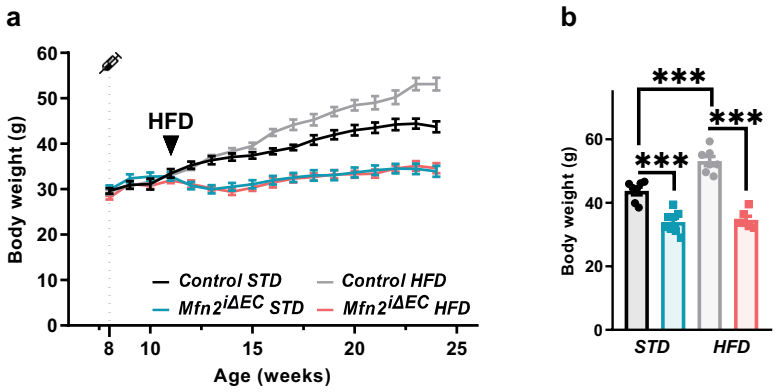

Figure 32: *Mfn2*$^{i\Delta EC}$ mice show resistance to HFD-induced obesity in a preventive manner
a) Weekly and b) final body weight of control and *Mfn2*$^{i\Delta EC}$ mice fed with STD or HFD for 19 weeks (n=6-8/genotype/diet). Statistical analysis was performed by one-way ANOVA test; corrected by two-stage step-up method of Benjamini, Krieger and Yekutieli. Data are expressed as mean ± SEM. ***P<0.001.

HFD-fed *Mfn2*$^{i\Delta EC}$ mice show similar adiposity to STD-fed mice

Consistent with body weight gain resistance, tissue collection at the end of the treatment showed a reduction in adiposity in HFD fed *Mfn2*$^{i\Delta EC}$ mice (Figure 33 a and b), when compared

with STD fed *Mfn2*$^{i\Delta EC}$ group. Notably, liver TG content in HFD-fed *Mfn2*$^{i\Delta EC}$ mice showed similar values to STD-fed groups suggesting no accumulation of ectopic fat (Figure 33 c).

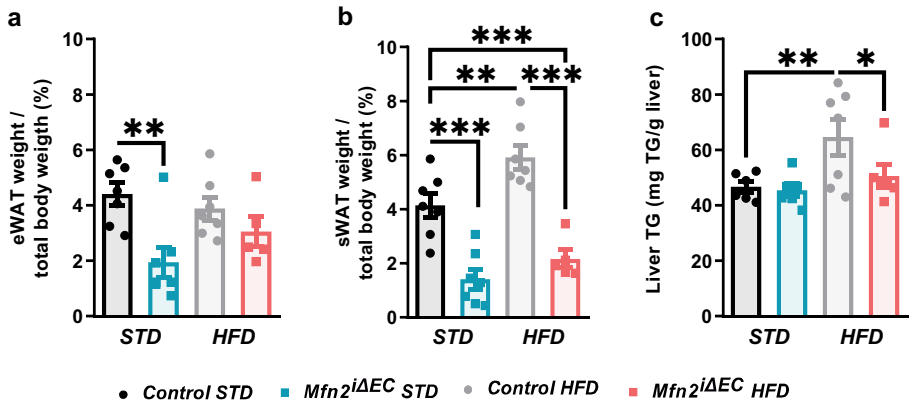

Figure 33: Reduced adiposity in *Mfn2*$^{i\Delta EC}$ mice when fed with HFD

a) eWAT and b) sWAT depots weight normalized by body weight. c) TG content in liver. All studies were conducted in control and *Mfn2*$^{i\Delta EC}$ mice fed with STD or HFD at 30 weeks of age (n=5-7/genotype). Statistical analysis was performed by one-way ANOVA test; corrected by two-stage step-up method of Benjamini, Krieger and Yekutieli. Data are expressed as mean ± SEM. *P<0.05; **P<0.01; ***P<0.001.

Improved metabolism in HFD-fed *Mfn2*$^{i\Delta EC}$ mice

Next, we examined glucose metabolism in control and *Mfn2*$^{i\Delta EC}$ mice under these experimental conditions. In line with diet-induced obesity resistance, similar results regarding diverse metabolic parameters were found in both *Mfn2*$^{i\Delta EC}$ groups irrespective of the diet. As expected,

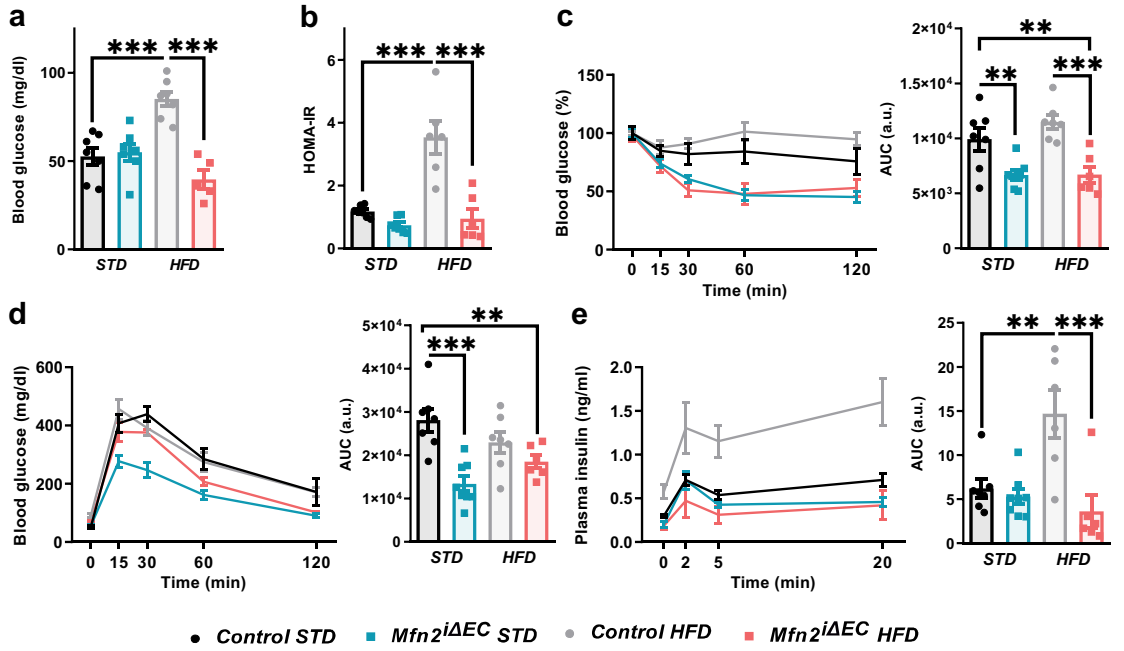

Figure 34: Improved glucose homeostasis in HFD-fed *Mfn2*$^{i\Delta EC}$ mice

a) Overnight fasting glucose levels. b) HOMA-IR values. b) ITT (0,3UI/Kg) and related area under the curve (AUC). d) GTT and related AUC. e) GSIS and related AUC. All studies were conducted in control and *Mfn2*$^{i\Delta EC}$ mice fed with STD or HFD at 25 weeks of age (n=6-8/genotype). Statistical analysis was performed by one-way ANOVA test; corrected by two-stage step-up method of Benjamini, Krieger and Yekutieli. Data are expressed as mean ± SEM. **P<0.01; ***P<0.001.

overnight fasting blood glucose levels were ~50% higher in HFD- versus STD-fed control mice. Remarkably, HFD-fed *Mfn2*$^{i\Delta EC}$ mice showed fully normalized glucose levels, similar to those observed in STD-fed groups (Figure 34 a). Besides, equivalent HOMA-IR was obtained between STD-fed groups and *Mfn2*$^{i\Delta EC}$ HFD-fed mice (Figure 34 b). To readily detect insulin sensitivity, we used an insulin dose that was ineffective in control mice (0,3UI/Kg). Under these conditions, increased insulin sensitivity was observed in *Mfn2*$^{i\Delta EC}$ HFD group in comparison with HFD-fed control mice (Figure 34 c). Glucose intolerance was attenuated in both *Mfn2*$^{i\Delta EC}$ groups (Figure 34 d) and complete normalization of GSIS levels were found in the *Mfn2*$^{i\Delta EC}$ group after 14 weeks of HFD administration. Together, these results indicate that *Mfn2*$^{i\Delta EC}$ mice are resistant to the HFD-induced obesogenic phenotype and associated glucose metabolism derangements.

3.2 Deletion of endothelial *Mfn2* reverses established obesity

Mfn2 loss in ECs counteract diet-induced body weight gain

To assess the possible effect of endothelial *Mfn2* deletion in counterbalancing established obesity, we administered HFD to control and *Mfn2*$^{i\Delta EC}$ mice littermates at 6 weeks of age. Control and mutant mice cohorts fed with STD were run in parallel.

Body weight was weekly monitored during the 12 weeks of HFD administration. At this time point, HFD-fed animals weighed ~26% more than STD-fed counterparts and tamoxifen was injected to promote *Mfn2* deletion. At 30 weeks of age, glucose metabolism was assessed, and tissues were collected at the end of the experiment (Figure 35).

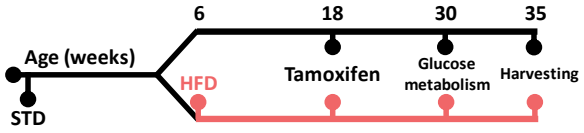

Figure 35: Experimental design for the curative strategy
Six-week-old mice were exposed to 45% fat-enriched diet for twelve weeks. Afterwards *Mfn2* deletion was induced via tamoxifen injection at 18 weeks of age. Glucose metabolism was assessed five weeks before the end of the experiment.

After tamoxifen administration, obese *Mfn2*$^{i\Delta EC}$ mice progressively reduced their body weight until reaching STD-fed control mice levels (Figure 36 a and b).

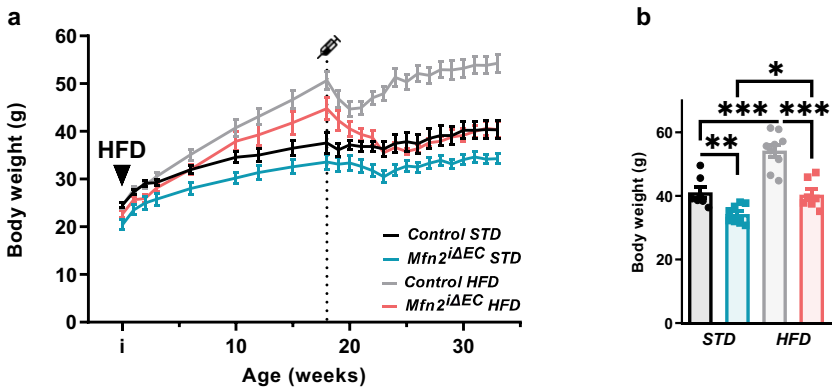

Figure 36: Obese *Mfn2*$^{i\Delta EC}$ mice reduce their body weight to control STD-fed mice levels

a) Weekly and b) final body weight of control and *Mfn2*$^{i\Delta EC}$ mice of 35 weeks of age fed with STD or HFD (n=7-9/genotype/diet). Statistical analysis was performed by one-way ANOVA test; corrected by two-stage step-up method of Benjamini, Krieger and Yekutieli. Data are expressed as mean ± SEM. *P<0.05; **P<0.01; ***P<0.001.

HFD-fed *Mfn2*$^{i\Delta EC}$ mice show similar adiposity than STD-fed mice

NMRI was performed in order to assess adiposity in control and *Mfn2*$^{i\Delta EC}$ mice fed with STD or HFD. This technique allowed us to measure whole intraperitoneal WAT, referred as vWAT, and the diverse subcutaneous depots. Reduced volume of vWAT and sWAT (Figure 37 a, b and c) was observed in *Mfn2*$^{i\Delta EC}$ mice fed with HFD in comparison with control-HFD group. In fact, AT reduction reached the levels of STD-fed control mice thus counterbalancing the AT expansion observed upon HFD administration.

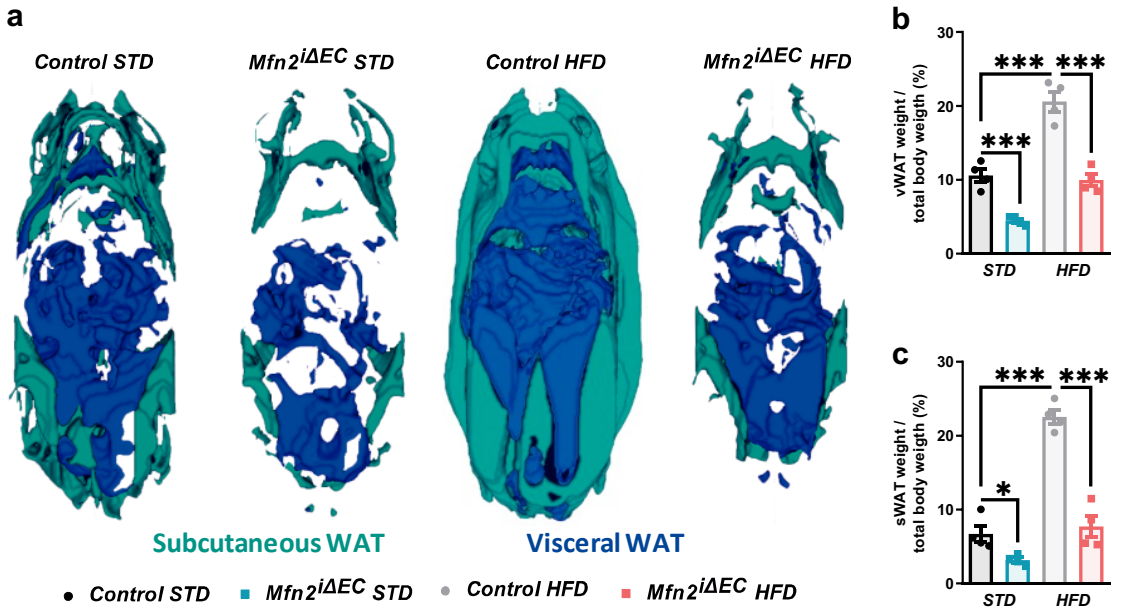

Figure 37: Obese *Mfn2*$^{i\Delta EC}$ mice reduce their adiposity to control STD-fed mice levels

a) Representative images of NMRI studies in control and *Mfn2*$^{i\Delta EC}$ mice fed with STD or HFD (n=4/genotype/diet). Quantification of the b) sWAT and c) vWAT volume from images in a). Statistical analysis was performed by one-way ANOVA test; corrected by two-stage step-up method of Benjamini, Krieger and Yekutieli. Data are expressed as mean ± SEM. *P<0.05; ***P<0.001.

Mfn2 deletion in ECs recovers obesity-related glucose metabolism impairment

To further verify if *Mfn2* deletion also recovers glucose metabolism impairment shown in obese mice, glucose homeostasis was assessed. Although overnight-fasting blood glucose levels were not different between the HFD-fed groups (Figure 38 a), most of the glucose homeostasis parameters associated with obesity were recovered after *Mfn2* ablation. Indeed, insulin sensitivity (assessed by HOMA-IR and the ITT) (Figure 38 b and c) and glucose tolerance (Figure 38 d) were fully recovered. Insulin secretion stimulated by glucose (Figure 38 e), was not improved in the *Mfn2*$^{i\Delta EC}$-HFD group probably due to an expanded β-cell mass as a consequence of the long HFD treatment.

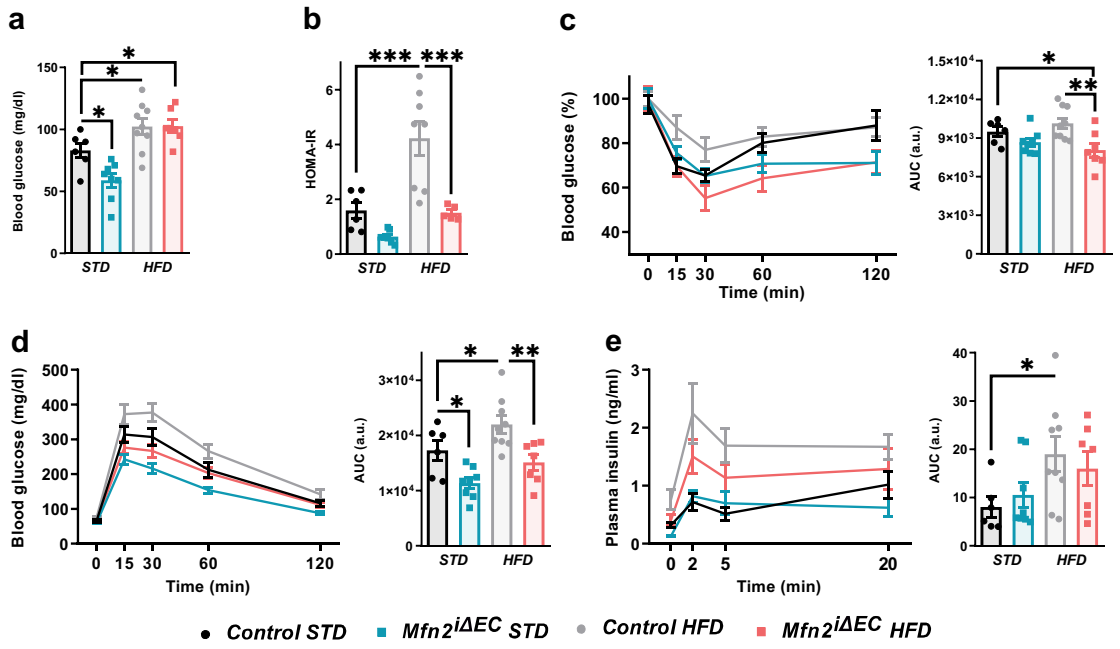

Figure 38: Glucose metabolism recovery in obese mice after *Mfn2* deletion
a) Overnight fasting glucose levels. b) HOMA-IR values. b) ITT (0,3UI/Kg) and related AUC. d) GTT and related AUC. e) GSIS and related AUC. All studies were conducted in control and *Mfn2*$^{i\Delta EC}$ mice fed with STD or HFD at 45 weeks of age (n=5-9/genotype). Statistical analysis was performed by one-way ANOVA test; corrected by two-stage step-up method of Benjamini, Krieger and Yekutieli. Data are expressed as mean ± SEM. *P<0.05; **P<0.01; ***P<0.001.

4. Mice with endothelial Mfn2 loss in the face of ageing

The free radical theory of ageing is based on the progressive mitochondrial dysfunction that occurs with ageing, which leads to increased ROS accumulation causing oxidative damage to numerous cellular structures (Harman, 1965). In contrast, physiological and highly controlled levels of ROS are required for many biological processes (Di Meo et al., 2016). Given that our mutant mice exhibited reduced levels of ROS across different metabolic tissues we wondered if this would cause a beneficial effect upon ageing.

4.1 Endothelial Mfn2 loss does not alter mice lifespan

Lifespan was assessed in group-housed control and *Mfn2*$^{i\Delta EC}$ mice. To minimize stress, mice were monitored weekly and weighed monthly, but otherwise left undisturbed until they died naturally. No differences were observed in lifespan between control and *Mfn2*$^{i\Delta EC}$ mice (Figure 39).

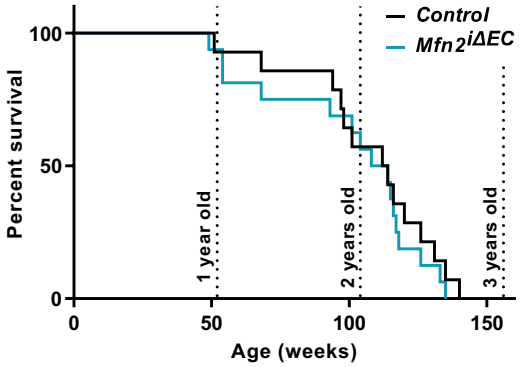

Figure 39: *Mfn2* deletion in ECs does not alter lifespan
Kaplan-Meier curves of control and *Mfn2*$^{i\Delta EC}$ mice (n=14-16/genotype). Statistical analysis was performed by Log-rank test.

4.2 Aged *Mfn2*$^{i\Delta EC}$ preserve young-like health parameters

Given that loss of Mfn2 in ECs did not alter lifespan, we next focused on potential beneficial effects on health-span during ageing. To this aim, we generated cohorts of control and *Mfn2*$^{i\Delta EC}$ mice of 16-20 (Young-adult group) and 70-75 (Old-adult group) weeks of age fed with STD diet. Several tests were performed to cover a wide range of behavioural and physiological parameters.

Neuro-state evaluation shows similar skills between young and old mice

Prior to the studies, a general neurological assessment was performed to control and *Mfn2*$^{i\Delta EC}$ mice. This consists in a battery of standardized tests that evaluate several parameters of the mice's appearance and reflex responses. These tests were conducted to ensure normal sensorimotor status of the mice and their ability to perform the subsequent behavioural tests. No significant differences were obtained amongst the four experimental groups (Figure 40). Of particular interest is the visual test, as well as the negative geotaxis or the flight responses, due to the importance of an optimal visual capacity and correct motor performance for subsequent tests.

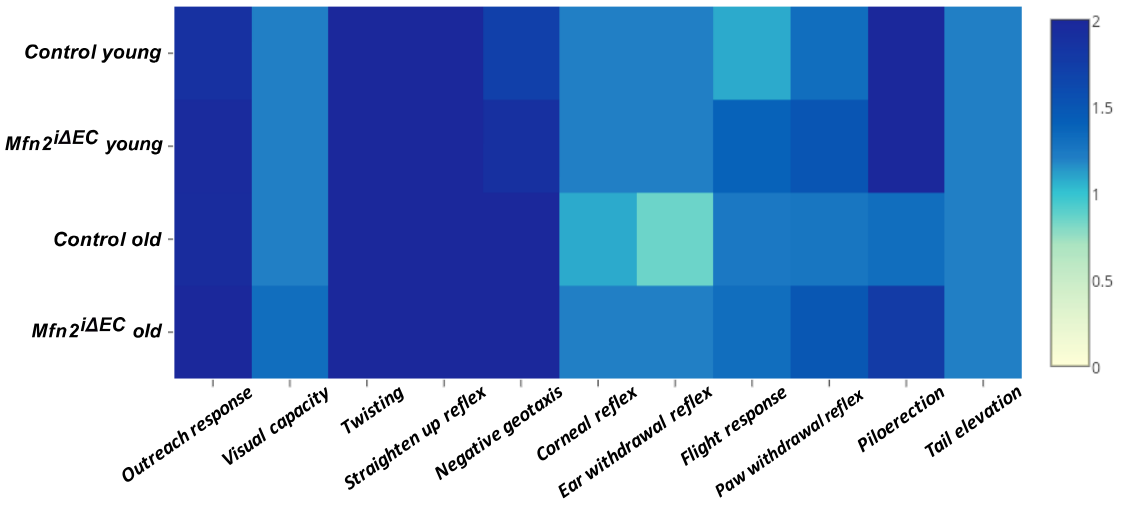

Figure 40: Young- and old-mice do not show differences in the neuro-state tests
Heat map of young and old control and *Mfn2*$^{i\Delta EC}$ mice performance on a standard neurological test (n=7-8/age/genotype).

Physiological parameters

a) Body composition, glucose homeostasis and bone analysis

<u>Old control and *Mfn2*$^{i\Delta EC}$ mice show equivalent body weight and glucose homeostasis</u>

Body weight and composition are affected by ageing and are considered health status predictors. It has been reported that weight loss is strongly predictive of mortality, independent of disease (Newman et al., 2001). Accordingly, body weight was recorded from weaning to late ages (Figure 41 a). A dramatic body weight and adiposity reduction in the control group was observed from 50 weeks of age onwards, indicative of physiological ageing. However, *Mfn2*$^{i\Delta EC}$ mice showed body weight and adiposity stability over the course of this study (Figure 41 a, b and c). Of note, equivalent adiposity and body weight observed in old mice groups exclude these parameters as confounding factors for the subsequent behavioural tests. As a consequence of equivalent body weights, no differences were observed when glucose homeostasis was assessed by insulin and glucose tolerance tests (Figure 41 d and e). These results further support the idea that changes in glucose metabolism seen in mutant mice are a secondary effect of body weight loss and reduced adiposity as shown previously (Figure 22).

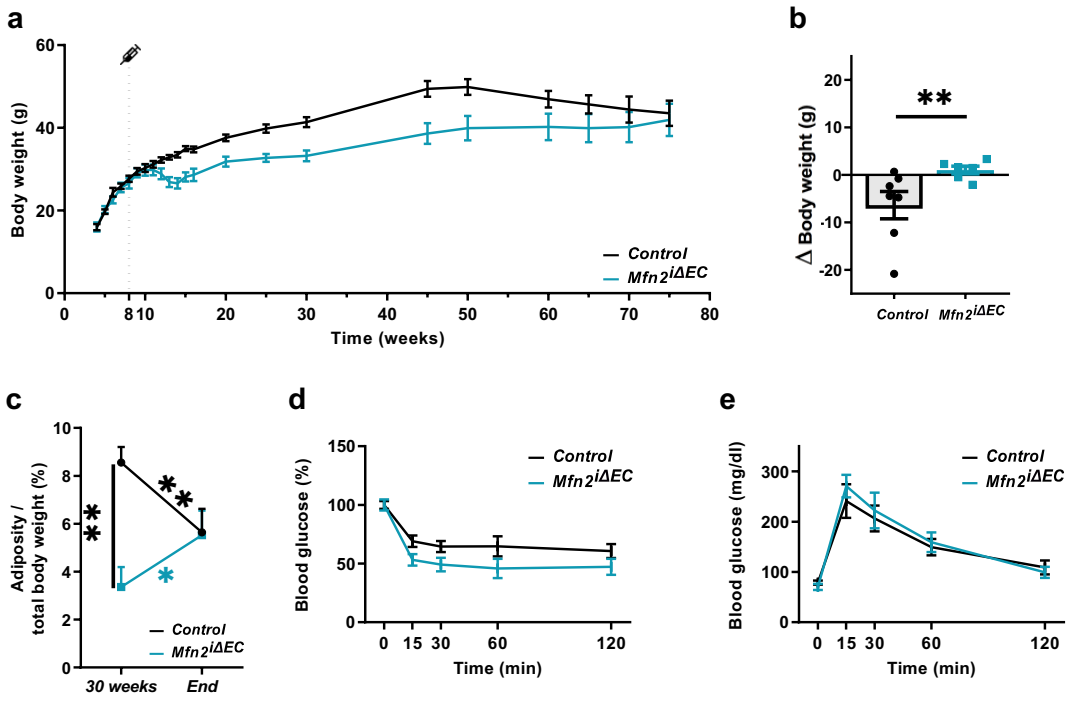

Figure 41: Aged-control and *Mfn2*$^{i\Delta EC}$ mice show equivalent adiposity and glucose metabolism homeostasis
a) Body weight profile. b) Body weight increase from 50 weeks of age to the end of the study. c) Adiposity changes between 30 weeks of age and the end of the experiment. Adiposity calculated by the combined sum of sWAT and eWAT depots weight normalized by body weight. d) ITT (0,4UI/Kg) and e) GTT performed at 65 weeks of age. All studies were conducted in control and *Mfn2*$^{i\Delta EC}$ mice (n=6-7/age/genotype). Statistical analysis was performed by One-way ANOVA test; corrected by two-stage step-up method of Benjamini, Krieger and Yekutieli (b and c) and by Two-Way ANOVA test (d and e). Data are expressed as mean ± SEM. *P<0.05; **P<0.01.

Old control and *Mfn2*$^{i\Delta EC}$ mice do not show differences in bone parameters

Ageing is associated with reduced bone mineral density and its progression results in bone diseases such as osteoporosis. High resolution imaging of femurs was acquired to perform measures of the cortical and trabecular bone. No differences were observed in trabecular/cortical thickness or bone volume/tissue volume ratio in aged *Mfn2*$^{i\Delta EC}$ mice when compared to the control group (Figure 42 a, b and c).

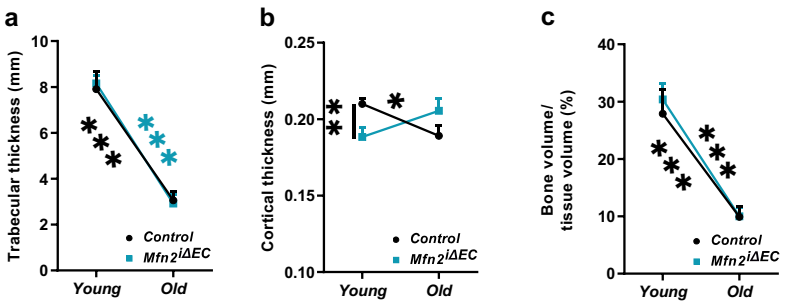

Figure 42: Mfn2 loss in ECs do not alter bone parameters during ageing
a) Trabecular thickness, b) cortical thickness and c) bone volume/tissue volume measured in femurs from young and old control and *Mfn2*$^{i\Delta EC}$ mice (n=6-7/age/genotype). Statistical analysis was performed by One-Way ANOVA test; corrected by two-stage step-up method of Benjamini, Krieger and Yekutieli. Data are expressed as mean ± SEM. *P<0.05; **P<0.01; ***P<0.001.

b) *Mfn2*$^{i\Delta EC}$ mice do not develop anaemia with age

Blood was collected to perform a complete hemogram. Total red blood cell number (Figure 43 a), haemoglobin concentration (Figure 43 b) and haematocrit (Figure 43 c) values showed a reduction with age in the control group. However, old *Mfn2*$^{i\Delta EC}$ mice exhibited similar values to their young counterparts. These results indicate that the control group is becoming anaemic (a marker of ageing) while *Mfn2*$^{i\Delta EC}$ mice not.

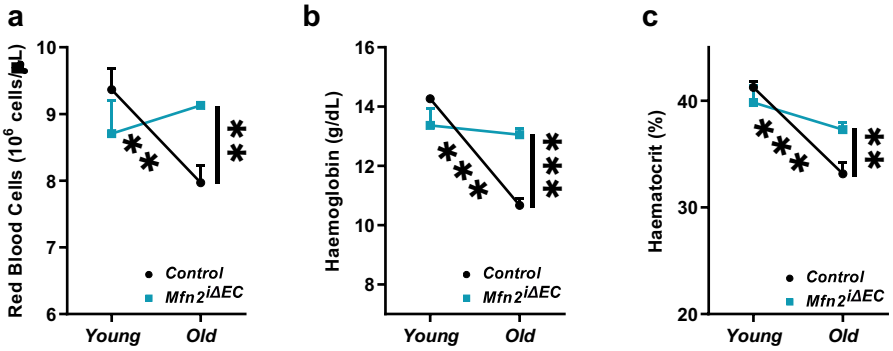

Figure 43: Old *Mfn2*$^{i\Delta EC}$ mice do not become anaemic with age
a) Number of red blood cells, b) haemoglobin and c) haematocrit values in blood from young and old control and *Mfn2*$^{i\Delta EC}$ mice (n=3-7/age/genotype). Statistical analysis was performed by One-Way ANOVA test; corrected by two-stage step-up method of Benjamini, Krieger and Yekutieli. Data are expressed as mean ± SEM. **P<0.01; ***P<0.001.

c) Kidney function is preserved in *Mfn2*$^{i\Delta EC}$ mice

Kidney function was determined by the albumin to creatinine ratio (ACR) levels in urine. Since creatinine, but not microalbumin, is normally excreted by urine, an increased ratio of these molecules is related with renal dysfunction. Age-associated increase in ACR was observed in the control group, but not in *Mfn2*$^{i\Delta EC}$ mice (Figure 44). This indicates that the age-related deterioration of kidney function is prevented in mouse lacking Mfn2 in ECs.

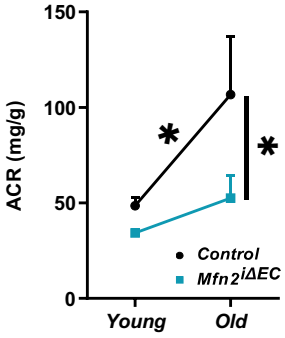

Figure 44: Improved kidney function in old *Mfn2*$^{i\Delta EC}$ mice
Albumin-creatinine ratio measured in urine from young and old control and *Mfn2*$^{i\Delta EC}$ mice (n=6-7/age/genotype). Statistical analysis was performed by One-Way ANOVA test; corrected by two-stage step-up method of Benjamini, Krieger and Yekutieli. Data are expressed as mean ± SEM. *P<0.05.

Behavioural and motor indicators of health-span

Behavioural parameters of health-span include gait/ataxia, motivated activity, cognition and affective function (Ackert-Bicknell et al., 2015). We conducted diverse tests to assess the aforementioned general parameters.

a) Preserved locomotor activity in *Mfn2*$^{i\Delta EC}$ mice

First, we assessed motor capacity, balance and fine coordination in our mouse model by performing an OF, balance beam and rotarod tests.

Open field

Mice were placed in a new arena and their motor and exploratory capacity was recorded by a camera. Automated tracking of mice (Figure 45 a) showed reduced LA in the old control group, while no differences were observed between young and old mutant groups. In the OF study, we analysed several parameters including total distance run (Figure 45 b), global activity of the mouse (Figure 45 c), mean speed (excluding resting time) (Figure 45 d) and time spent resting (Figure 45 e). Automatic software analysis of the OF videos revealed a decrease in performance by the control group as they age in all the parameters measured. Interestingly, no impairment

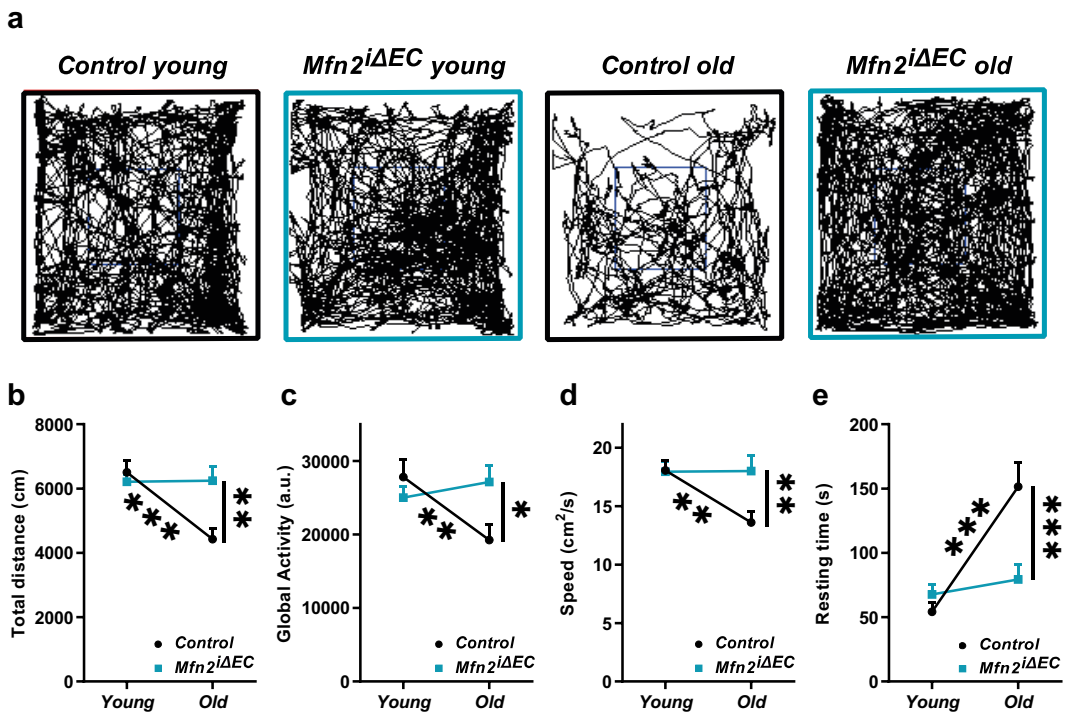

Figure 45: *Mfn2*$^{i\Delta EC}$ mice preserved their locomotor capacity during ageing

a) Representative images of the track trajectories performed by mice in the OF test. b) Total distance, c) global activity, d) mean speed excluding resting time and e) resting time from young and old control and *Mfn2*$^{i\Delta EC}$ mice, measured during the OF test (n=7-8/age/genotype). Statistical analysis was performed by One-Way ANOVA test; corrected by two-stage step-up method of Benjamini, Krieger and Yekutieli. Data are expressed as mean ± SEM. *P<0.05; **P<0.01; ***P<0.001.

was observed between the young and old *Mfn2*$^{i\Delta EC}$ group (Figure 45). These results suggest that the locomotor capacity in *Mfn2*$^{i\Delta EC}$ mice is preserved along their life.

Balance beam

The balance beam test was performed to assess the ability of mice to maintain the equilibrium when crossing a narrow beam. The time needed to walk the first 30 frames was recorded. *Mfn2*$^{i\Delta EC}$ mice showed better performance at young and old ages when compared to the control group (Figure 46).

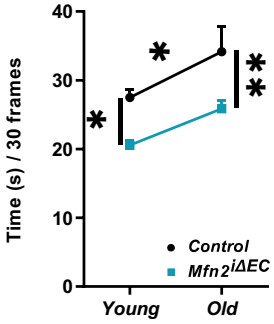

Figure 46: *Mfn2*$^{i\Delta EC}$ mice cross faster the beam than control mice irrespective of their age
Time spent by young and old control and *Mfn2*$^{i\Delta EC}$ mice to cover 30 frames of the beam (n=7-8/age/genotype). Statistical analysis was performed by One-Way ANOVA test; corrected by two-stage step-up method of Benjamini, Krieger and Yekutieli. Data are expressed as mean ± SEM. *P<0.05; **P<0.01.

Rotarod

The rotarod is a commonly used test to assess motor function in mice. Mice were forced to walk in an accelerating rotating rod, and the latency to fall was recorded. We observed a decreased latency to fall in the old control group when compared to the old *Mfn2*$^{i\Delta EC}$ group (Figure 47). This suggests that *Mfn2* deletion in ECs prevents the aged-associated loss of fine coordination and balance.

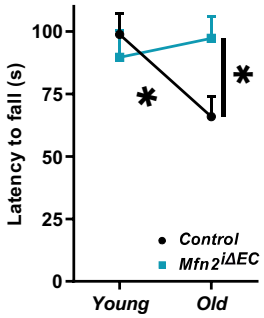

Figure 47: The latency to fall from the rotarod is preserved in aged *Mfn2*$^{i\Delta EC}$ mice
Latency to fall from the rotarod by young and old control and *Mfn2*$^{i\Delta EC}$ mice (n=6-7/age/genotype). Statistical analysis was performed by One-Way ANOVA test; corrected by two-stage step-up method of Benjamini, Krieger and Yekutieli. Data are expressed as mean ± SEM. *P<0.05.

b) Endothelial *Mfn2* deletion does not alter muscular function

Another hallmark of ageing is the muscular function. To assess this, mice were placed on a grid upside down and the latency to fall was recorded. A similar aged-associated decline in muscular function was observed between genotypes (Figure 48). This suggests that muscle function is not affected in *Mfn2*$^{i\Delta EC}$ mice, and that the locomotor improvements shown in the previous section could be driven by central effects.

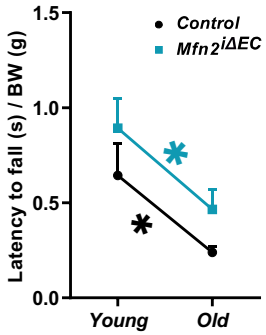

Figure 48. Mfn2 loss in ECs does not alter muscular function
Latency to fall from the grid by young and old control and *Mfn2*$^{i\Delta EC}$ mice (n=6-7/age/genotype). Statistical analysis was performed by One-Way ANOVA test; corrected by two-stage step-up method of Benjamini, Krieger and Yekutieli. Data are expressed as mean ± SEM. *P<0.05.

c) Memory function is preserved in *Mfn2*$^{i\Delta EC}$ mice

Next we assessed age-related cognitive decline. To this aim, we performed the NORT as ageing is associated with memory impairment. Consistently, our results showed that control mice reduced their ability to remember a previously exposed object as they age. Interestingly, *Mfn2*$^{i\Delta EC}$ mice exhibited preserved NORT performance irrespective of their age (Figure 49), indicating improved cognitive function along *Mfn2*$^{i\Delta EC}$ mice life.

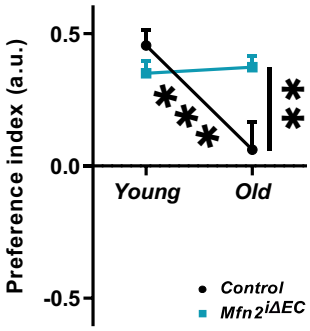

Figure 49: Old *Mfn2*$^{i\Delta EC}$ mice show better cognitive function than old control mice
Preference index, based on the time of exploration of the new and the previously exposed object, from young and old control and *Mfn2*$^{i\Delta EC}$ mice (n=6-8/age/genotype). Statistical analysis was performed by One-Way ANOVA test; corrected by two-stage step-up method of Benjamini, Krieger and Yekutieli. Data are expressed as mean ± SEM. **P<0.01; ***P<0.001.

DISCUSSION

Numerous studies have reported a direct connection between metabolic disorders and vascular dysfunction considering it a hallmark of obesity (Zaborska et al., 2017). In fact, dysfunctional endothelium can cause by itself secondary pathologies associated with such metabolic disorders (Rajendran et al., 2013), thus contributing to the progression and worsening of these diseases. However, emerging evidences have reported that genetic loss of certain proteins in the endothelium results in systemic metabolism alterations (Hashimoto et al., 2015; Sawada et al., 2014; Yokoyama et al., 2014). These observations suggest a primary role of ECs as systemic metabolism modulators (Graupera and Claret, 2018; Pi et al., 2018).

Mitochondria are considered the "powerhouse" of the cell since they provide the required energy for cellular processes. Given the pivotal role of mitochondria in cellular bioenergetics, mitochondrial dysfunction is present in many pathophysiological processes, including metabolic disorders such as obesity and T2D (Gao et al., 2014). Excessive ROS production and oxidative stress are thought to be involved in mitochondrial function impairment. Intimately linked to ROS production and mitochondrial performance is the well-known process of mitochondrial dynamics. Impairment of this process has been associated with metabolic disorders, and conversely, metabolic diseases have been directly connected with mitochondrial dynamics dysregulation (Bhatti et al., 2017). Therefore, mitochondrial dynamics is crucial for adequate mitochondrial function and is considered a bioenergetic adaptation process to the metabolic needs and demands of the cell (Westermann, 2012).

Most of the vascular studies reported so far have been focused on understanding the process of angiogenesis, in which ECs are in a proliferative state. However, in adults, ECs usually are in a quiescent state and rarely proliferate. In fact, proliferative ECs in adult organisms have been often related to diseases like cancer, obesity, vascular malformations and blindness among others (Carmeliet, 2003). However, the role of quiescent ECs in maintaining blood and tissue homeostasis, likely via sensing of environmental cues and generating responses in accordance, remains relatively unexplored. Mitochondria have been suggested to be the endothelial sensors, integrators and modulators of the ECs responses, rather than energy suppliers (Caja and Antonio Enríquez, 2017; Davidson and Duchen, 2007; Tang et al., 2014).

Therefore, a detailed study of diverse mitochondrial processes, such as mitochondrial dynamics, in ECs is necessary to understand the connection between vascular biology, mitochondrial function and metabolism.

1. Mitofusins; siblings rather than twins

As mentioned in the Introduction section, despite Mfn1 and 2 exhibit high degree of homology they exert both redundant and distinct functions. This observation was evidenced in *in vivo* studies in which double KO mice died at mid-gestation due to insufficient fusion (Chen et al., 2003a). Interestingly, either single mutant embryos live longer than double mutants, suggesting non-redundant functions (Chen et al., 2007). Non-overlapping functions of Mfns have also been demonstrated in adulthood. For instance, liver Mfn1 KOs are protected against diet-induced insulin resistance (Kulkarni et al., 2016), while hepatic *Mfn2* deletion in mice led to metabolic abnormalities, such as glucose intolerance, enhanced hepatic gluconeogenesis and impaired insulin signalling (Sebastián et al., 2012). Moreover, in POMC neurons, while *Mfn1* deletion leads to defective pancreatic insulin release in the face of unaltered energy homeostasis (Ramírez et al., 2017), Mfn2 ablation causes a completely different phenotype characterized by obesity due to ER stress-mediated leptin resistance (Schneeberger et al., 2013).

Little is known about the role of Mfns in ECs. In fact, only one study has initially investigated their functions *in vitro* in HUVECs. Absence of both Mfn proteins disrupts mitochondrial networks and reduces mitochondrial membrane potential, thus decreasing VEGF-mediated migration and differentiation. However, Mfn2 ablation resulted in decreased ROS generation probably due to the stimulation of the Akt/eNOS signalling pathway, while in *Mfn1* deleted ECs these parameters remain unaltered (Lugus et al., 2011). In our study, we do also report differential phenotypes upon *Mfn1* or *Mfn2* specific deletion in ECs *in vivo*. In fact, Mfn1 loss does not support our hypothesis, since its deletion does not lead to any systemic metabolic alteration. However, upon Mfn2 loss, we observed a marked beneficial metabolic phenotype.

The phenotype differences seen in several studies investigating Mfn1 and Mfn2 mutants, including ours, could be explained by divergent Mfns expression patterns amongst diverse tissues. Although RNA-seq analysis suggest low expression levels in most rodent tissues (Eura et al., 2003), it has been reported that Mfn1 is ubiquitously expressed but particularly abundant in heart, liver, pancreas and testis (Eura et al., 2003; Santel et al., 2003). However, Mfn2 is preferentially expressed in heart, skeletal muscle, brain and iBAT (Bach et al., 2005; Eura et al., 2003). In HUVECs, *MFN2* expression is 8-fold higher than *MFN1*. Besides, upon VEGF stimulation, *MFN2* expression was 3-fold higher than *MFN1* (Lugus et al., 2011). Altogether, these observations could explain, at least in part, the differential phenotype observed upon Mfns deletion in our study.

2. Tissue specificity

Mitochondria are widely present in almost every cell of the organism but erythrocytes. Mitochondrial content within different cell types varies significantly, occupying from 2 to 6% of the cytoplasm volume in ECs and up to 32% in cardiac myocytes (Barth et al., 1992; Oldendorf et al., 1977), according to the energy requirements and the specific functions of the cells. Consequently, mitochondrial related proteins, such as Mfns, are differentially expressed among tissues, as shown in the previous section, suggesting cell-specific functions.

In addition to the studies mentioned in the previous section, a variety of phenotypes are reported upon *Mfn2* deletion in diverse tissues. For instance, *Mfn2* deletion in hippocampus and cortex results in oxidative stress and neuronal death (Jiang et al., 2018). Moreover, knocking out Mfn2 in mouse white adipocytes results in an obese phenotype (Mancini et al., 2019). Deletion of *Mfn2* in brown adipocytes causes BAT hypertrophy and cold intolerance (Boutant et al., 2017), although Mfn2 seems to have a beneficial effect in HFD-BAT adaptation. Surprisingly in our case, we observed that deficiency of Mfn2 in ECs decreases body weight and fat mass, likely due to enhanced EE and lipolytic activity thus conferring resistance to diet-induced obesity. Mouse studies in muscle, show that Mfn2 deficiency accelerates the age-related detrimental effects (Sebastián et al., 2016). In contrast, we report improved age-associated biomarkers, as demonstrated by improved locomotor activity, cognition and several physiological parameters in aged $Mfn2^{i\Delta EC}$ mice. So generally speaking, although reduced expression of Mfn2 in diverse tissues or cell-types has been associated with harmful effects for the organism, our mouse model reveals that knocking out *Mfn2* in ECs could be systemically beneficial.

The broad ranges of phenotypes reported upon same-gene deletion suggest tissue/cell-specific actions of Mfn2, and this could also be the case within the endothelium. It is known that the ECs are not all alike. In fact, there is a notable heterogeneity across the endothelium. ECs heterogeneity is mediated, at least in part, by site-specific and time-dependent differences in gene transcription (Minami and Aird, 2005). Depending on the type of vessel or organ in which they are located, ECs exhibit differential molecular patterns of expression and functional properties (Aird, 2007; Herron et al., 2019; Marcu et al., 2018; Nolan et al., 2013).

Although the vasculature are amongst the first organs to form during development (Carmeliet and Collen, 1997), vessel growth continues after birth in lung (deMello et al., 1997), heart (Hudlicka and Brown, 1996), brain (Ment et al., 1997; Wang et al., 1992) and retina (Stone et al., 1995). Deletion of *Mfn1* and *2* is embryonically lethal. Hence, we decided to induce DNA recombination in 8-week-old mice, with the aim of avoiding possible interferences during the

vascular network development. We have demonstrated that the recombination event of the gene of interest was extended across the endothelium, except retina and pituitary. However, the extent of deletion was only assessed in lung given the abundant presence of ECs in this tissue. Indeed, based on the observations that around 20% of adult mouse lungs are ECs (Singer et al., 2016), we show a significant decrease in *Mfn2* expression in this tissue reflecting ECs-*Mfn2* deletion. Analysis of vessel structure and functionality reveal no overt abnormalities caused by *Mfn2* deletion. Thus, we concluded that our model is suitable to study the role of Mfn2 in adult mouse vasculature.

3. Enhanced lipid metabolism

Adult mice with endothelial *Mfn2* deletion display decreased adiposity likely due to enhanced EE and reduced RQ. Excluding alterations in food intake, locomotor activity or thermogenesis, augmented BMR seems to be the likely cause for the increased energy consumption. EE is usually increased during the active phase (night, for rodents) and decreased during the inactive period (day, for rodents). Interestingly, we do detect slightly higher rates of EE in the inactive phase when compared to controls. This observation further reinforces the idea of increased BMR as a putative cause of the increased EE, since during this phase, basal metabolism is the major contributor to EE. Conversely, during the dark-active phase, locomotor activity and the thermogenic effect associated to food intake are the major sponsors of EE. Given that, it is likely that the tiny contributions of BMR to EE during this phase, could be masked, thus explaining the equivalent EE detected in the dark phase.

Moreover, RQ values also oscillate during night and day. It is generally reduced during the light-inactive-fasting phase, indicating a higher oxidation of the lipid storages. However, in the darkactive-fed period, mice metabolize more carbohydrates, thus increasing the RQ values close to 1. In contrast, mice with *Mfn2* deletion in ECs show a significantly attenuated fluctuation of the RQ pattern throughout the 48h period, indicating a sustained tendency to utilize fat as substrate.

The capacity of an organism to adapt their metabolism to the energy demands, as well as prevailing conditions or activity, is known as metabolic flexibility. This concept was defined in the context of fuel selection in the transition from fasting to fed states (Galgani et al., 2008; Goodpaster and Sparks, 2017; Kelley and Mandarino, 2000). Metabolic inflexibility has been associated to obese and T2D patients (Goodpaster and Sparks, 2017; Kelley et al., 1999). In fact, mouse studies show that metabolic inflexibility precede glucose intolerance and obesity-induced alterations (Muoio and Neufer, 2012; Noland et al., 2009).

Our results show that upon fed/fast transition, *Mfn2*$^{i\Delta EC}$ mice activate the lipolytic machinery to a similar extent as their control counterparts thus adapting its metabolism to energy demand. However, the continuous tendency to metabolize fat, shown by low RQ values throughout the day, suggests certain metabolic inflexibility. In fact, the increased lipid oxidation shown during the dark-fed phase correlates with the higher activation of HSL in WAT in fed conditions. This observation points towards a basal and sustained fat mobilization and oxidation irrespective of the metabolic state. This observation could actually explain the decreased adiposity and body weight, as well as the resistance to diet-induced obesity shown by *Mfn2*$^{i\Delta EC}$ mice.

Although the obtained results point towards WAT as the putative tissue underlying the *Mfn2*$^{i\Delta EC}$ mice phenotype, further experiments are needed to uncover why FAO is increased. One possible explanation would be that ECs lacking Mfn2 are promoting FAO via crosstalk between the endothelium and the adipocytes through existing mechanisms such as extracellular vesicles (Crewe et al., 2018) or release of angiocrine factors. This would enhance fatty acid consumption by peripheral tissues such as muscle, thus explaining the increased EE and the decreased RQ.

However, with the available data, we cannot exclude that changes in endothelium metabolism itself are the responsible of the observed phenotype. The aforementioned mouse models lacking Mfn2 in diverse tissues displayed deleterious cellular and systemic effects due to oxidative stress. Taking this into consideration, we cannot rule out the possibility that ROS production and accumulation is increased in the endothelium of our mouse model. Importantly, the observation that the deletion of *Mfn2* in ECs does not cause deleterious systemic effects would suggest an EC-intrinsic machinery in charge of ROS detoxification, thus preventing oxidative stress. In fact, ROS accumulation was significantly decreased in hypothalamus, liver, eWAT and iBAT in our model. Interestingly, as mentioned in the introduction, quiescent ECs upregulate FAO as a protective mechanism against oxidative stress (Kalucka et al., 2018). Therefore, we cannot discard that *Mfn2* deleted ECs could rely on FAO as a ROS-detoxification mechanism.

4. Calorie restriction-like phenotype

Calorie restriction (CR) refers to the chronic reduction of the total caloric intake without causing malnutrition. CR has emerged as the most efficient non-genetic intervention to extend both health- and life-span in multiple animal models including yeast, fruit flies, worms, rodents and monkeys (Fontana et al., 2010; De Guzman et al., 2013). Some of the metabolic improvements upon CR, such as reduced body weight and fat mass, decreased fasting blood glucose and plasma insulin concentrations, as well as increased insulin sensitivity and glucose uptake, have been observed in mice and monkeys (Roth et al., 2006). Moreover, recent studies suggest that the

beneficial metabolic effects of CR observed in mice and other species, could be relevant for human physiology (Racette et al., 2006; Redman et al., 2018). CR has also been associated with reduced risk of developing age-associated diseases such as diabetes, cancer and cardiovascular diseases, as well as with the prevention of age-associated impairments in memory and learning. Besides, studies in calorie-restricted aged rats show improved locomotor activity and age-associated renal disease (Jiang et al., 2005; Masoro, 2000; Salvatore et al., 2016; Stewarrt et al., 1989; Witte et al., 2009).

Interestingly, *Mfn2*$^{i\Delta EC}$ mice share several phenotypical features with the calorie-restricted mice. Both models exhibit body weight, adiposity reduction and resistance to develop metabolic diseases such as obesity and TD2 similar. Moreover, our mutant mice preserve young-like age-associated parameters such as improved cognition, locomotor activity and coordination, show preserved kidney function and do not develop anaemia upon ageing thus indicating improved health-span. In contrast, unlike the CR model, lifespan in endothelial *Mfn2* deleted mice is not extended. This is in line with recent studies indicating that life- and health-span are not necessarily correlated (Fischer et al., 2016).

Moreover, as reported by short CR intervention studies, reduced body weight and adiposity is limited to the time in which feeding is restricted. However, health-span benefits persist long time after the CR intervention (Hornsby et al., 2016; Melo et al., 2019), suggesting that the mechanisms involved in health-span are established early and linked to the adiposity reduction. Unlike the CR model, body weight loss in *Mfn2*$^{i\Delta EC}$ mice is not recovered but the initial tendency becomes stable around six weeks after recombination. After this time point, control and *Mfn2*$^{i\Delta EC}$ mice described parallel body weight curves. These observations suggest that the mechanisms governing health-span could be related, but are not coupled, with body weight reduction in both models. Moreover, given the observed similarities we cannot exclude analogous molecular mechanisms underlying both phenotypes. For this reason, I will briefly summarize the current hypotheses that could explain the health-span improvements found in CR mice, to find a suitable explanation for our phenotype.

Several hypotheses exist in the literature linking CR and ageing. First, the “growth retardation hypothesis” proposes that CR increases the longevity of mice by delaying development. This hypothesis is illustrated by reduced body and organs size, including reduced femur length, in CR-rats (McCay et al., 1935). Consistent with growth retardation, it has also been reported decreased levels of insulin-like growth factor-1 (Igf-1) in calorie-restricted rats and mice (Breese et al., 1991; D’Costa et al., 1993; Sonntag et al., 1992). Given that aged controls and *Mfn2*$^{i\Delta EC}$

mice show equivalent body and organs weight, as well as femur length and plasma Igf-1 (data not shown), this theory does not explain the phenotype observed in our study.

Reduced fat mass has also been proposed as a mechanism underlying CR beneficial effects. This observation was based on the fact that fat accumulation is associated with premature death in humans and that CR rodents exhibit decreased visceral fat (Barzilai and Gupta, 1999). Although there is some controversy linking reduced fat mass and lifespan, it is unquestionable that excessive fat accumulation, particularly in the abdominal region, compromise health-span since it is associated with TD2 and insulin resistance in several tissues (Fagot-Campagna et al., 2001; Ford et al., 1997; Mokdad et al., 2003; Urbanavičius et al., 2013). Therefore, the hypothesis based on reduced fat mass, could explain in part the phenotype observed in *Mfn2*$^{i\Delta EC}$ mice. In fact, reduction in total fat mass (including visceral adiposity) was observed in *Mfn2*$^{i\Delta EC}$ mice fed with HFD. Nevertheless, the improvements shown by *Mfn2*$^{i\Delta EC}$ mice upon ageing will remain vaguely justified by this theory, since aged *Mfn2*$^{i\Delta EC}$ mice show improved health parameters in the face of unaltered body weigh when compared to controls. Other suggested hypothesis that could mimic better the phenotype observed by *Mfn2*$^{i\Delta EC}$ mice, will be explained in the following sections.

4.1 Oxidative damage attenuation hypothesis

Another hypothesis is based on the oxidative stress theory that proposes that ageing is a consequence of molecular damage caused by excessive ROS production (Harman, 1965). This line of thought evolved into the mitochondrial theory of ageing, since mitochondria are major sources of ROS (Barja, 2002; Beckman and Ames, 1998). As explained in the Introduction section, oxidative stress damages biological molecules, such as DNA, proteins or lipids, altering cellular functions thus compromising life. In fact, it is established that CR delays age-associated accumulation of oxidative damage in mice and also in monkeys (Fontana et al., 2010; Sohal and Weindruch, 1996; Someya et al., 2010; Weindruch and Sohal, 1997; Yu, 1996; Zaninal et al., 2000). Of note, reduced ROS levels (assessed by H_2O_2 measurements) were found in tissues from young *Mfn2*$^{i\Delta EC}$ mice when compared to controls, suggesting that the cumulative oxidative damage of these tissues could be reduced upon ageing. Whether this lower H_2O_2 content is due to a decreased production or to increased ROS-scavenger mechanisms is still under investigation.

Interestingly, higher levels of NO were found exclusively in sWAT. This result raises a key question: could NO be an angiocrine factor secreted in all vascular beds or only by the ECs

located in the sWAT? It is known that NO is secreted by ECs in response to some stressors such as shear stress (Kabirian et al., 2015). Besides, in 1992, it was suggested that the endothelium could be regarded as an endocrine organ in its own right with a paracrine secretion of NO (Vane and Botting, 1992). Therefore, assuming that *Mfn2* deleted endothelium secretes NO in a paracrine manner, and knowing that NO and H_2O_2 react (Nappi and Vass, 1998), this theory would explain the lower H_2O_2 release detected in several tissues of our mutant mice. However, we detected an increased release of NO in the sWAT. Therefore, we cannot exclude the possibility of an endocrine effect specific of the endothelium form of the sWAT. Thus, NO produced by ECs in sWAT will act in an endocrine manner reducing ROS levels systemically.

Vascular Nitric Oxide

NO is generated by NOS and in mammals three isoenzymes are found: nNOS (neuronal), iNOS (inducible) and eNOS (endothelial). Interestingly, it has been reported that CR induces eNOS expression but not other isoenzymes (Nisoli et al., 2005). This study also reports that this induction is observed in several tissues (brain, liver, iBAT and heart), but it is particularly high in WAT. CR is also accompanied by increased mitochondrial biogenesis, oxygen consumption and ATP production as well as enhanced expression of sirtuin 1 (SIRT-1) (Nisoli et al., 2005). Importantly, SIRT-1 (the mammalian form of *Sir2* gene that mediates lifespan extension upon CR in yeast) (Anderson et al., 2003; Lin et al., 2000), has also been reported to promote fat mobilization (Picard et al., 2004). Nisoli and colleagues have also shown that upon eNOS inactivation mitochondrial biogenesis is blunted and SIRT-1 levels are decreased. This suggests that under stress conditions (in this case CR) eNOS expression increases its activity, as a putative compensatory mechanism.

Other studies have investigated the role of eNOS by knocking-down or overexpressing it *in vivo*. In fact, HFD-fed and *db/db* mice exhibit decreased eNOS protein levels in AT (Sansbury et al., 2012). Interestingly, overexpression of eNOS ($eNOS^{TG}$) in mice mimics the phenotype observed upon endothelial *Mfn2* deletion. Sansbury and colleagues reported that $eNOS^{TG}$ mice show reduced adiposity and resistance to body weight gain upon HFD administration, due to an increased metabolic rate. Although these mice were insulin resistant and glucose intolerant, they exhibited a higher fatty acid metabolism in AT, thus preventing lipid accumulation and adipocyte expansion. Since increased FAO suggests higher mitochondrial activity, oxygen consumption was measured in AT explants. This experiment revealed enhanced oxygen consumption in the AT of $eNOS^{TG}$ mice when compared to controls. All in all, Sansbury and colleagues concluded that overexpressing eNOS causes a hypermetabolic state in the AT that

could explain the increased energy consumption and diet-induced obesity resistance (Sansbury et al., 2012).

Conversely, the eNOS KO mouse phenotype opposes the phenotype observed in *Mfn2*$^{i\Delta EC}$ mice, reporting reduced EE and oxygen consumption (Le Gouill et al., 2007). Another study demonstrates a role for eNOS in the control of glucose and lipid homeostasis (Duplain et al., 2001). Furthermore, aged-eNOS KO mice show higher mortality and reduced locomotor activity in the open field test (Dere et al., 2002), as well as renal failure progression (Forbes et al., 2007). Collectively, the strong phenotypical similarities between *in vivo* genetic manipulations of eNOS and *Mfn2*$^{i\Delta EC}$ mouse suggest that NO may mediate some of the metabolic and ageing improvements observed in our model. Therefore, an in-depth assessment of eNOS function in *Mfn2*$^{i\Delta EC}$ mice is mandatory.

4.2 Hormetic response

Hormesis is defined as the beneficial effects resulting from the response of an organism to a sustained low-intensity stressor (Furst, 1987; Masoro, 2005). The hormesis response has been suggested as another hypothesis underlying the beneficial effects observed in CR conditions, including increased life- and health-span. Moreover, CR has been associated with increased metabolic rate (Schulz et al., 2007; Walker et al., 2005) and higher mitochondrial metabolism. Therefore, it is likely that as a by-product of mitochondrial metabolism, ROS production is increased (Schulz et al., 2007). While excessive ROS has been associated with cellular damage and ageing, low levels may induce an adaptive response. This type of hormesis, when the low-intensity stressor is referred to mitochondrial ROS, is known as mitochondrial hormesis or mitohormesis. Of note, it has been reported that CR induces stress defence mechanisms, in particular those in charge of ROS-detoxification, such as eNOS (Nisoli et al., 2005; Ristow and Schmeisser, 2014). These two situations associated with CR (that is increased mitochondrial ROS and stress defences induction), may secondarily reduce mitochondrial ROS in a time-resolved manner (Zarse et al., 2012). This indicates that the mitohormetic ROS signals are transient or even abolished due to an adaptive response mediated by antioxidative mechanisms and stress defences. In fact, under CR conditions it has been described a primary ROS generation, followed by a reduction of ROS levels due to the activation of the detoxification mechanisms (Agarwal et al., 2005). Although these studies were performed in yeast, carbonylated protein concentrations (a marker of oxidative protein damage) were found in brains of mice shortly after CR. However, in steady-state, after the acute insult, these levels were significantly lower than controls (Dubey et al., 1996).

Given these observations, a parallelism with the endothelial Mfn2 KO mice phenotype can be inferred from the body weight curves either under STD or HFD conditions. Upon Mfn2 recombination in ECs, reduction in body weight is observed for few weeks. However, after that time, mice stop to lose weight and the slope of the curve changes. In fact, *Mfn2*$^{i\Delta EC}$ mice re-start to gain weight and body weight curves continue parallel to the control ones. Thus, it is likely that the initial impact of *Mfn2* deletion is progressively compensated via a mitohormesis mechanism. As mentioned, high levels of ROS cause cellular damage, promoting ageing. It is known that high ROS levels activate anti-ROS-defences, thus preventing oxidative damage via an adaptive response. The reduced ROS levels observed in several tissues of *Mfn2*$^{i\Delta EC}$ mice could result from enhanced systemic antioxidative defences, thus decreasing ROS levels in the context of a hormetic response.

5. Limitations of the study and ongoing research

5.1 Endothelial transcriptome analysis

One of the major challenges of this study is the assessment of the molecular underpinnings of ECs *in vivo*. Given that endothelial mitochondria integrate and respond to environmental cues, those strategies involving stressful procedures such as tissue homogenization, enzymatic digestion or cell sorting are not adequate. For this reason, we generated a mouse line that permits the *in vivo* isolation of EC-RNA. We took advantage of the *RiboTag* mouse line, which allows Cre-mediated tagging of polyribosomes and subsequent isolation of mRNA in a cell-specific manner via immunoprecipitation (Sanz et al., 2009). We crossed the *Pdgfb-iCre-ER*^{T2}-*Mfn2*$^{flox/flox}$ mice with the *RiboTag* mice, that upon tamoxifen administration generates the *Mfn2*$^{i\Delta EC}$*-RiboTag* mouse model.

The endothelial transcriptome analysis will confirm the extension of *Mfn2* gene deletion in the different vascular beds and will help to unravel crucial aspects of the intriguing phenotype of our mutant mice. Based on H_2O_2 and NO release results, we anticipate alterations in the expression patterns of ROS- and NO-related genes in ECs. This may help to understand the role of these signalling molecules in our experimental settings.

5.2 Mitochondrial ultrastructure and functionality studies

Another notable omission of this study is the evaluation of the mitochondrial ultrastructure and functionality. Since time and resources are limited and given the heterogeneity of ECs, we

decided to pair this decision to the EC transcriptome analysis. Therefore, knowing the contribution of the different vascular beds to the phenotype observed, this study will be performed in the most appropriate ECs populations.

Most of the publications targeting Mfn2 in different tissues, show diminished mitochondrial network, increased fragmentation (by showing decreased AR and FF) and more rounded and enlarged mitochondria (Boutant et al., 2017; Lee et al., 2012; Mahdaviani et al., 2017; Schneeberger et al., 2013; Sebastián et al., 2012; Yang et al., 2018), including ECs in vitro studies (Lugus et al., 2011). In our case, we report bigger mitochondria, without alterations in AR and FF. This discrepancy could be due to the limited accuracy of the confocal microscopy technique that we initially used for the assessment of the mitochondrial network. We are currently planning to conduct electron microscopy studies to precisely assess mitochondrial ultrastructure and morphology.

Furthermore, specific mitochondrial functionality studies are required for the adequate characterization of our mutant mice. For this reason, assessment of mitochondrial respiration in isolated ECs and tissues are planned. The results derived from the endothelial transcriptome analysis will likely reveal the specific tissues and vascular beds to perform this assessment. EC-specific mitochondrial respiratory alterations without changes in the residing organ will suggest EC-specific defects. However, if we detect respiratory alterations also in the residing tissue, this observation will point towards a specific crosstalk between ECs and the residing organ.

6. Concluding remarks

The correct function of the vascular system is essential for life. Blood vessels are lined by ECs and allow the distribution of oxygen and nutrients, crucially regulating the passage of substances to satisfy the necessities of every organ. Therefore, ECs are crucially positioned to sense diverse environmental cues and respond in accordance. Mitochondria have emerged as key endothelial sensors, integrators and modulators of the ECs responses, being ROS a key signalling molecule. Here we show that *in vivo* endothelial mitochondrial function is implicated in the regulation of systemic energy balance as well as in ageing progression.

The precise molecular mechanism underlying the phenotype observed upon endothelial *Mfn2* deletion is incompletely understood. However, based on the described results in this report and the previous observations from the literature, we can propose that *Mfn2*$^{i\Delta EC}$ mice mimic, at least partially, the CR model. CR results in excessive generation of ROS, which in turn activates the detoxification machinery and eventually reducing ROS levels (Agarwal et al., 2005). CR also

induces eNOS expression (Nisoli et al., 2005) which acts a as a putative mechanism to compensate high ROS levels.

Consistently, elevated ROS levels are also reported in mouse models of *Mfn2* deletion in diverse tissues (Jiang et al., 2018; Schneeberger et al., 2013; Sebastián et al., 2012). However, specific deletion of endothelial *Mfn2 in vitro* reduces ROS production and increases eNOS activity (Lugus et al., 2011), suggesting the existance of an intrinsic EC ROS-eNOS axis involved in oxidative stress detoxification. We have not directly assessed eNOS activity in this study. However, ROS and NO release levels measured in several tissues points towards an enhanced eNOS function either across the endothelium or specifically in the ECs residing in the sWAT. In addition, the described phenotypes upon global eNOS overexpression or eNOS ablation (Dere et al., 2002; Duplain et al., 2001; Forbes et al., 2007; Le Gouill et al., 2007; Sansbury et al., 2012), reflect and opposes respectively the phenotype observed in our mutant mice. These mechanisms could explain at least in part the HFD-resistance and improved health-span found in $Mfn2^{i\Delta EC}$ mice.

CONCLUSIONS

Chapter I: Endothelial Mfn1 function assessment

1. Adult endothelial deletion of *Mfn1* does not alter the EC population.
2. Loss of Mfn1 in ECs does not cause systemic metabolic alterations when fed standard or high-fat diet.

Chapter II: Decoding the function of Mfn2 in ECs

1. Loss of endothelial Mfn2 in adult mice does not cause histopathological or vascular function alteration.
2. Endothelial *Mfn2* deletion in adult male and female mice causes body weight reduction as a consequence of decreased adiposity, both under standard or high-fat diet conditions.
3. The leaner phenotype of $Mfn2^{i\Delta EC}$ mice is a consequence of increased EE, and the sustained mobilization and oxidation of the lipid storages.
4. Mice lacking Mfn2 in ECs are resistant to diet-induced obesity, as shown in both preventive and curative studies.
5. Aged $Mfn2^{i\Delta EC}$ mice exhibit improved health-span despite unaltered lifespan.

REFERENCES

REFERENCES

Abou-Mohamed, G., Kaesemeyer, W.H., Caldwell, R.B., and Caldwell, R.W. (2000). Role of L-arginine in the vascular actions and development of tolerance to nitroglycerin. Br. J. Pharmacol. *130*, 211–218.

Ackert-Bicknell, C.L., Anderson, L., Sheehan, S., Hill, W.G., Chang, B., Churchill, G.A., Chesler, E.J., Korstanje, R., and Peters, L.L. (2015). Aging Research Using Mouse Models. Curr Protoc Mouse Biol *5*, 95–133.

Adams, R.H., and Alitalo, K. (2007). Molecular regulation of angiogenesis and lymphangiogenesis. Nat. Rev. Mol. Cell Biol. *8*, 464–478.

Afolayan, A.J., Eis, A., Alexander, M., Michalkiewicz, T., Teng, R.-J., Lakshminrusimha, S., and Konduri, G.G. (2016). Decreased endothelial nitric oxide synthase expression and function contribute to impaired mitochondrial biogenesis and oxidative stress in fetal lambs with persistent pulmonary hypertension. Am. J. Physiol. Cell. Mol. Physiol. *310*, L40–L49.

Agarwal, S., Sharma, S., Agrawal, V., and Roy, N. (2005). Caloric restriction augments ROS defense in S. cerevisiae, by a Sir2p independent mechanism. Free Radic. Res. *39*, 55–62.

Agouni, A., Lagrue-Lak-Hal, A.-H., Mostefai, H.A., Tesse, A., Mulder, P., Rouet, P., Desmoulin, F., Heymes, C., Martínez, M.C., and Andriantsitohaina, R. (2009). Red Wine Polyphenols Prevent Metabolic and Cardiovascular Alterations Associated with Obesity in Zucker Fatty Rats (Fa/Fa). PLoS One *4*, e5557.

Aird, W.C. (2007). Phenotypic Heterogeneity of the Endothelium I. Structure, Function, and Mechanisms.

Al-Mehdi, A.-B., Pastukh, V.M., Swiger, B.M., Reed, D.J., Patel, M.R., Bardwell, G.C., Pastukh, V. V., Alexeyev, M.F., and Gillespie, M.N. (2012). Perinuclear Mitochondrial Clustering Creates an Oxidant-Rich Nuclear Domain Required for Hypoxia-Induced Transcription. Sci. Signal. *5*, ra47–ra47.

Amanso, A.M., and Griendling, K.K. (2012). Differential roles of NADPH oxidases in vascular physiology and pathophysiology. Front. Biosci. (Schol. Ed). *4*, 1044–1064.

American Diabetes Association, A.D. (2014). Diagnosis and classification of diabetes mellitus. Diabetes Care *37 Suppl 1*, S81-90.

An, Y.A., Sun, K., Joffin, N., Zhang, F., Deng, Y., Donzé, O., Kusminski, C.M., and Scherer, P.E. (2017). Angiopoietin-2 in white adipose tissue improves metabolic homeostasis through enhanced angiogenesis. Elife *6*.

REFERENCES

Anderson, R.M., Bitterman, K.J., Wood, J.G., Medvedik, O., and Sinclair, D.A. (2003). Nicotinamide and PNC1 govern lifespan extension by calorie restriction in Saccharomyces cerevisiae. Nature *423*, 181–185.

Andreyev, A.Y., Kushnareva, Y.E., Murphy, A.N., and Starkov, A.A. (2015). Mitochondrial ROS Metabolism: 10 Years Later. Biochemistry. (Mosc). *80*, 517–531.

Araki, E., Oyadomari, S., and Mori, M. (2003). Impact of Endoplasmic Reticulum Stress Pathway on Pancreatic β-Cells and Diabetes Mellitus. Exp. Biol. Med. *228*, 1213–1217.

Bach, D., Pich, S., Soriano, F.X., Vega, N., Baumgartner, B., Oriola, J., Daugaard, J.R., Lloberas, J., Camps, M., Zierath, J.R., et al. (2003). Mitofusin-2 determines mitochondrial network architecture and mitochondrial metabolism. A novel regulatory mechanism altered in obesity. J. Biol. Chem. *278*, 17190–17197.

Bach, D., Naon, D., Pich, S., Soriano, F.X., Vega, N., Rieusset, J., Laville, M., Guillet, C., Boirie, Y., Wallberg-Henriksson, H., et al. (2005). Expression of Mfn2, the Charcot-Marie-Tooth Neuropathy Type 2A Gene, in Human Skeletal Muscle: Effects of Type 2 Diabetes, Obesity, Weight Loss, and the Regulatory Role of Tumor Necrosis Factor and Interleukin-6. Diabetes *54*, 2685–2693.

Barja, G. (2002). Endogenous oxidative stress: relationship to aging, longevity and caloric restriction. Ageing Res. Rev. *1*, 397–411.

Barth, E., Stämmler, G., Speiser, B., and Schaper, J. (1992). Ultrastructural quantitation of mitochondria and myofilaments in cardiac muscle from 10 different animal species including man. J. Mol. Cell. Cardiol. *24*, 669–681.

Barzilai, N., and Gupta, G. (1999). Revisiting the role of fat mass in the life extension induced by caloric restriction. J. Gerontol. A. Biol. Sci. Med. Sci. *54*, B89-96; discussion B97-8.

Basen-Engquist, K., and Chang, M. (2011). Obesity and Cancer Risk: Recent Review and Evidence. Curr. Oncol. Rep. *13*, 71–76.

Beckman, K.B., and Ames, B.N. (1998). The Free Radical Theory of Aging Matures. Physiol. Rev. *78*, 547–581.

Bell, M.B., Bush, Z., Mcginnis, G.R., Glenn, X., and Rowe, C. (2019). Adult skeletal muscle deletion of Mitofusin 1 and 2 impedes exercise performance and training capacity. J Appl Physiol *126*, 341–353.

REFERENCES

Bereiter-Hahn, J. (1990). Behavior of Mitochondria in the Living Cell. Int. Rev. Cytol. *122*, 1–63.

Berg, A.H., Combs, T.P., Du, X., Brownlee, M., and Scherer, P.E. (2001). The adipocyte-secreted protein Acrp30 enhances hepatic insulin action. Nat. Med. *7*, 947–953.

Bhatti, J.S., Bhatti, G.K., and Reddy, P.H. (2017). Mitochondrial dysfunction and oxidative stress in metabolic disorders — A step towards mitochondria based therapeutic strategies. Biochim. Biophys. Acta - Mol. Basis Dis. *1863*, 1066–1077.

Bianconi, E., Piovesan, A., Facchin, F., Beraudi, A., Casadei, R., Frabetti, F., Vitale, L., Pelleri, M.C., Tassani, S., Piva, F., et al. (2013). An estimation of the number of cells in the human body. Ann. Hum. Biol. *40*, 463–471.

Blanquicett, C., Graves, A., Kleinhenz, D.J., and Hart, M.C. (2007). Attenuation of Signaling and Nitric Oxide Production following Prolonged Leptin Exposure in Human Aortic Endothelial Cells. J. Investig. Med. *55*, 368–377.

Blouin, A., Bolender, R.P., and Weibel, E.R. (1977). Distribution of organelles and membranes between hepatocytes and nonhepatocytes in the rat liver parenchyma. A stereological study. J. Cell Biol. *72*, 441–455.

De Bock, K., Georgiadou, M., Schoors, S., Kuchnio, A., Wong, B.W., Cantelmo, A.R., Quaegebeur, A., Ghesquière, B., Cauwenberghs, S., Eelen, G., et al. (2013). Role of PFKFB3-driven glycolysis in vessel sprouting. Cell *154*, 651–663.

Bourgoin, F., Bachelard, H., Badeau, M., Mélançon, S., Pitre, M., Larivière, R., and Nadeau, A. (2008). Endothelial and vascular dysfunctions and insulin resistance in rats fed a high-fat, high-sucrose diet. Am. J. Physiol. Circ. Physiol. *295*, H1044–H1055.

Boutant, M., Kulkarni, S.S., Joffraud, M., Ratajczak, J., Valera-Alberni, M., Combe, R., Zorzano, A., and Cantó, C. (2017). Mfn2 is critical for brown adipose tissue thermogenic function. EMBO J. *36*, 1543.

Brand, M.D. (2000). Uncoupling to survive? The role of mitochondrial inefficiency in ageing. Exp. Gerontol. *35*, 811–820.

Bray, G.A., and Tartaglia, L.A. (2000). Medicinal strategies in the treatment of obesity. Nature *404*, 672–677.

Breese, C.R., Ingram, R.L., and Sonntag, W.E. (1991). Influence of age and long-term dietary restriction on plasma insulin-like growth factor-1 (IGF-1), IGF-1 gene expression, and IGF-1

binding proteins. J. Gerontol. *46*, B180-7.

de Brito, O.M., and Scorrano, L. (2008). Mitofusin 2 tethers endoplasmic reticulum to mitochondria. Nature *456*, 605–610.

Brook, R.D., Bard, R.L., Rubenfire, M., Ridker, P.M., and Rajagopalan, S. (2001). Usefulness of visceral obesity (waist/hip ratio) in predicting vascular endothelial function in healthy overweight adults. Am. J. Cardiol. *88*, 1264–1269.

Bui, H.T., and Shaw, J.M. (2013). Dynamin Assembly Strategies and Adaptor Proteins in Mitochondrial Fission. Curr. Biol. *23*, R891–R899.

Bult, H., Meyer, G.R.Y., and Herman, A.G. (1995). Influence of chronic treatment with a nitric oxide donor on fatty streak development and reactivity of the rabbit aorta. Br. J. Pharmacol. *114*, 1371–1382.

Butler, A.E., Janson, J., Bonner-Weir, S., Ritzel, R., Rizza, R.A., and Butler, P.C. (2003). Beta-cell deficit and increased beta-cell apoptosis in humans with type 2 diabetes. Diabetes *52*, 102–110.

Caja, S., and Antonio Enríquez, J. (2017). Mitochondria in endothelial cells: Sensors and integrators of environmental cues. Redox Biol. *12*, 821–827.

Camici, G.G., Schiavoni, M., Francia, P., Bachschmid, M., Martin-Padura, I., Hersberger, M., Tanner, F.C., Pelicci, P., Volpe, M., Anversa, P., et al. (2007). Genetic deletion of p66Shc adaptor protein prevents hyperglycemia-induced endothelial dysfunction and oxidative stress. Proc. Natl. Acad. Sci. *104*, 5217–5222.

Cardillo, C., Kilcoyne, C.M., Cannon, R.O., Quyyumi, A.A., and Panza, J.A. (1997). Xanthine oxidase inhibition with oxypurinol improves endothelial vasodilator function in hypercholesterolemic but not in hypertensive patients. Hypertens. (Dallas, Tex. 1979) *30*, 57–63.

Carmeliet, P. (2000). Mechanisms of angiogenesis and arteriogenesis. Nat. Med. *6*, 389–395.

Carmeliet, P. (2003). Angiogenesis in health and disease. Nat. Med. *9*, 653–660.

Carmeliet, P. (2005). Angiogenesis in life, disease and medicine. Nature *438*, 932–936.

Carmeliet, P., and Collen, D. (1997). Genetic Analysis of Blood Vessel Formation. Trends Cardiovasc. Med. *7*, 271–281.

Chatzizisis, Y.S., Coskun, A.U., Jonas, M., Edelman, E.R., Feldman, C.L., and Stone, P.H. (2007).

Role of Endothelial Shear Stress in the Natural History of Coronary Atherosclerosis and Vascular Remodeling. J. Am. Coll. Cardiol. *49*, 2379–2393.

Chemaly, E.R., Hadri, L., Zhang, S., Kim, M., Kohlbrenner, E., Sheng, J., Liang, L., Chen, J., K-Raman, P., Hajjar, R.J., et al. (2011). Long-term in vivo resistin overexpression induces myocardial dysfunction and remodeling in rats. J. Mol. Cell. Cardiol. *51*, 144–155.

Chen, C., Jiang, J., Lü, J.-M., Chai, H., Wang, X., Lin, P.H., and Yao, Q. (2010a). Resistin decreases expression of endothelial nitric oxide synthase through oxidative stress in human coronary artery endothelial cells. Am. J. Physiol. Circ. Physiol. *299*, H193–H201.

Chen, F., Haigh, S., Barman, S., and Fulton, D.J.R. (2012). From form to function: the role of Nox4 in the cardiovascular system. Front. Physiol. *3*, 412.

Chen, H., Detmer, S.A., Ewald, A.J., Griffin, E.E., Fraser, S.E., and Chan, D.C. (2003a). Mitofusins Mfn1 and Mfn2 coordinately regulate mitochondrial fusion and are essential for embryonic development. J. Cell Biol. *160*, 189–200.

Chen, H., Montagnani, M., Funahashi, T., Shimomura, I., and Quon, M.J. (2003b). Adiponectin Stimulates Production of Nitric Oxide in Vascular Endothelial Cells. J. Biol. Chem. *278*, 45021–45026.

Chen, H., Chomyn, A., and Chan, D.C. (2005). Disruption of Fusion Results in Mitochondrial Heterogeneity and Dysfunction. J. Biol. Chem. *280*, 26185–26192.

Chen, H., McCaffery, J.M., and Chan, D.C. (2007). Mitochondrial Fusion Protects against Neurodegeneration in the Cerebellum. Cell *130*, 548–562.

Chen, H., Vermulst, M., Wang, Y.E., Chomyn, A., Prolla, T.A., McCaffery, J.M., and Chan, D.C. (2010b). Mitochondrial Fusion Is Required for mtDNA Stability in Skeletal Muscle and Tolerance of mtDNA Mutations. Cell *141*, 280–289.

Chen, K., Li, F., Li, J., Cai, H., Strom, S., Bisello, A., Kelley, D.E., Friedman-Einat, M., Skibinski, G.A., McCrory, M.A., et al. (2006). Induction of leptin resistance through direct interaction of C-reactive protein with leptin. Nat. Med. *12*, 425–432.

Cheng, K.K.Y., Lam, K.S.L., Wang, Y., Huang, Y., Carling, D., Wu, D., Wong, C., and Xu, A. (2007). Adiponectin-induced endothelial nitric oxide synthase activation and nitric oxide production are mediated by APPL1 in endothelial cells. Diabetes *56*, 1387–1394.

Cinti, S., Mitchell, G., Barbatelli, G., Murano, I., Ceresi, E., Faloia, E., Wang, S., Fortier, M.,

REFERENCES

Greenberg, A.S., and Obin, M.S. (2005). Adipocyte death defines macrophage localization and function in adipose tissue of obese mice and humans. J. Lipid Res. *46*, 2347–2355.

Claxton, S., Kostourou, V., Jadeja, S., Chambon, P., Hodivala-Dilke, K., and Fruttiger, M. (2008). Efficient, inducible Cre-recombinase activation in vascular endothelium. Genesis *46*, 74–80.

Cogliati, S., Enriquez, J.A., and Scorrano, L. (2016). Mitochondrial Cristae: Where Beauty Meets Functionality. Trends Biochem. Sci. *41*, 261–273.

Cohen, S.S., Palmieri, R.T., Nyante, S.J., Koralek, D.O., Kim, S., Bradshaw, P., and Olshan, A.F. (2008). A review. Cancer *112*, 1892–1904.

Collins, T.J. (2002). Mitochondria are morphologically and functionally heterogeneous within cells. EMBO J. *21*, 1616–1627.

Colombini, M., Blachly-Dyson, E., and Forte, M. (1996). VDAC, a channel in the outer mitochondrial membrane. Ion Channels *4*, 169–202.

Cortese, J.D., Voglino, A.L., and Hackenbrock, C.R. (1992). The ionic strength of the intermembrane space of intact mitochondria is not affected by the pH or volume of the intermembrane space. Biochim. Biophys. Acta *1100*, 189–197.

Couper, J., and Donaghue, K.C. (2009). Phases of diabetes in children and adolescents. Pediatr. Diabetes *10*, 13–16.

Craige, S.M., Kröller-Schön, S., Li, C., Kant, S., Cai, S., Chen, K., Contractor, M.M., Pei, Y., Schulz, E., and Keaney, J.F. (2016). PGC-1α dictates endothelial function through regulation of eNOS expression. Sci. Rep. *6*, 38210.

Crewe, C., Joffin, N., Rutkowski, J.M., Kim, M., Zhang, F., Towler, D.A., Gordillo, R., and Scherer, P.E. (2018). An Endothelial-to-Adipocyte Extracellular Vesicle Axis Governed by Metabolic State. Cell *175*, 695-708.e13.

Crewe, H.K., Notley, L.M., Wunsch, R.M., Lennard, M.S., and Gillam, E.M.J. (2002). Metabolism of Tamoxifen by Recombinant Human Cytochrome P450 Enzymes: Formation of the 4-Hydroxy, 4'-Hydroxy and *N*- Desmethyl Metabolites and Isomerization of *trans* -4-Hydroxytamoxifen. Drug Metab. Dispos. *30*, 869–874.

D'Costa, A.P., Lenham, J.E., Ingram, R.L., and Sonntag, W.E. (1993). Moderate caloric restriction increases type 1 IGF receptors and protein synthesis in aging rats. Mech. Ageing Dev. *71*, 59–71.

Dagher, Z., Ruderman, N., Tornheim, K., and Ido, Y. (2001). Acute Regulation of Fatty Acid

Oxidation and AMP-Activated Protein Kinase in Human Umbilical Vein Endothelial Cells. Circ. Res. *88*, 1276–1282.

Daiber, A. (2010). Redox signaling (cross-talk) from and to mitochondria involves mitochondrial pores and reactive oxygen species. Biochim. Biophys. Acta - Bioenerg. *1797*, 897–906.

Darley-Usmar, V. (2004). The powerhouse takes control of the cell; the role of mitochondria in signal transduction. Free Radic. Biol. Med. *37*, 753–754.

Darvall, K.A.L., Sam, R.C., Silverman, S.H., Bradbury, A.W., and Adam, D.J. (2007). Obesity and Thrombosis. Eur. J. Vasc. Endovasc. Surg. *33*, 223–233.

Davidge, S.T. (2001). Prostaglandin H Synthase and Vascular Function. Circ. Res. *89*, 650–660.

Davidson, S.M., and Duchen, M.R. (2007). Endothelial mitochondria: contributing to vascular function and disease. Circ. Res. *100*, 1128–1141.

De Bock, K., Georgiadou, M., and Carmeliet, P. (2013). Role of Endothelial Cell Metabolism in Vessel Sprouting. Cell Metab. *18*, 634–647.

DeFronzo, R.A. (2010). Insulin resistance, lipotoxicity, type 2 diabetes and atherosclerosis: the missing links. The Claude Bernard Lecture 2009. Diabetologia *53*, 1270–1287.

deMello, D.E., Sawyer, D., Galvin, N., and Reid, L.M. (1997). Early fetal development of lung vasculature. Am. J. Respir. Cell Mol. Biol. *16*, 568–581.

Dere, E., De Souza Silva, M.A., Topic, B., Fiorillo, C., Li, J.S., Sadile, A.G., Frisch, C., and Huston, J.P. (2002). Aged endothelial nitric oxide synthase knockout mice exhibit higher mortality concomitant with impaired open-field habituation and alterations in forebrain neurotransmitter levels. Genes. Brain. Behav. *1*, 204–213.

Detmer, S.A., and Chan, D.C. (2007). Functions and dysfunctions of mitochondrial dynamics. Nat. Rev. Mol. Cell Biol. *8*, 870–879.

Devendra, D., Liu, E., and Eisenbarth, G.S. (2004). Type 1 diabetes: recent developments. BMJ *328*, 750–754.

Dhawan, V. (2014). Reactive Oxygen and Nitrogen Species: General Considerations. (Humana Press, New York, NY), p.

Donath, M.Y., and Halban, P.A. (2004). Decreased beta-cell mass in diabetes: significance, mechanisms and therapeutic implications. Diabetologia *47*, 581–589.

REFERENCES

Doughan, A.K., Harrison, D.G., and Dikalov, S.I. (2008). Molecular Mechanisms of Angiotensin II–Mediated Mitochondrial Dysfunction. Circ. Res. *102*, 488–496.

Draoui, N., De Zeeuw, P., and Carmeliet, P. (2017). Angiogenesis revisited from a metabolic perspective: Role and therapeutic implications of endothelial cell metabolism. Open Biol. *7*.

Dröge, W. (2002). Free Radicals in the Physiological Control of Cell Function. Physiol. Rev. *82*, 47–95.

Dubey, A., Forster, M.J., Lal, H., and Sohal, R.S. (1996). Effect of Age and Caloric Intake on Protein Oxidation in Different Brain Regions and on Behavioral Functions of the Mouse. Arch. Biochem. Biophys. *333*, 189–197.

Duncan, J.G. (2008). Lipotoxicity: what is the fate of fatty acids? J. Lipid Res. *49*, 1375–1376.

Duplain, H., Burcelin, R., Sartori, C., Cook, S., Egli, M., Lepori, M., Vollenweider, P., Pedrazzini, T., Nicod, P., Thorens, B., et al. (2001). Insulin Resistance, Hyperlipidemia, and Hypertension in Mice Lacking Endothelial Nitric Oxide Synthase. Circulation *104*, 342–345.

Eckel, R.H., Grundy, S.M., and Zimmet, P.Z. (2005). The metabolic syndrome. Lancet *365*, 1415–1428.

Eelen, G., de Zeeuw, P., Treps, L., Harjes, U., Wong, B.W., and Carmeliet, P. (2018). Endothelial Cell Metabolism. Physiol. Rev. *98*, 3–58.

Egan, K., and FitzGerald, G.A. (2006). Eicosanoids and the vascular endothelium. Handb. Exp. Pharmacol. 189–211.

Ennaceur, A., and Meliani, K. (1992). A new one-trial test for neurobiological studies of memory in rats. III. Spatial vs. non-spatial working memory. Behav. Brain Res. *51*, 83–92.

Erdei, N., Tóth, A., Pásztor, E.T., Papp, Z., Édes, I., Koller, A., and Bagi, Z. (2006). High-fat diet-induced reduction in nitric oxide-dependent arteriolar dilation in rats: role of xanthine oxidase-derived superoxide anion. Am. J. Physiol. Circ. Physiol. *291*, H2107–H2115.

Erdos, B., Snipes, J.A., Miller, A.W., and Busija, D.W. (2004). Cerebrovascular Dysfunction in Zucker Obese Rats Is Mediated by Oxidative Stress and Protein Kinase C. Diabetes *53*, 1352–1359.

Erdös, B., Snipes, J.A., Tulbert, C.D., Katakam, P., Miller, A.W., and Busija, D.W. (2006). Rosuvastatin improves cerebrovascular function in Zucker obese rats by inhibiting NAD(P)H oxidase-dependent superoxide production. Am. J. Physiol. Circ. Physiol. *290*, H1264–H1270.

Eura, Y., Ishihara, N., Yokota, S., and Mihara, K. (2003). Two Mitofusin Proteins, Mammalian Homologues of FZO, with Distinct Functions Are Both Required for Mitochondrial Fusion. J. Biochem. *134*, 333–344.

Fadini, G.P., Sartore, S., Agostini, C., and Avogaro, A. (2007). Significance of Endothelial Progenitor Cells in Subjects With Diabetes. Diabetes Care *30*, 1305–1313.

Fagot-Campagna, A., Narayan, K.M., and Imperatore, G. (2001). Type 2 diabetes in children. BMJ *322*, 377–378.

Fang, L., Choi, S.-H., Baek, J.S., Liu, C., Almazan, F., Ulrich, F., Wiesner, P., Taleb, A., Deer, E., Pattison, J., et al. (2013). Control of angiogenesis by AIBP-mediated cholesterol efflux. Nature *498*, 118–122.

Fawcett, D.W. (1975). The mammalian spermatozoon. Dev. Biol. *44*, 394–436.

Ferrara, N., and Kerbel, R.S. (2005). Angiogenesis as a therapeutic target. Nature *438*, 967–974.

Ferri, C., Bellini, C., Desideri, G., Baldoncini, R., Properzi, G., Santucci, A., and De Mattia, G. (2009). Circulating endothelin-1 levels in obese patients with the metabolic syndrome. Exp. Clin. Endocrinol. Diabetes *105*, 38–40.

Filadi, R., Pendin, D., and Pizzo, P. (2018). Mitofusin 2: from functions to disease. Cell Death Dis. *9*, 330.

Fischer, K.E., Hoffman, J.M., Sloane, L.B., Gelfond, J.A.L., Soto, V.Y., Richardson, A.G., and Austad, S.N. (2016). A cross-sectional study of male and female C57BL/6Nia mice suggests lifespan and healthspan are not necessarily correlated. Aging (Albany. NY). *8*, 2370–2391.

Flegal, K.M., Williamson, D.F., Pamuk, E.R., and Rosenberg, H.M. (2004). Estimating deaths attributable to obesity in the United States. Am. J. Public Health *94*, 1486–1489.

Fontana, L., Partridge, L., and Longo, V.D. (2010). Extending healthy life span--from yeast to humans. Science *328*, 321–326.

Forbes, M.S., Thornhill, B.A., Park, M.H., and Chevalier, R.L. (2007). Lack of endothelial nitric-oxide synthase leads to progressive focal renal injury. Am. J. Pathol. *170*, 87–99.

Ford, E.S., Williamson, D.F., and Liu, S. (1997). Weight Change and Diabetes Incidence: Findings from a National Cohort of US Adults. Am. J. Epidemiol. *146*, 214–222.

Frezza, C., Cipolat, S., Martins de Brito, O., Micaroni, M., Beznoussenko, G. V., Rudka, T., Bartoli,

REFERENCES

D., Polishuck, R.S., Danial, N.N., De Strooper, B., et al. (2006). OPA1 Controls Apoptotic Cristae Remodeling Independently from Mitochondrial Fusion. Cell *126*, 177–189.

Frisbee, J.C., and Stepp, D.W. (2001). Impaired NO-dependent dilation of skeletal muscle arterioles in hypertensive diabetic obese Zucker rats. Am. J. Physiol. Circ. Physiol. *281*, H1304–H1311.

Fruebis, J., Tsao, T.S., Javorschi, S., Ebbets-Reed, D., Erickson, M.R., Yen, F.T., Bihain, B.E., and Lodish, H.F. (2001). Proteolytic cleavage product of 30-kDa adipocyte complement-related protein increases fatty acid oxidation in muscle and causes weight loss in mice. Proc. Natl. Acad. Sci. *98*, 2005–2010.

Furst, A. (1987). Hormetic Effects in Pharmacology. Health Phys. *52*, 527–530.

Furukawa, S., Fujita, T., Shimabukuro, M., Iwaki, M., Yamada, Y., Nakajima, Y., Nakayama, O., Makishima, M., Matsuda, M., and Shimomura, I. (2004). Increased oxidative stress in obesity and its impact on metabolic syndrome. J. Clin. Invest. *114*, 1752–1761.

Galgani, J.E., Moro, C., and Ravussin, E. (2008). Metabolic flexibility and insulin resistance. Am. J. Physiol. Metab. *295*, E1009–E1017.

Galili, O., Versari, D., Sattler, K.J., Olson, M.L., Mannheim, D., McConnell, J.P., Chade, A.R., Lerman, L.O., and Lerman, A. (2007). Early experimental obesity is associated with coronary endothelial dysfunction and oxidative stress. Am. J. Physiol. Circ. Physiol. *292*, H904–H911.

Galloway, C.A., and Yoon, Y. (2013). Mitochondrial Morphology in Metabolic Diseases. Antioxid. Redox Signal. *19*, 415–430.

Gao, A.W., Cantó, C., and Houtkooper, R.H. (2014). Mitochondrial response to nutrient availability and its role in metabolic disease. EMBO Mol. Med. *6*, 580–589.

Garlanda, C., and Dejana, E. (1997). Heterogeneity of endothelial cells. Specific markers. Arterioscler. Thromb. Vasc. Biol. *17*, 1193–1202.

Gilkerson, R.W., Selker, J.M.L., and Capaldi, R.A. (2003). The cristal membrane of mitochondria is the principal site of oxidative phosphorylation. FEBS Lett. *546*, 355–358.

Giorgio, M., Migliaccio, E., Orsini, F., Paolucci, D., Moroni, M., Contursi, C., Pelliccia, G., Luzi, L., Minucci, S., Marcaccio, M., et al. (2005). Electron Transfer between Cytochrome c and p66Shc Generates Reactive Oxygen Species that Trigger Mitochondrial Apoptosis. Cell *122*, 221–233.

Golub, A.S., Song, B.K., and Pittman, R.N. (2011). The rate of O_2 loss from mesenteric arterioles

is not unusually high. Am. J. Physiol. Circ. Physiol. *301*, H737–H745.

Goodpaster, B.H., and Sparks, L.M. (2017). Metabolic Flexibility in Health and Disease. Cell Metab. *25*, 1027–1036.

Le Gouill, E., Jimenez, M., Binnert, C., Jayet, P.-Y., Thalmann, S., Nicod, P., Scherrer, U., and Vollenweider, P. (2007). Endothelial nitric oxide synthase (eNOS) knockout mice have defective mitochondrial beta-oxidation. Diabetes *56*, 2690–2696.

Graupera, M., and Claret, M. (2018). Endothelial Cells: New Players in Obesity and Related Metabolic Disorders. Trends Endocrinol. Metab. *29*, 781–794.

Green, D.R., Galluzzi, L., and Kroemer, G. (2014). Metabolic control of cell death. Science (80-.). *345*, 1250256–1250256.

Guzik, T.J., Skiba, D.S., Touyz, R.M., and Harrison, D.G. (2017). The role of infiltrating immune cells in dysfunctional adipose tissue. Cardiovasc. Res. *113*, 1009–1023.

De Guzman, J.M., Ku, G., Fahey, R., Youm, Y.-H., Kass, I., Ingram, D.K., Dixit, V.D., and Kheterpal, I. (2013). Chronic caloric restriction partially protects against age-related alteration in serum metabolome. Age (Dordr). *35*, 1091–1104.

Hagberg, C.E., Falkevall, A., Wang, X., Larsson, E., Huusko, J., Nilsson, I., Van Meeteren, L.A., Samen, E., Lu, L., Vanwildemeersch, M., et al. (2010). Vascular endothelial growth factor B controls endothelial fatty acid uptake. Nature *464*, 917–921.

Hajnóczky, G., Robb-Gaspers, L.D., Seitz, M.B., and Thomas, A.P. (1995). Decoding of cytosolic calcium oscillations in the mitochondria. Cell *82*, 415–424.

Halban, P.A., Polonsky, K.S., Bowden, D.W., Hawkins, M.A., Ling, C., Mather, K.J., Powers, A.C., Rhodes, C.J., Sussel, L., and Weir, G.C. (2014). β-Cell Failure in Type 2 Diabetes: Postulated Mechanisms and Prospects for Prevention and Treatment. Diabetes Care *37*, 1751–1758.

Halberg, N., Khan, T., Trujillo, M.E., Wernstedt-Asterholm, I., Attie, A.D., Sherwani, S., Wang, Z. V., Landskroner-Eiger, S., Dineen, S., Magalang, U.J., et al. (2009). Hypoxia-Inducible Factor 1 Induces Fibrosis and Insulin Resistance in White Adipose Tissue. Mol. Cell. Biol. *29*, 4467–4483.

Halliwell, B., and Gutteridge, J.M.C. (2015). Free Radicals in Biology and Medicine (Oxford University Press).

Harman, D. (1965). The Free Radical Theory of Aging: Effect of Age on Serum Copper Levels. J. Gerontol. *20*, 151–153.

REFERENCES

Harman, D. (1981). The aging process. Proc. Natl. Acad. Sci. *78*, 7124–7128.

Hasegawa, Y., Saito, T., Ogihara, T., Ishigaki, Y., Yamada, T., Imai, J., Uno, K., Gao, J., Kaneko, K., Shimosawa, T., et al. (2012). Blockade of the Nuclear Factor-κB Pathway in the endothelium prevents insulin resistance and prolongs life spans. Circulation *125*, 1122–1133.

Hashimoto, S., Kubota, N., Sato, H., Sasaki, M., Takamoto, I., Kubota, T., Nakaya, K., Noda, M., Ueki, K., and Kadowaki, T. (2015). Insulin receptor substrate-2 (Irs2) in endothelial cells plays a crucial role in insulin secretion. Diabetes *64*, 876–886.

Heiss, C., Rodriguez-Mateos, A., and Kelm, M. (2015). Central Role of eNOS in the Maintenance of Endothelial Homeostasis. Antioxid. Redox Signal. *22*, 1230–1242.

Helmlinger, G., Endo, M., Ferrara, N., Hlatky, L., and Jain, R.K. (2000). Formation of endothelial cell networks. Nature *405*, 139–141.

Herrmann, J.M., and Riemer, J. (2010). The Intermembrane Space of Mitochondria. Antioxid. Redox Signal. *13*, 1341–1358.

Herron, L.A., Hansen, C.S., and Abaci, H.E. (2019). Engineering tissue-specific blood vessels. Bioeng. Transl. Med. *4*.

Hirase, T., and Node, K. (2012). Endothelial dysfunction as a cellular mechanism for vascular failure. Am. J. Physiol. Circ. Physiol. *302*, H499–H505.

Hornsby, A.K.E., Redhead, Y.T., Rees, D.J., Ratcliff, M.S.G., Reichenbach, A., Wells, T., Francis, L., Amstalden, K., Andrews, Z.B., and Davies, J.S. (2016). Short-term calorie restriction enhances adult hippocampal neurogenesis and remote fear memory in a Ghsr-dependent manner. Psychoneuroendocrinology *63*, 198–207.

Hsieh, H.-J., Liu, C.-A., Huang, B., Tseng, A.H., and Wang, D. (2014). Shear-induced endothelial mechanotransduction: the interplay between reactive oxygen species (ROS) and nitric oxide (NO) and the pathophysiological implications. J. Biomed. Sci. *21*, 3.

Huang, C.-J., McAllister, M.J., Slusher, A.L., Webb, H.E., Mock, J.T., and Acevedo, E.O. (2015). Obesity-Related Oxidative Stress: the Impact of Physical Activity and Diet Manipulation. Sport. Med. - Open *1*, 32.

Hudlicka, O., and Brown, D. (1996). Postnatal Growth of the Heart and Its Blood Vessels. J. Vasc. Res. *33*, 266–287.

Hussain, Z., and Khan, J.A. (2017). Food intake regulation by leptin: Mechanisms mediating

gluconeogenesis and energy expenditure. Asian Pac. J. Trop. Med.

International Diabetes Federation (2017). IDF Diabetes Atlas 8th Edition Country.

Ishihara, N., Eura, Y., and Mihara, K. (2004). Mitofusin 1 and 2 play distinct roles in mitochondrial fusion reactions via GTPase activity. J. Cell Sci. *117*, 6535–6546.

Ishihara, N., Fujita, Y., Oka, T., and Mihara, K. (2006). Regulation of mitochondrial morphology through proteolytic cleavage of OPA1. EMBO J. *25*, 2966–2977.

Jabs, M., Rose, A.J., Lehmann, L.H., Taylor, J., Moll, I., Sijmonsma, T.P., Herberich, S.E., Sauer, S.W., Poschet, G., Federico, G., et al. (2018). Inhibition of Endothelial Notch Signaling Impairs Fatty Acid Transport and Leads to Metabolic and Vascular Remodeling of the Adult Heart. Circulation *137*, 2592–2608.

Jaffe, E.A. (1987). Cell biology of endothelial cells. Hum. Pathol. *18*, 234–239.

Jheng, H.-F., Huang, S.-H., Kuo, H.-M., Hughes, M.W., and Tsai, Y.-S. (2015). Molecular insight and pharmacological approaches targeting mitochondrial dynamics in skeletal muscle during obesity. Ann. N. Y. Acad. Sci. *1350*, 82–94.

Ji, L.L. (1999). Antioxidants and Oxidative Stress in Exercise. Proc. Soc. Exp. Biol. Med. *222*, 283–292.

Jiang, S., Nandy, P., Wang, W., Ma, X., Hsia, J., Wang, C., Wang, Z., Niu, M., Siedlak, S.L., Torres, S., et al. (2018). Mfn2 ablation causes an oxidative stress response and eventual neuronal death in the hippocampus and cortex. Mol. Neurodegener. *13*.

Jiang, T., Liebman, S.E., Lucia, M.S., Phillips, C.L., and Levi, M. (2005). Calorie Restriction Modulates Renal Expression of Sterol Regulatory Element Binding Proteins, Lipid Accumulation, and Age-Related Renal Disease. J. Am. Soc. Nephrol. *16*, 2385–2394.

Johnson, I.T., and Lund, E.K. (2007). Review article: nutrition, obesity and colorectal cancer. Aliment. Pharmacol. Ther. *26*, 161–181.

Kabirian, F., Amoabediny, G., Haghighipour, N., Salehi-Nik, N., and Zandieh-Doulabi, B. (2015). Nitric oxide secretion by endothelial cells in response to fluid shear stress, aspirin, and temperature. J. Biomed. Mater. Res. - Part A *103*, 1231–1237.

Kähler, J., Ewert, A., Weckmüller, J., Stobbe, S., Mittmann, C., Köster, R., Paul, M., Meinertz, T., and Münzel, T. (2001). Oxidative Stress Increases Endothelin-1 Synthesis in Human Coronary Artery Smooth Muscle Cells. J. Cardiovasc. Pharmacol. *38*, 49–57.

REFERENCES

Kahn, C.R. (1994). Insulin Action, Diabetogenes, and the Cause of Type II Diabetes. Diabetes *43*, 1066–1085.

Kajimoto, Y., and Kaneto, H. (2004). Role of Oxidative Stress in Pancreatic β-Cell Dysfunction. In Mitochondrial Pathogenesis, (Berlin, Heidelberg: Springer Berlin Heidelberg), pp. 168–176.

Kalucka, J., Bierhansl, L., Conchinha, N.V., Missiaen, R., Elia, I., Brüning, U., Scheinok, S., Treps, L., Cantelmo, A.R., Dubois, C., et al. (2018). Quiescent Endothelial Cells Upregulate Fatty Acid β-Oxidation for Vasculoprotection via Redox Homeostasis. Cell Metab. *28*, 881-894.e13.

Kaludercic, N., Takimoto, E., Nagayama, T., Feng, N., Lai, E.W., Bedja, D., Chen, K., Gabrielson, K.L., Blakely, R.D., Shih, J.C., et al. (2010). Monoamine Oxidase A–Mediated Enhanced Catabolism of Norepinephrine Contributes to Adverse Remodeling and Pump Failure in Hearts With Pressure Overload. Circ. Res. *106*, 193–202.

Kanda, T., Brown, J.D., Orasanu, G., Vogel, S., Gonzalez, F.J., Sartoretto, J., Michel, T., and Plutzky, J. (2009). PPARγ in the endothelium regulates metabolic responses to high-fat diet in mice. J. Clin. Invest. *119*, 110–124.

Karpoff, L., Vinet, A., Schuster, I., Oudot, C., Goret, L., Dauzat, M., Obert, P., and Perez-Martin, A. (2009). Abnormal vascular reactivity at rest and exercise in obese boys. Eur. J. Clin. Invest. *39*, 94–102.

Kelley, D.E. (2002). Dysfunction of Mitochondria in Human Skeletal Muscle in Type 2 Diabetes. Diabetes *51*, 2944–2950.

Kelley, D.E., and Mandarino, L.J. (2000). Fuel selection in human skeletal muscle in insulin resistance: a reexamination. Diabetes *49*, 677–683.

Kelley, D.E., Goodpaster, B., Wing, R.R., and Simoneau, J.-A. (1999). Skeletal muscle fatty acid metabolism in association with insulin resistance, obesity, and weight loss. Am. J. Physiol. Metab. *277*, E1130–E1141.

Ketonen, J., Pilvi, T., and Mervaala, E. (2010a). Caloric restriction reverses high-fat diet-induced endothelial dysfunction and vascular superoxide production in C57Bl/6 mice. Heart Vessels *25*, 254–262.

Ketonen, J., Shi, J., Martonen, E., and Mervaala, E. (2010b). Periadventitial adipose tissue promotes endothelial dysfunction via oxidative stress in diet-induced obese C57Bl/6 mice. Circ. J. *74*, 1479–1487.

Kharroubi, A.T., and Darwish, H.M. (2015). Diabetes mellitus: The epidemic of the century. World J. Diabetes *6*, 850–867.

Kim, F., Tysseling, K.A., Rice, J., Pham, M., Haji, L., Gallis, B.M., Baas, A.S., Paramsothy, P., Giachelli, C.M., Corson, M.A., et al. (2005). Free Fatty Acid Impairment of Nitric Oxide Production in Endothelial Cells Is Mediated by IKKβ. Arterioscler. Thromb. Vasc. Biol. *25*, 989–994.

Kim, F., Pham, M., Luttrell, I., Bannerman, D.D., Tupper, J., Thaler, J., Hawn, T.R., Raines, E.W., and Schwartz, M.W. (2007). Toll-Like Receptor-4 Mediates Vascular Inflammation and Insulin Resistance in Diet-Induced Obesity. Circ. Res. *100*, 1589–1596.

Kim, F., Pham, M., Maloney, E., Rizzo, N.O., Morton, G.J., Wisse, B.E., Kirk, E.A., Chait, A., and Schwartz, M.W. (2008). Vascular Inflammation, Insulin Resistance, and Reduced Nitric Oxide Production Precede the Onset of Peripheral Insulin Resistance. Arterioscler. Thromb. Vasc. Biol. *28*, 1982–1988.

Kim, J., Montagnani, M., Koh, K.K., and Quon, M.J. (2006). Reciprocal Relationships Between Insulin Resistance and Endothelial Dysfunction. Circulation *113*, 1888–1904.

Kim, S.-H., Park, H.-S., Hong, M.J., Yoo, J.Y., Lee, H., Lee, J.A., Hur, J., Kwon, D.Y., and Kim, M.-S. (2016). Tongqiaohuoxue decoction ameliorates obesity-induced inflammation and the prothrombotic state by regulating adiponectin and plasminogen activator inhibitor-1. J. Ethnopharmacol. *192*, 201–209.

Kleikers, P.W.., Dao, V.., Göb, E., Hooijmans, C., Debets, J., van Essen, H., Kleinschnitz, C., and Schmidt, H.H.H.. (2014). SFRR-E Young Investigator AwardeeNOXing out stroke: Identification of NOX4 and 5as targets in blood-brain-barrier stabilisation and neuroprotection. Free Radic. Biol. Med. *75*, S16.

Kluge, M.A. (2013). Mitochondria and Endothelial Function. Circ. Res. *112*, 1171–1188.

Knudson, J.D., Dincer, Ü.D., Zhang, C., Swafford, A.N., Koshida, R., Picchi, A., Focardi, M., Dick, G.M., and Tune, J.D. (2005). Leptin receptors are expressed in coronary arteries, and hyperleptinemia causes significant coronary endothelial dysfunction. Am. J. Physiol. Circ. Physiol. *289*, H48–H56.

Kobayasi, R., Akamine, E.H., Davel, A.P., Rodrigues, M.A., Carvalho, C.R., and Rossoni, L. V (2010). Oxidative stress and inflammatory mediators contribute to endothelial dysfunction in high-fat diet-induced obesity in mice. J. Hypertens. *28*, 2111–2119.

Kondoh, H., Lleonart, M.E., Nakashima, Y., Yokode, M., Tanaka, M., Bernard, D., Gil, J., and

REFERENCES

Beach, D. (2007). A High Glycolytic Flux Supports the Proliferative Potential of Murine Embryonic Stem Cells. Antioxid. Redox Signal. *9*, 293–299.

Konishi, M., Sakaguchi, M., Lockhart, S.M., Cai, W., Li, M.E., Homan, E.P., Rask-Madsen, C., and Kahn, C.R. (2017). Endothelial insulin receptors differentially control insulin signaling kinetics in peripheral tissues and brain of mice. Proc. Natl. Acad. Sci. U. S. A. *114*, E8478–E8487.

Kopelman, P.G. (2000). Obesity as a medical problem. Nature *404*, 635–643.

Korda, M., Kubant, R., Patton, S., and Malinski, T. (2008). Leptin-induced endothelial dysfunction in obesity. Am. J. Physiol. Circ. Physiol. *295*, H1514–H1521.

Koshiba, T., Detmer, S.A., Kaiser, J.T., Chen, H., McCaffery, J.M., and Chan, D.C. (2004). Structural Basis of Mitochondrial Tethering by Mitofusin Complexes. Science (80-.). *305*, 858–862.

Kubota, T., Kubota, N., Kumagai, H., Yamaguchi, S., Kozono, H., Takahashi, T., Inoue, M., Itoh, S., Takamoto, I., Sasako, T., et al. (2011). Impaired Insulin Signaling in Endothelial Cells Reduces Insulin-Induced Glucose Uptake by Skeletal Muscle. Cell Metab. *13*, 294–307.

Kulkarni, S.S., Joffraud, M., Boutant, M., Ratajczak, J., Gao, A.W., Maclachlan, C., Isabel Hernandez-Alvarez, M., Raymond, F., Metairon, S., Descombes, P., et al. (2016). Mfn1 Deficiency in the Liver Protects Against Diet-Induced Insulin Resistance and Enhances the Hypoglycemic Effect of Metformin.

Kusminski, C.M., and Scherer, P.E. (2012). Mitochondrial dysfunction in white adipose tissue. Trends Endocrinol. Metab. *23*, 435–443.

Kusminski, C.M., Mcternan, P.G., and Kumar, S. (2005). Role of resistin in obesity, insulin resistance and Type II diabetes. Clin. Sci. *109*, 243–256.

Van Der Laan, M., Horvath, S.E., and Pfanner, N. (2016). Mitochondrial contact site and cristae organizing system This review comes from a themed issue on Cell Organelles. Curr. Opin. Cell Biol. *41*, 33–42.

Lahera, V., de las Heras, N., López-Farré, A., Manucha, W., and Ferder, L. (2017). Role of Mitochondrial Dysfunction in Hypertension and Obesity. Curr. Hypertens. Rep. *19*, 11.

Landmesser, U., Dikalov, S., Price, S.R., McCann, L., Fukai, T., Holland, S.M., Mitch, W.E., and Harrison, D.G. (2003). Oxidation of tetrahydrobiopterin leads to uncoupling of endothelial cell nitric oxide synthase in hypertension. J. Clin. Invest. *111*, 1201–1209.

Laurens, C., Abot, A., Delarue, A., and Knauf, C. (2019). Central Effects of Beta-Blockers May Be

Due to Nitric Oxide and Hydrogen Peroxide Release Independently of Their Ability to Cross the Blood-Brain Barrier. Front. Neurosci. *13*, 33.

Lee, S., Sterky, F.H., Mourier, A., Terzioglu, M., Cullheim, S., Olson, L., and Larsson, N.-G. (2012). Mitofusin 2 is necessary for striatal axonal projections of midbrain dopamine neurons. Hum. Mol. Genet. *21*, 4827–4835.

Leone, T.C., and Kelly, D.P. (2011). Transcriptional control of cardiac fuel metabolism and mitochondrial function. Cold Spring Harb. Symp. Quant. Biol. *76*, 175–182.

Li, J., Zhang, Y., Liu, Y., Shen, T., Zhang, H., Xing, Y., and Zhu, D. (2015). PGC-1α plays a major role in the anti-apoptotic effect of 15-HETE in pulmonary artery endothelial cells. Respir. Physiol. Neurobiol. *205*, 84–91.

Li, T.-B., Zhang, J.-J., Liu, B., Liu, W.-Q., Wu, Y., Xiong, X.-M., Luo, X.-J., Ma, Q.-L., and Peng, J. (2016). Involvement of NADPH oxidases and non-muscle myosin light chain in senescence of endothelial progenitor cells in hyperlipidemia. Naunyn. Schmiedebergs. Arch. Pharmacol. *389*, 289–302.

Liesa, M., and Shirihai, O.S. (2013). Mitochondrial Dynamics in the Regulation of Nutrient Utilization and Energy Expenditure. Cell Metab. *17*, 491–506.

Liesa, M., Palacín, M., and Zorzano, A. (2009). Mitochondrial Dynamics in Mammalian Health and Disease. Physiol. Rev. *89*, 799–845.

Lin, S.-J., Defossez, P.A., and Guarente, L. (2000). Requirement of NAD and SIR2 for Life-Span Extension by Calorie Restriction in Saccharomyces cerevisiae. Science (80-.). *289*, 2126–2128.

Lind, L., Siegbahn, A., Ingelsson, E., Sundström, J., and Ärnlöv, J. (2011). A Detailed Cardiovascular Characterization of Obesity Without the Metabolic Syndrome. Arterioscler. Thromb. Vasc. Biol. *31*, e27-34.

Liu, R., Jin, P., LiqunYu, L., Wang, Y., Han, L., Shi, T., Li, X., and Li, X. (2014). Impaired Mitochondrial Dynamics and Bioenergetics in Diabetic Skeletal Muscle. PLoS One *9*, e92810.

Liu, Y., Li, H., Bubolz, A.H., Zhang, D.X., and Gutterman, D.D. (2008). Endothelial cytoskeletal elements are critical for flow-mediated dilation in human coronary arterioles. Med. Biol. Eng. Comput. *46*, 469–478.

Lobato, N.S., Filgueira, F.P., Akamine, E.H., Davel, A.P.C., Rossoni, L.V., Tostes, R.C., Carvalho, M.H.C., and Fortes, Z.B. (2011). Obesity induced by neonatal treatment with monosodium

glutamate impairs microvascular reactivity in adult rats: Role of NO and prostanoids. Nutr. Metab. Cardiovasc. Dis. *21*, 808–816.

Lohmann, R., Souba, W.W., and Bode, B.P. (1999). Rat liver endothelial cell glutamine transporter and glutaminase expression contrast with parenchymal cells. Am. J. Physiol. Liver Physiol. *276*, G743–G750.

Lugus, J.J., Ngoh, G.A., Bachschmid, M.M., and Walsh, K. (2011). Mitofusins are required for angiogenic function and modulate different signaling pathways in cultured endothelial cells. J. Mol. Cell. Cardiol. *51*, 885–893.

Maahs, D.M., West, N.A., Lawrence, J.M., and Mayer-Davis, E.J. (2010). Epidemiology of Type 1 Diabetes. Endocrinol. Metab. Clin. North Am. *39*, 481–497.

Maedler, K., Sergeev, P., Ris, F., Oberholzer, J., Joller-Jemelka, H.I., Spinas, G.A., Kaiser, N., Halban, P.A., and Donath, M.Y. (2002). Glucose-induced β cell production of IL-1β contributes to glucotoxicity in human pancreatic islets. J. Clin. Invest. *110*, 851–860.

Mahdaviani, K., Benador, I.Y., Su, S., Gharakhanian, R.A., Stiles, L., Trudeau, K.M., Cardamone, M., Enríquez-Zarralanga, V., Ritou, E., Aprahamian, T., et al. (2017). Mfn2 deletion in brown adipose tissue protects from insulin resistance and impairs thermogenesis. EMBO Rep. *18*, 1123.

Mai, S., Klinkenberg, M., Auburger, G., Bereiter-Hahn, J., and Jendrach, M. (2010). Decreased expression of Drp1 and Fis1 mediates mitochondrial elongation in senescent cells and enhances resistance to oxidative stress through PINK1. J. Cell Sci. *123*, 917–926.

Mancini, G., Pirruccio, K., Yang, X., Bl€, M., Rodeheffer, M., and Horvath, T.L. (2019). Mitofusin 2 in Mature Adipocytes Controls Adiposity and Body Weight In Brief. Cell Rep. *26*.

Marchesi, C., Ebrahimian, T., Angulo, O., Paradis, P., and Schiffrin, E.L. (2009). Endothelial Nitric Oxide Synthase Uncoupling and Perivascular Adipose Oxidative Stress and Inflammation Contribute to Vascular Dysfunction in a Rodent Model of Metabolic Syndrome. Hypertension *54*, 1384–1392.

Marcu, R., Jung Choi, Y., Xue, J., Himmelfarb, J., Schwartz, S.M., Zheng, Y., Fortin, C.L., Wang, Y., Nagao, R.J., Xu, J., et al. (2018). Human Organ-Specific Endothelial Cell Heterogeneity.

Maruthur, N.M., Bolen, S., Brancati, F.L., and Clark, J.M. (2009). Obesity and Mammography: A Systematic Review and Meta-Analysis. J. Gen. Intern. Med. *24*, 665–677.

Masoro, E.J. (2000). Caloric restriction and aging: an update. Exp. Gerontol. *35*, 299–305.

Masoro, E.J. (2005). Overview of caloric restriction and ageing. Mech. Ageing Dev. *126*, 913–922.

McCay, C.M., Crowell, M.F., and Maynard, L.A. (1935). The Effect of Retarded Growth Upon the Length of Life Span and Upon the Ultimate Body Size. J. Nutr. *10*, 63–79.

Melo, D. de S., Santos, C.S., Pereira, L.C., Mendes, B.F., Jesus, L.S., Pelaez, J.M.N., Aguilar, E.C., Nascimento, D.R., Martins, A. de S., Magalhães, F. de C., et al. (2019). Refeeding abolishes beneficial effects of severe calorie restriction from birth on adipose tissue and glucose homeostasis of adult rats. Nutrition *66*, 87–93.

Ment, L.R., Stewart, W.B., Fronc, R., Seashore, C., Mahooti, S., Scaramuzzino, D., and Madri, J.A. (1997). Vascular endothelial growth factor mediates reactive angiogenesis in the postnatal developing brain. Brain Res. Dev. Brain Res. *100*, 52–61.

Di Meo, S., Reed, T.T., Venditti, P., and Victor, V.M. (2016). Role of ROS and RNS Sources in Physiological and Pathological Conditions. Oxid. Med. Cell. Longev. *2016*, 1245049.

Méresse, S., Dehouck, M.-P., Delorme, P., Bensaïd, M., Tauber, J.-P., Delbart, C., Fruchart, J.-C., and Cecchelli, R. (1989). Bovine Brain Endothelial Cells Express Tight Junctions and Monoamine Oxidase Activity in Long-Term Culture. J. Neurochem. *53*, 1363–1371.

Mertens, S., Noll, T., Spahr, R., Krutzfeldt, A., and Piper, H.M. (1990). Energetic response of coronary endothelial cells to hypoxia. Am. J. Physiol. Circ. Physiol. *258*, H689–H694.

Meyer, A.A., Kundt, G., Steiner, M., Schuff-Werner, P., and Kienast, W. (2006). Impaired Flow-Mediated Vasodilation, Carotid Artery Intima-Media Thickening, and Elevated Endothelial Plasma Markers in Obese Children: The Impact of Cardiovascular Risk Factors. Pediatrics *117*, 1560–1567.

De Meyer, G.R.Y., Bult, H., Kockx, M.M., and Herman, A.G. (1997). The effect of chronic treatment with NO donors during intimal thickening and fatty streak formation. BioFactors *6*, 209–215.

Minami, T., and Aird, W.C. (2005). Endothelial Cell Gene Regulation. Trends Cardiovasc. Med. *15*, 174.e1-174.e24.

Mishiro, K., Imai, T., Sugitani, S., Kitashoji, A., Suzuki, Y., Takagi, T., Chen, H., Oumi, Y., Tsuruma, K., Shimazawa, M., et al. (2014). Diabetes Mellitus Aggravates Hemorrhagic Transformation after Ischemic Stroke via Mitochondrial Defects Leading to Endothelial Apoptosis. PLoS One *9*, e103818.

REFERENCES

Mokdad, A.H., Ford, E.S., Bowman, B.A., Dietz, W.H., Vinicor, F., Bales, V.S., and Marks, J.S. (2003). Prevalence of Obesity, Diabetes, and Obesity-Related Health Risk Factors, 2001. JAMA *289*, 76.

Mombouli, J.-V., and Vanhoutte, P.M. (1999). Endothelial Dysfunction: From Physiology to Therapy. J. Mol. Cell. Cardiol. *31*, 61–74.

Moncada, S., and Higgs, E.A. (2006). Nitric oxide and the vascular endothelium. Handb. Exp. Pharmacol. 213–254.

Motoshima, H., Wu, X., Mahadev, K., and Goldstein, B.J. (2004). Adiponectin suppresses proliferation and superoxide generation and enhances eNOS activity in endothelial cells treated with oxidized LDL. Biochem. Biophys. Res. Commun. *315*, 264–271.

Muniyappa, R., and Sowers, J.R. (2013). Role of insulin resistance in endothelial dysfunction. Rev. Endocr. Metab. Disord. *14*, 5–12.

Muoio, D.M., and Neufer, P.D. (2012). Lipid-Induced Mitochondrial Stress and Insulin Action in Muscle. Cell Metab. *15*, 595–605.

Murphy, M.P. (2009). How mitochondria produce reactive oxygen species. Biochem. J. *417*, 1–13.

Naderali, E.K., Brown, M.J., Pickavance, L.C., Wilding, J.P., Doyle, P.J., and Williams, G. (2001). Dietary obesity in the rat induces endothelial dysfunction without causing insulin resistance: a possible role for triacylglycerols. Clin. Sci. (Lond). *101*, 499–506.

Nappi, A.J., and Vass, E. (1998). Hydroxyl radical formation resulting from the interaction of nitric oxide and hydrogen peroxide. Biochim. Biophys. Acta *1380*, 55–63.

Neuspiel, M., Zunino, R., Gangaraju, S., Rippstein, P., and McBride, H. (2005). Activated mitofusin 2 signals mitochondrial fusion, interferes with Bax activation, and reduces susceptibility to radical induced depolarization. J. Biol. Chem. *280*, 25060–25070.

Newman, A.B., Yanez, D., Harris, T., Duxbury, A., Enright, P.L., Fried, L.P., and Cardiovascular Study Research Group (2001). Weight change in old age and its association with mortality. J. Am. Geriatr. Soc. *49*, 1309–1318.

Ngoh, G.A., Papanicolaou, K.N., and Walsh, K. (2012). Loss of Mitofusin 2 Promotes Endoplasmic Reticulum Stress. J. Biol. Chem. *287*, 20321–20332.

De Nigris, V., Pujadas, G., La Sala, L., Testa, R., Genovese, S., and Ceriello, A. (2015). Short-term

high glucose exposure impairs insulin signaling in endothelial cells. Cardiovasc. Diabetol. *14*, 114.

Nisoli, E., Clementi, E., Paolucci, C., Cozzi, V., Tonello, C., Sciorati, C., Bracale, R., Valerio, A., Francolini, M., Moncada, S., et al. (2003). Mitochondrial Biogenesis in Mammals: The Role of Endogenous Nitric Oxide. Science (80-.). *299*, 896–899.

Nisoli, E., Tonello, C., Cardile, A., Cozzi, V., Bracale, R., Tedesco, L., Falcone, S., Valerio, A., Cantoni, O., Clementi, E., et al. (2005). Calorie restriction promotes mitochondrial biogenesis by inducing the expression of eNOS. Science *310*, 314–317.

Nolan, D.J., Ginsberg, M., Israely, E., Palikuqi, B., Poulos, M.G., James, D., Ding, B. Sen, Schachterle, W., Liu, Y., Rosenwaks, Z., et al. (2013). Molecular Signatures of Tissue-Specific Microvascular Endothelial Cell Heterogeneity in Organ Maintenance and Regeneration. Dev. Cell *26*, 204–219.

Noland, R.C., Koves, T.R., Seiler, S.E., Lum, H., Lust, R.M., Ilkayeva, O., Stevens, R.D., Hegardt, F.G., and Muoio, D.M. (2009). Carnitine Insufficiency Caused by Aging and Overnutrition Compromises Mitochondrial Performance and Metabolic Control. J. Biol. Chem. *284*, 22840–22852.

Obligado, S.H., and Goldfarb, D.S. (2008). The Association of Nephrolithiasis With Hypertension and Obesity: A Review. Am. J. Hypertens. *21*, 257–264.

Ogata, T., and Murata, F. (1969). Cytological Features of Three Fiber Types in Human Striated Muscle*.

Ogata, T., and Yamasaki, Y. (1985). Scanning electron-microscopic studies on the three-dimensional structure of sarcoplasmic reticulum in the mammalian red, white and intermediate muscle fibers. Cell Tissue Res. *242*, 461–467.

Oldendorf, W.H., Cornford, M.E., and Brown, W.J. (1977). The large apparent work capability of the blood-brain barrier: A study of the mitochondrial content of capillary endothelial cells in brain and other tissues of the rat. Ann. Neurol. *1*, 409–417.

Olichon, A., Baricault, L., Gas, N., Guillou, E., Valette, A., Belenguer, P., and Lenaers, G. (2003). Loss of OPA1 perturbates the mitochondrial inner membrane structure and integrity, leading to cytochrome c release and apoptosis. J. Biol. Chem. *278*, 7743–7746.

Osellame, L.D., Blacker, T.S., and Duchen, M.R. (2012). Cellular and molecular mechanisms of mitochondrial function. Best Pract. Res. Clin. Endocrinol. Metab. *26*, 711–723.

REFERENCES

Ouchi, N., Kihara, S., Arita, Y., Okamoto, Y., Maeda, K., Kuriyama, H., Hotta, K., Nishida, M., Takahashi, M., Muraguchi, M., et al. (2000). Adiponectin, an adipocyte-derived plasma protein, inhibits endothelial NF-kappaB signaling through a cAMP-dependent pathway. Circulation *102*, 1296–1301.

Ouchi, N., Parker, J.L., Lugus, J.J., and Walsh, K. (2011). Adipokines in inflammation and metabolic disease. Nat. Rev. Immunol. *11*, 85–97.

Ouedraogo, R., Gong, Y., Berzins, B., Wu, X., Mahadev, K., Hough, K., Chan, L., Goldstein, B.J., and Scalia, R. (2007). Adiponectin deficiency increases leukocyte-endothelium interactions via upregulation of endothelial cell adhesion molecules in vivo. J. Clin. Invest. *117*, 1718.

Pagliarini, D.J., Calvo, S.E., Chang, B., Sheth, S.A., Vafai, S.B., Ong, S.-E., Walford, G.A., Sugiana, C., Boneh, A., Chen, W.K., et al. (2008). A Mitochondrial Protein Compendium Elucidates Complex I Disease Biology. Cell *134*, 112–123.

Palmer, R.M.J., Ferrige, A.G., and Moncada, S. (1987). Nitric oxide release accounts for the biological activity of endothelium-derived relaxing factor. Nature *327*, 524–526.

Paneni, F., and Cosentino, F. (2012). p66 Shc as the engine of vascular aging. Curr. Vasc. Pharmacol. *10*, 697–699.

Paneni, F., Mocharla, P., Akhmedov, A., Costantino, S., Osto, E., Volpe, M., Lüscher, T.F., and Cosentino, F. (2012). Gene Silencing of the Mitochondrial Adaptor p66 ^{Shc} Suppresses Vascular Hyperglycemic Memory in Diabetes. Circ. Res. *111*, 278–289.

Pangare, M., and Makino, A. (2012). Mitochondrial function in vascular endothelial cell in diabetes. J. Smooth Muscle Res. *48*, 1–26.

Park, J., Lee, J., and Choi, C. (2011). Mitochondrial Network Determines Intracellular ROS Dynamics and Sensitivity to Oxidative Stress through Switching Inter-Mitochondrial Messengers. PLoS One *6*, e23211.

Park, Y., Booth, F.W., Lee, S., Laye, M.J., and Zhang, C. (2012). Physical activity opposes coronary vascular dysfunction induced during high fat feeding in mice. J. Physiol. *590*, 4255–4268.

Patten, I.S., and Arany, Z. (2012). PGC-1 coactivators in the cardiovascular system. Trends Endocrinol. Metab. *23*, 90–97.

Perticone, F., Ceravolo, R., Candigliota, M., Ventura, G., Iacopino, S., Sinopoli, F., and Mattioli, P.L. (2001). Obesity and Body Fat Distribution Induce Endothelial Dysfunction by Oxidative

Stress: Protective Effect of Vitamin C. Diabetes *50*, 159–165.

Pfanner, N., and Wiedemann, N. (2002). Mitochondrial protein import: two membranes, three translocases. Curr. Opin. Cell Biol. *14*, 400–411.

Pfanner, N., van der Laan, M., Amati, P., Capaldi, R.A., Caudy, A.A., Chacinska, A., Darshi, M., Deckers, M., Hoppins, S., Icho, T., et al. (2014). Uniform nomenclature for the mitochondrial contact site and cristae organizing system. J. Cell Biol. *204*, 1083–1086.

Phoebe A.Stapleton (2008). Obesity and vascular dysfunction. Pathophysiology *15*, 79–89.

Pi, X., Xie, L., and Patterson, C. (2018). Emerging roles of vascular endothelium in metabolic homeostasis. Circ. Res. *123*, 477–494.

Picard, F., Kurtev, M., Chung, N., Topark-Ngarm, A., Senawong, T., Machado de Oliveira, R., Leid, M., McBurney, M.W., and Guarente, L. (2004). Sirt1 promotes fat mobilization in white adipocytes by repressing PPAR-γ. Nature *429*, 771–776.

Pierce, G.L., Lesniewski, L.A., Lawson, B.R., Beske, S.D., and Seals, D.R. (2009). Nuclear Factor-κB Activation Contributes to Vascular Endothelial Dysfunction via Oxidative Stress in Overweight/Obese Middle-Aged and Older Humans. Circulation *119*, 1284–1292.

Polet, F., and Feron, O. (2013). Endothelial cell metabolism and tumour angiogenesis: glucose and glutamine as essential fuels and lactate as the driving force. J. Intern. Med. *273*, 156–165.

Porcelli, A.M., Ghelli, A., Zanna, C., Pinton, P., Rizzuto, R., and Rugolo, M. (2005). pH difference across the outer mitochondrial membrane measured with a green fluorescent protein mutant q. Biochem. Biophys. Res. Commun. *326*, 799–804.

Potente, M., and Carmeliet, P. (2017). The Link Between Angiogenesis and Endothelial Metabolism. Annu. Rev. Physiol. *79*, 43–66.

Potente, M., and Mäkinen, T. (2017). Vascular heterogeneity and specialization in development and disease. Nat. Rev. Mol. Cell Biol. *18*, 477–494.

Potente, M., Gerhardt, H., and Carmeliet, P. (2011). Basic and therapeutic aspects of angiogenesis. Cell *146*, 873–887.

Potenza, M.A., Addabbo, F., and Montagnani, M. (2009). Vascular actions of insulin with implications for endothelial dysfunction. Am. J. Physiol. Metab. *297*, E568–E577.

Poulain, M. (2006). The effect of obesity on chronic respiratory diseases: pathophysiology and

therapeutic strategies. Can. Med. Assoc. J. *174*, 1293–1299.

Prieto, D., Kaminski, P.M., Bagi, Z., Ahmad, M., and Wolin, M.S. (2010). Hypoxic relaxation of penile arteries: involvement of endothelial nitric oxide and modulation by reactive oxygen species. Am. J. Physiol. Circ. Physiol. *299*, H915–H924.

Procopio, C., Andreozzi, F., Laratta, E., Cassese, A., Beguinot, F., Arturi, F., Hribal, M.L., Perticone, F., and Sesti, G. (2009). Leptin-Stimulated Endothelial Nitric-Oxide Synthase via an Adenosine 5'-Monophosphate-Activated Protein Kinase/Akt Signaling Pathway Is Attenuated by Interaction with C-Reactive Protein. Endocrinology *150*, 3584–3593.

Quintero, M., Colombo, S.L., Godfrey, A., and Moncada, S. (2006). Mitochondria as signaling organelles in the vascular endothelium. Proc. Natl. Acad. Sci. *103*, 5379–5384.

Racette, S.B., Weiss, E.P., Villareal, D.T., Arif, H., Steger-May, K., Schechtman, K.B., Fontana, L., Klein, S., Holloszy, J.O., and Washington University School of Medicine CALERIE Group (2006). One Year of Caloric Restriction in Humans: Feasibility and Effects on Body Composition and Abdominal Adipose Tissue. Journals Gerontol. Ser. A Biol. Sci. Med. Sci. *61*, 943–950.

Radu, M., and Chernoff, J. (2013). An in vivo assay to test blood vessel permeability. J. Vis. Exp. e50062.

Rajendran, P., Rengarajan, T., Thangavel, J., Nishigaki, Y., Sakthisekaran, D., Sethi, G., and Nishigaki, I. (2013). The vascular endothelium and human diseases. Int. J. Biol. Sci. *9*, 1057–1069.

Ramírez, S., Gómez-Valadés, A.G., Schneeberger, M., Varela, L., Haddad-Tóvolli, R., Altirriba, J., Noguera, E., Drougard, A., Flores-Martínez, Á., Imbernón, M., et al. (2017). Mitochondrial Dynamics Mediated by Mitofusin 1 Is Required for POMC Neuron Glucose-Sensing and Insulin Release Control. Cell Metab. *25*, 1390-1399.e6.

Rausch, M.E., Weisberg, S., Vardhana, P., and Tortoriello, D. V (2008). Obesity in C57BL/6J mice is characterized by adipose tissue hypoxia and cytotoxic T-cell infiltration. Int. J. Obes. *32*, 451–463.

Redman, L.M., Smith, S.R., Burton, J.H., Martin, C.K., Il'yasova, D., and Ravussin, E. (2018). Metabolic Slowing and Reduced Oxidative Damage with Sustained Caloric Restriction Support the Rate of Living and Oxidative Damage Theories of Aging. Cell Metab. *27*, 805-815.e4.

Reinehr, T. (2013). Type 2 diabetes mellitus in children and adolescents. World J. Diabetes *4*, 270.

Reis, A., Hauache, O., and Velho, G. (2005). Vitamin D endocrine system and the genetic susceptibility to diabetes, obesity and vascular disease. A review of evidence. Diabetes Metab. *31*, 318–325.

Risau, W., and Flamme, I. (1995). Vasculogenesis. Annu. Rev. Cell Dev. Biol. *11*, 73–91.

Ristow, M., and Schmeisser, K. (2014). Mitohormesis: Promoting health and lifespan by increased levels of reactive oxygen species (ROS). Dose-Response *12*, 288–341.

Rizzuto, R., Pinton, P., Carrington, W., Fay, F.S., Fogarty, K.E., Lifshitz, L.M., Tuft, R.A., and Pozzan, T. (1998). Close Contacts with the Endoplasmic Reticulum as Determinants of Mitochondrial Ca2+ Responses. Science (80-.). *280*, 1763–1766.

Robbins, S.L. (Stanley L., Kumar, V., and Cotran, R.S. (2010). Robbins and Cotran pathologic basis of disease. (Saunders/Elsevier).

Robciuc, M.R., Kivelä, R., Williams, I.M., Wasserman, D.H., Groen, A.K., and Alitalo, K. (2016). VEGFB/VEGFR1-Induced Expansion of Adipose Vasculature Counteracts Obesity and Related Metabolic Complications. Cell Metab. *23*, 712–724.

Robertson, R.P. (1995). Antagonist: diabetes and insulin resistance--philosophy, science, and the multiplier hypothesis. J. Lab. Clin. Med. *125*, 560–564; discussion 565.

Rogge, M.M. (2009). The Role of Impaired Mitochondrial Lipid Oxidation in Obesity. Biol. Res. Nurs. *10*, 356–373.

Rönnemaa, T., Karonen, S.L., Rissanen, A., Koskenvuo, M., and Koivisto, V.A. (1997). Relation between plasma leptin levels and measures of body fat in identical twins discordant for obesity. Ann. Intern. Med. *126*, 26–31.

Roth, G.S., Ingram, D.K., and Lane, M.A. (2006). Caloric Restriction in Primates and Relevance to Humans. Ann. N. Y. Acad. Sci. *928*, 305–315.

Rudnicki, M., Abdifarkosh, G., Nwadozi, E., Ramos, S. V., Makki, A., Sepa-Kishi, D.M., Ceddia, R.B., Perry, C.G.R., Roudier, E., and Haas, T.L. (2018). Endothelial-specific FoxO1 depletion prevents obesity-related disorders by increasing vascular metabolism and growth. Elife *7*.

Rupnick, M.A., Panigrahy, D., Zhang, C.Y., Dallabrida, S.M., Lowell, B.B., Langer, R., and Folkman, M.J. (2002). Adipose tissue mass can be regulated through the vasculature. Proc. Natl. Acad. Sci. U. S. A. *99*, 10730–10735.

Ryan, M.T., and Hoogenraad, N.J. (2007). Mitochondrial-Nuclear Communications. Annu. Rev.

REFERENCES

Biochem. *76*, 701–722.

Salgado-Somoza, A., Teijeira-Fernández, E., Fernández, Á.L., González-Juanatey, J.R., and Eiras, S. (2010). Proteomic analysis of epicardial and subcutaneous adipose tissue reveals differences in proteins involved in oxidative stress. Am. J. Physiol. Circ. Physiol. *299*, H202–H209.

Salvatore, M.F., Terrebonne, J., Fields, V., Nodurft, D., Runfalo, C., Latimer, B., and Ingram, D.K. (2016). Initiation of calorie restriction in middle-aged male rats attenuates aging-related motoric decline and bradykinesia without increased striatal dopamine. Neurobiol. Aging *37*, 192–207.

Sánchez, A., Contreras, C., Martínez, M.P., Climent, B., Benedito, S., García-Sacristán, A., Hernández, M., and Prieto, D. (2012). Role of Neural NO Synthase (nNOS) Uncoupling in the Dysfunctional Nitrergic Vasorelaxation of Penile Arteries from Insulin-Resistant Obese Zucker Rats. PLoS One *7*, e36027.

Sansbury, B.E., Cummins, T.D., Tang, Y., Hellmann, J., Holden, C.R., Harbeson, M.A., Chen, Y., Patel, R.P., Spite, M., Bhatnagar, A., et al. (2012). Overexpression of Endothelial Nitric Oxide Synthase Prevents Diet-Induced Obesity and Regulates Adipocyte Phenotype. Circ. Res. *111*, 1176–1189.

Santel, A., and Fuller, M.T. (2001). Control of mitochondrial morphology by a human mitofusin. J. Cell Sci. *114*, 867–874.

Santel, A., Frank, S., Gaume, B., Herrler, M., Youle, R.J., and Fuller, M.T. (2003). Mitofusin-1 protein is a generally expressed mediator of mitochondrial fusion in mammalian cells. J. Cell Sci. *114*, 867–874.

Santillo, M., Colantuoni, A., Mondola, P., Guida, B., and Damiano, S. (2015). NOX signaling in molecular cardiovascular mechanisms involved in the blood pressure homeostasis. Front. Physiol. *6*, 194.

Sanz, E., Yang, L., Su, T., Morris, D.R., McKnight, G.S., and Amieux, P.S. (2009). Cell-type-specific isolation of ribosome-associated mRNA from complex tissues. Proc. Natl. Acad. Sci. U. S. A. *106*, 13939–13944.

Sawada, N., Jiang, A., Takizawa, F., Safdar, A., Manika, A., Tesmenitsky, Y., Kang, K.-T., Bischoff, J., Kalwa, H., Sartoretto, J.L., et al. (2014). Endothelial PGC-1a Mediates Vascular Dysfunction in Diabetes. Cell Metab. *19*, 246–258.

Scheitlin, C.G., Nair, D.M., Crestanello, J.A., Zweier, J.L., and Alevriadou, B.R. (2014). Fluid Mechanical Forces and Endothelial Mitochondria: A Bioengineering Perspective. Cell. Mol.

Bioeng. *7*, 483–496.

Schmidt, O., Pfanner, N., and Meisinger, C. (2010). Mitochondrial protein import: from proteomics to functional mechanisms. Nat. Rev. Mol. Cell Biol. *11*, 655–667.

Schneeberger, M., Dietrich, M.O., Sebastián, D., Imbernón, M., Castaño, C., Garcia, A., Esteban, Y., Gonzalez-Franquesa, A., Rodríguez, I.C., Bortolozzi, A., et al. (2013). Mitofusin 2 in POMC Neurons Connects ER Stress with Leptin Resistance and Energy Imbalance. Cell *155*, 172–187.

Schulz, T.J., Zarse, K., Voigt, A., Urban, N., Birringer, M., and Ristow, M. (2007). Glucose Restriction Extends Caenorhabditis elegans Life Span by Inducing Mitochondrial Respiration and Increasing Oxidative Stress. Cell Metab. *6*, 280–293.

Sebastián, D., Hernández-Alvarez, M.I., Segalés, J., Sorianello, E., Muñoz, J.P., Sala, D., Waget, A., Liesa, M., Paz, J.C., Gopalacharyulu, P., et al. (2012). Mitofusin 2 (Mfn2) links mitochondrial and endoplasmic reticulum function with insulin signaling and is essential for normal glucose homeostasis. PNAS *109*, 5523–5528.

Sebastián, D., Sorianello, E., Segalés, J., Irazoki, A., Ruiz-Bonilla, V., Sala, D., Planet, E., Berenguer-Llergo, A., Pablo Muñoz, J., Sánchez-Feutrie, M., et al. (2016). Mfn2 deficiency links age-related sarcopenia and impaired autophagy to activation of an adaptive mitophagy pathway. EMBO J. *35*, 1677–1693.

Segalés, J., Paz, J.C., Hernández-Alvarez, M.I., Sala, D., Muñoz, J.P., Noguera, E., Pich, S., Palacín, M., Enríquez, J.A., and Zorzano, A. (2013). A form of mitofusin 2 (Mfn2) lacking the transmembrane domains and the COOH-terminal end stimulates metabolism in muscle and liver cells. Am. J. Physiol. Metab. *305*, E1208–E1221.

Seki, T., Hosaka, K., Fischer, C., Lim, S., Andersson, P., Abe, M., Iwamoto, H., Gao, Y., Wang, X., Fong, G.-H., et al. (2018). Ablation of endothelial VEGFR1 improves metabolic dysfunction by inducing adipose tissue browning. J. Exp. Med. *215*, 611–626.

Shenouda, S.M., Widlansky, M.E., Chen, K., Xu, G., Holbrook, M., Tabit, C.E., Hamburg, N.M., Frame, A.A., Caiano, T.L., Kluge, M.A., et al. (2011). Altered mitochondrial dynamics contributes to endothelial dysfunction in diabetes mellitus. Circulation *124*, 444–453.

Shibata, R., Skurk, C., Ouchi, N., Galasso, G., Kondo, K., Ohashi, T., Shimano, M., Kihara, S., Murohara, T., and Walsh, K. (2008). Adiponectin promotes endothelial progenitor cell number and function. FEBS Lett. *582*, 1607–1612.

Singer, G., and Granger, D.N. (2007). Inflammatory Responses Underlying the Microvascular

REFERENCES

Dysfunction Associated with Obesity and Insulin Resistance. Microcirculation *14*, 375–387.

Singer, B.D., Mock, J.R., D'Alessio, F.R., Aggarwal, N.R., Mandke, P., Johnston, L., and Damarla, M. (2016). Flow-cytometric method for simultaneous analysis of mouse lung epithelial, endothelial, and hematopoietic lineage cells. Am. J. Physiol. - Lung Cell. Mol. Physiol. *310*, L796–L801.

Skulachev, V.P. (2001). Mitochondrial filaments and clusters as intracellular power-transmitting cables. Trends Biochem. Sci. *26*, 23–29.

Sohal, R.S., and Weindruch, R. (1996). Oxidative Stress, Caloric Restriction, and Aging. Science (80-.). *273*, 59–63.

Someya, S., Yu, W., Hallows, W.C., Xu, J., Vann, J.M., Leeuwenburgh, C., Tanokura, M., Denu, J.M., and Prolla, T.A. (2010). Sirt3 Mediates Reduction of Oxidative Damage and Prevention of Age-Related Hearing Loss under Caloric Restriction. Cell *143*, 802–812.

Son, N.H., Basu, D., Samovski, D., Pietka, T.A., Peche, V.S., Willecke, F., Fang, X., Yu, S.Q., Scerbo, D., Chang, H.R., et al. (2018). Endothelial cell CD36 optimizes tissue fatty acid uptake. J. Clin. Invest. *128*, 4329–4342.

Sonntag, W.E., Lenham, J.E., and Ingram, R.L. (1992). Effects of aging and dietary restriction on tissue protein synthesis: relationship to plasma insulin-like growth factor-1. J. Gerontol. *47*, B159-63.

Sorescu, G.P., Song, H., Tressel, S.L., Hwang, J., Dikalov, S., Smith, D.A., Boyd, N.L., Platt, M.O., Lassègue, B., Griendling, K.K., et al. (2004). Bone Morphogenic Protein 4 Produced in Endothelial Cells by Oscillatory Shear Stress Induces Monocyte Adhesion by Stimulating Reactive Oxygen Species Production From a Nox1-Based NADPH Oxidase. Circ. Res. *95*, 773–779.

Speakman, J.R. (2013). Measuring energy metabolism in the mouse - theoretical, practical, and analytical considerations. Front. Physiol. *4*, 34.

Spiegelman, B.M., and Flier, J.S. (2001). Obesity and the regulation of energy balance. Cell *104*, 531–543.

Stayner, L.T., Dannenberg, A.L., Thun, M., Reeve, G., Bloom, T.F., Boeniger, M., and Halperin, W. (1992). Cardiovascular mortality among munitions workers exposed to nitroglycerin and dinitrotoluene. Scand. J. Work. Environ. Health *18*, 34–43.

Steinberg, H.O., Chaker, H., Leaming, R., Johnson, A., Brechtel, G., and Baron, A.D. (1996).

Obesity/insulin resistance is associated with endothelial dysfunction. Implications for the syndrome of insulin resistance. J. Clin. Invest. *97*, 2601–2610.

Stewarrt, J., Mitchell, J., and Kalant, N. (1989). The effects of life-long food restriction on spatial memory in young and aged Fischer 344 rats measured in the eight-arm radial and the Morris water mazes. Neurobiol. Aging *10*, 669–675.

Stone, J., Itin, A., Alon, T., Pe'er, J., Gnessin, H., Chan-Ling, T., and Keshet, E. (1995). Development of retinal vasculature is mediated by hypoxia-induced vascular endothelial growth factor (VEGF) expression by neuroglia. J. Neurosci. *15*, 4738–4747.

Sung, H.K., Doh, K.O., Son, J.E., Park, J.G., Bae, Y., Choi, S., Nelson, S.M.L., Cowling, R., Nagy, K., Michael, I.P., et al. (2013). Adipose vascular endothelial growth factor regulates metabolic homeostasis through angiogenesis. Cell Metab. *17*, 61–72.

Tahmin Sarnali, T., Moyenuddin Tanjila Tahmin Sarnali, M.P., and Khan, A. (2010). Obesity and Disease Association: A Review. AKMMC *1*, 21–24.

Tan, C.Y., and Vidal-Puig, A. (2008). Adipose tissue expandability: the metabolic problems of obesity may arise from the inability to become more obese. Biochem. Soc. Trans. *36*, 935–940.

Tang, X., Luo, Y.X., Chen, H.Z., and Liu, D.P. (2014). Mitochondria, endothelial cell function, and vascular diseases. Front. Physiol. *5 MAY*.

Touyz, R.M., and Briones, A.M. (2011). Reactive oxygen species and vascular biology: implications in human hypertension. Hypertens. Res. *34*, 5–14.

Traaseth, N., Elfering, S., Solien, J., Haynes, V., and Giulivi, C. (2004). Role of calcium signaling in the activation of mitochondrial nitric oxide synthase and citric acid cycle. Biochim. Biophys. Acta - Bioenerg. *1658*, 64–71.

Triggle, C.R., Samuel, S.M., Ravishankar, S., Marei, I., Arunachalam, G., and Ding, H. (2012). The endothelium: influencing vascular smooth muscle in many ways. Can. J. Physiol. Pharmacol. *90*, 713–738.

Trinei, M., Berniakovich, I., Beltrami, E., Migliaccio, E., Fassina, A., Pelicci, P., and Giorgio, M. (2009). P66Shc signals to age. Aging (Albany. NY). *1*, 503–510.

Tukker, A., Visscher, T., and Picavet, H. (2008). Overweight and health problems of the lower extremities: osteoarthritis, pain and disability. Public Health Nutr. *12*, 1.

Twig, G., Elorza, A., Molina, A.J.A., Mohamed, H., Wikstrom, J.D., Walzer, G., Stiles, L., Haigh,

REFERENCES

S.E., Katz, S., Las, G., et al. (2008). Fission and selective fusion govern mitochondrial segregation and elimination by autophagy. EMBO J. *27*, 433–446.

Ulrich, C.M., Steindorf, K., and Berger, N.A. (2013). Exercise, Energy Balance and Cancer. In Exercise, Energy Balance, and Cancer, (New York, NY: Springer New York), pp. 1–5.

Unger, R.H., and Orci, L. (2001). Diseases of liporegulation: new perspective on obesity and related disorders. FASEB J. *15*, 312–321.

Unterluggauer, H., Mazurek, S., Lener, B., Hütter, E., Eigenbrodt, E., Zwerschke, W., and Jansen-Dürr, P. (2008). Premature senescence of human endothelial cells induced by inhibition of glutaminase. Biogerontology *9*, 247–259.

Urbanavičius, V., Abalikšta, T., Brimas, G., Abraitienė, A., Gogelienė, L., and Strupas, K. (2013). Comparison of Changes in Blood Glucose, Insulin Resistance Indices, and Adipokine Levels in Diabetic and Nondiabetic Subjects With Morbid Obesity After Laparoscopic Adjustable Gastric Banding. Medicina (B. Aires). *49*, 2.

Valle, I., Alvarezbarrientos, A., Arza, E., Lamas, S., and Monsalve, M. (2005). PGC-1α regulates the mitochondrial antioxidant defense system in vascular endothelial cells. Cardiovasc. Res. *66*, 562–573.

Vance, J.E. (1990). Phospholipid synthesis in a membrane fraction associated with mitochondria. J. Biol. Chem. *265*, 7248–7256.

Vandekeere, S., Dewerchin, M., and Carmeliet, P. (2015). Angiogenesis Revisited: An Overlooked Role of Endothelial Cell Metabolism in Vessel Sprouting. Microcirculation *22*, 509–517.

Vane, J.R., and Botting, R.M. (1992). Secretory functions of the vascular endothelium. J. Physiol. Pharmacol. *43*, 195–207.

Vetere, A., Choudhary, A., Burns, S.M., and Wagner, B.K. (2014). Targeting the pancreatic β-cell to treat diabetes. Nat. Rev. Drug Discov. *13*, 278–289.

Vicent, D., Ilany, J., Kondo, T., Naruse, K., Fisher, S.J., Kisanuki, Y.Y., Bursell, S., Yanagisawa, M., King, G.L., and Kahn, C.R. (2003). The role of endothelial insulin signaling in the regulation of vascular tone and insulin resistance. J. Clin. Invest. *111*, 1373–1380.

Vigili de Kreutzenberg, S., Crepaldi, C., Marchetto, S., Calò, L., Tiengo, A., Del Prato, S., and Avogaro, A. (2000). Plasma Free Fatty Acids and Endothelium-Dependent Vasodilation: Effect of Chain-Length and Cyclooxygenase Inhibition. J. Clin. Endocrinol. Metab. *85*, 793–798.

Virdis, A., Santini, F., Colucci, R., Duranti, E., Salvetti, G., Rugani, I., Segnani, C., Anselmino, M., Bernardini, N., Blandizzi, C., et al. (2011). Vascular Generation of Tumor Necrosis Factor-α Reduces Nitric Oxide Availability in Small Arteries From Visceral Fat of Obese Patients. J. Am. Coll. Cardiol. *58*, 238–247.

Virdis, A., Duranti, E., Rossi, C., Dell'Agnello, U., Santini, E., Anselmino, M., Chiarugi, M., Taddei, S., and Solini, A. (2015). Tumour necrosis factor-alpha participates on the endothelin-1/nitric oxide imbalance in small arteries from obese patients: role of perivascular adipose tissue. Eur. Heart J. *36*, 784–794.

Walker, G., Houthoofd, K., Vanfleteren, J.R., and Gems, D. (2005). Dietary restriction in C. elegans: From rate-of-living effects to nutrient sensing pathways. Mech. Ageing Dev. *126*, 929–937.

Wallin, I. (1927). Symbionticism and the origin of species, (Baltimore: Williams & Wilkins Company).

Wang, D.-B., Blocher, N.C., Spence, M.E., Rovainen, C.M., and Woolsey, T.A. (1992). Development and Remodeling of Cerebral Blood Vessels and Their Flow in Postnatal Mice Observed with in vivo Videomicroscopy. J. Cereb. Blood Flow Metab. *12*, 935–946.

van de Weijer, T., Schrauwen-Hinderling, V.B., and Schrauwen, P. (2011). Lipotoxicity in type 2 diabetic cardiomyopathy. Cardiovasc. Res. *92*, 10–18.

Weindruch, R., and Sohal, R.S. (1997). Caloric Intake and Aging. N. Engl. J. Med. *337*, 986–994.

Weir, J.B. d. V. (1949). New methods for calculating metabolic rate with special reference to protein metabolism. J. Physiol. *109*, 1–9.

Weisberg, S.P., McCann, D., Desai, M., Rosenbaum, M., Leibel, R.L., and Ferrante, A.W. (2003). Obesity is associated with macrophage accumulation in adipose tissue. J. Clin. Invest. *112*, 1796–1808.

Westermann, B. (2010). Mitochondrial fusion and fission in cell life and death. Nat. Rev. Mol. Cell Biol. *11*, 872–884.

Westermann, B. (2012). Bioenergetic role of mitochondrial fusion and fission. Biochim. Biophys. Acta - Bioenerg. *1817*, 1833–1838.

WHO-Diabetes (2018). WHO | Diabetes. WHO.

WHO-Obesity (2018). WHO | Obesity. WHO.

REFERENCES

Widlansky, M.E., and Gutterman, D.D. (2011). Regulation of Endothelial Function by Mitochondrial Reactive Oxygen Species. Antioxid. Redox Signal. *15*, 1517–1530.

Wilson, A.M., Harada, R., Nair, N., Balasubramanian, N., and Cooke, J.P. (2007). l -Arginine Supplementation in Peripheral Arterial Disease. Circulation *116*, 188–195.

Witte, A. V., Fobker, M., Gellner, R., Knecht, S., and Floel, A. (2009). Caloric restriction improves memory in elderly humans. Proc. Natl. Acad. Sci. *106*, 1255–1260.

Wolin, M.S. (2000). Interactions of oxidants with vascular signaling systems. Arterioscler. Thromb. Vasc. Biol. *20*, 1430–1442.

Wooley, D.M. (1970). The Midpiece of the Mouse Spermatozoon: Its Form and Development as Seen by Surface Replication. J. Cell Sci. *6*.

Worthen, L.M., and Nollert, M.U. (2000). Intracellular calcium response of endothelial cells exposed to flow in the presence of thrombin or histamine. J. Vasc. Surg. *32*, 593–601.

Wrede, C.E., Dickson, L.M., Lingohr, M.K., Briaud, I., and Rhodes, C.J. (2002). Protein kinase B/Akt prevents fatty acid-induced apoptosis in pancreatic beta-cells (INS-1). J. Biol. Chem. *277*, 49676–49684.

Wright, G.L., Maroulakou, I.G., Eldridge, J., Liby, T.L., Sridharan, V., Tsichlis, P.N., and Muise-Helmericks, R.C. (2008). VEGF stimulation of mitochondrial biogenesis: requirement of AKT3 kinase. FASEB J. *22*, 3264–3275.

Wu, W., Xu, H., Wang, Z., Mao, Y., Yuan, L., Luo, W., Cui, Z., Cui, T., Wang, X.L., and Shen, Y.H. (2015). PINK1-Parkin-Mediated Mitophagy Protects Mitochondrial Integrity and Prevents Metabolic Stress-Induced Endothelial Injury. PLoS One *10*, e0132499.

Xu, A., Wang, Y., Keshaw, H., Xu, L.Y., Lam, K.S.L., and Cooper, G.J.S. (2003). The fat-derived hormone adiponectin alleviates alcoholic and nonalcoholic fatty liver diseases in mice. J. Clin. Invest. *112*, 91–100.

Yamauchi, T., Kamon, J., Waki, H., Terauchi, Y., Kubota, N., Hara, K., Mori, Y., Ide, T., Murakami, K., Tsuboyama-Kasaoka, N., et al. (2001). The fat-derived hormone adiponectin reverses insulin resistance associated with both lipoatrophy and obesity. Nat. Med. *7*, 941–946.

Yang, Y., Xue, L.J., Xue, X., Ou, Z., Jiang, T., and Zhang, Y.D. (2018). MFN2 ameliorates cell apoptosis in a cellular model of parkinson's disease induced by rotenone. Exp. Ther. Med. *16*, 3680–3685.

Yin, J., Gao, Z., He, Q., Zhou, D., Guo, Z., and Ye, J. (2009). Role of hypoxia in obesity-induced disorders of glucose and lipid metabolism in adipose tissue. Am. J. Physiol. Metab. *296*, E333–E342.

Yokoyama, H., Emoto, M., Fujiwara, S., Motoyama, K., Morioka, T., Komatsu, M., Tahara, H., Shoji, T., Okuno, Y., and Nishizawa, Y. (2003). Quantitative insulin sensitivity check index and the reciprocal index of homeostasis model assessment in normal range weight and moderately obese type 2 diabetic patients. Diabetes Care *26*, 2426–2432.

Yokoyama, M., Okada, S., Nakagomi, A., Moriya, J., Shimizu, I., Nojima, A., Yoshida, Y., Ichimiya, H., Kamimura, N., Kobayashi, Y., et al. (2014). Inhibition of endothelial p53 improves metabolic abnormalities related to dietary obesity. CellReports *7*, 1691–1703.

Youle, R.J., and Narendra, D.P. (2011). Mechanisms of mitophagy. Nat. Rev. Mol. Cell Biol. *12*, 9–14.

Yu, B.P. (1996). Aging and oxidative stress: Modulation by dietary restriction. Free Radic. Biol. Med. *21*, 651–668.

Yushkevich, P.A., Piven, J., Hazlett, H.C., Smith, R.G., Ho, S., Gee, J.C., and Gerig, G. (2006). User-guided 3D active contour segmentation of anatomical structures: Significantly improved efficiency and reliability. Neuroimage *31*, 1116–1128.

Zaborska, K.E., Wareing, M., and Austin, C. (2017). Comparisons between perivascular adipose tissue and the endothelium in their modulation of vascular tone. Br. J. Pharmacol. *174*, 3388–3397.

Zaninal, T.A., Oberley, T.D., Allison, D.B., Szweda, L.I., and Weindruch, R. (2000). Caloric restriction of rhesus monkeys lowers oxidative damage in skeletal muscle. FASEB J. *14*, 1825–1836.

Zarse, K., Schmeisser, S., Groth, M., Priebe, S., Beuster, G., Kuhlow, D., Guthke, R., Platzer, M., Kahn, C.R., and Ristow, M. (2012). Impaired insulin/IGF1 signaling extends life span by promoting mitochondrial L-proline catabolism to induce a transient ROS signal. Cell Metab. *15*, 451–465.

Zeeshan, H.M.A., Lee, G.H., Kim, H.-R., and Chae, H.-J. (2016). Endoplasmic Reticulum Stress and Associated ROS. Int. J. Mol. Sci. *17*, 327.

Zembowicz, A., Hecker, M., Macarthur, H., Sessa, W.C., and Vane, J.R. (1991). Nitric oxide and another potent vasodilator are formed from NG-hydroxy-L-arginine by cultured endothelial cells. Proc. Natl. Acad. Sci. U. S. A. *88*, 11172–11176.

REFERENCES

Zheng, J. (2012). Energy metabolism of cancer: Glycolysis versus oxidative phosphorylation (Review). Oncol. Lett. *4*, 1151–1157.

Zorov, D.B., Juhaszova, M., and Sollott, S.J. (2014). Mitochondrial Reactive Oxygen Species (ROS) and ROS-Induced ROS Release. Physiol. Rev. *94*, 909–950.

Zorzano, A., Liesa, M., Sebastián, D., Segalés, J., and Palacín, M. (2010). Mitochondrial fusion proteins: Dual regulators of morphology and metabolism. Semin. Cell Dev. Biol. *21*, 566–574.

Zou, M.-H., Shi, C., and Cohen, R.A. (2002a). Oxidation of the zinc-thiolate complex and uncoupling of endothelial nitric oxide synthase by peroxynitrite. J. Clin. Invest. *109*, 817–826.

Zou, M.-H., Hou, X.-Y., Shi, C.-M., Nagata, D., Walsh, K., and Cohen, R.A. (2002b). Modulation by Peroxynitrite of Akt- and AMP-activated Kinase-dependent Ser ^{1179} Phosphorylation of Endothelial Nitric Oxide Synthase. J. Biol. Chem. *277*, 32552–32557.

(2000). Type 2 diabetes in children and adolescents. American Diabetes Association. Diabetes Care *23*, 381–389.

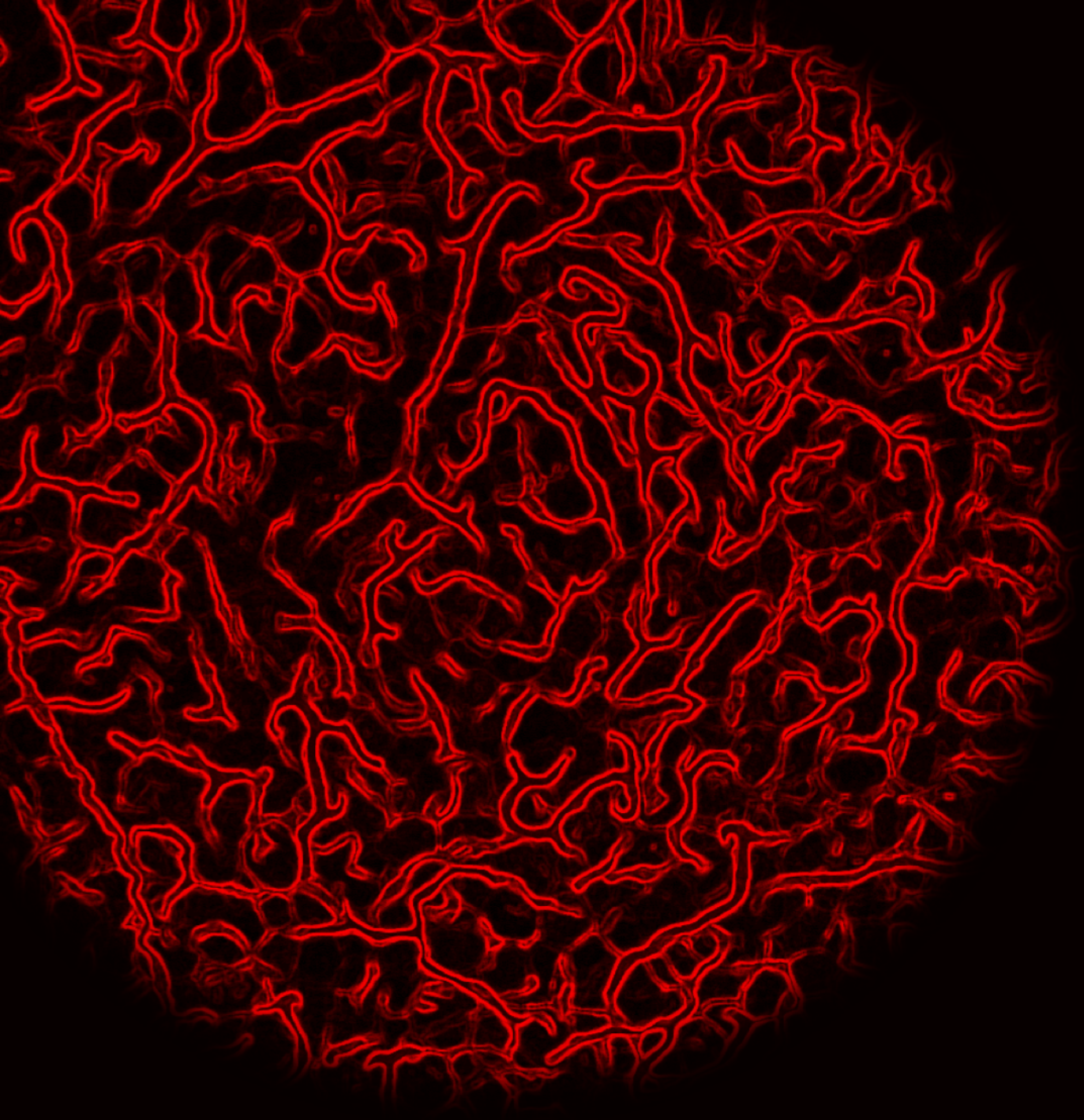

UNIVERSITAT DE BARCELONA

NeuCoMe Laboratory

IDIBAPS